University of Dundee

University of Dundee

DOCTOR OF PHILOSOPHY

Anti-Adhesive Si-and F-Doped DLC Coatings and Micro-Nanostructured Surfaces for Medical Implants

Ren, Dawei

Award date:
2015

Link to publication

General rights
Copyright and moral rights for the publications made accessible in the public portal are retained by the authors and/or other copyright owners and it is a condition of accessing publications that users recognise and abide by the legal requirements associated with these rights.

- Users may download and print one copy of any publication from the public portal for the purpose of private study or research.
- You may not further distribute the material or use it for any profit-making activity or commercial gain
- You may freely distribute the URL identifying the publication in the public portal

Take down policy
If you believe that this document breaches copyright please contact us providing details, and we will remove access to the work immediately and investigate your claim.

Download date: 05. May. 2023

Mechanical Engineering and Mechatronics

School of Engineering, Physics and Mathematics

Anti-Adhesive Si-and F-Doped DLC Coatings and Micro-Nanostructured Surfaces for Medical Implants

Dawei Ren

A Thesis Submitted to University of Dundee, in Fulfilment of the Requirements for the Degree of Doctor of Philosophy (Ph.D.)

CONTENTS

ABSTRACT .....

1. Introduction 1

1.1. Biomaterials 1

1.1.1. Metals and alloys.....2

1.1.2. Polymeric materials.....4

1.1.3. Ceramic materials and bioactive glasses.....6

1.2. Biocompatibility and corrosion.....7

1.2.1 Infection 9

1.2.1.1. Pin tract infections ·····11

1.2.1.2. Catheter-related bloodstream infections ·····12

1.2.1.3. Catheter-associated urinary tract infection ·····14

1.2.1.4. Other device-associated infections ·····16

1.2.2 Urinary encrustation.....17

1.2.3 Corrosion.....18

1.2.3.1 Corrosion of biomaterials in biological environment. ·····19

1.2.3.2 Marine Corrosion ·····20

1.2.3.3 Corrosion and associated problem of 316L stainless steel in biological environment ·····22

1.3. Improvements of biomaterials 26

1.3.1. Improvements of rejection 27

1.3.2. Improvements of anti-infection ability.....30

1.3.2.1. Biofilm on materials ·····30

1.3.2.2. Bacteriostatic strategy ·····33

1.3.2.3. Anti-adhesion strategy ……39

1.3.3. Improvement of urinary encrustation resistance 49

1.3.4. Improvement of corrosion resistance 50

1.4. Aim of study 52

1.4.1 Development and evaluation of doped diamond-like carbon (DLC) coatings 52

1.4.2 Development and evaluation of micro-nanostructured surfaces 52

2. Preparation of Doped DLC Coatings and Micro-nanostructured Surfaces ..54

2.1. Preparation of DLC and Si-and F-doped DLC coatings 54

2.2. Preparation of PDMS samples with surface micro-nanostructure 55

2.2.1 Soft lithography techniques.....55

2.2.2 Design of pattern 59

2.2.3 Fabrication of master.....61

2.2.4 Preparation of PDMS sample.....61

3. Characterization of Coatings and Micro-nanostructured Surfaces 64

3.1. Scanning electron microscope 64

3.2. Energy dispersive X-ray spectroscopy 64

3.3. Contact angle method 65

3.3.1 Sessile drop method 65

3.3.2 Captive bubble method 66

3.4. Surface energy 67

3.2.1 Calculation of surface energy by sessile drop method.....68

3.2.2 Calculation of surface energy by captive bubble method 70

3.2.3 The surface energy and zeta potential of bacteria.....72

4. Experiments and Methods.....74

4.1. Bacterial adhesion assays.....74

4.1.1. Bacterial culture 74

4.1.2. Bacterial growth curve 75

4.1.3. Bacterial suspension.....77

4.1.4. Simulation of bacterial adhesion.....78

4.1.5. Observation of bacterial adhesion and data statistics.....80

4.1.5.1 Plate count method ·····80

4.1.5.2 Fluorescence microscope method. ·····82

4.2. QCM-D method.....83

4.2.1. QCM-D system and its principle.....83

4.2.2. Measurement of bacterial adhesion by QCM-D system 85

4.3. Corrosion resistance test.....88

4.3.1. Electrochemical corrosion test 89

4.3.2. Test procedures.....91

4.4. Encrustation test.....94

5. Modelling of Interaction Energy Between Bacteria and Surfaces.....96

5.1 Extended DLVO theory.....96

5.1.1 Lifshitz-van der Waals interaction component (E^{LW}).....96

5.1.2 Lewis Acid–Base Interaction (E^{AB}) 98

5.1.3 Electrostatic Double-Layer Interaction (E^{EL}) 99

5.1.4 Brownian motion component (E^{Br}) 100

5.2 Surface integral method for ccalculating interaction energy.....100

5.2.1 Interaction energy between spherical bacteria and flat surface.....100

5.2.2Interaction energy between rod bacteria (cylinder model) and flat surface 102

5.2.3 Interaction energy between rod bacteria (cylinder model) and nanocube array surface.....103

6. Results and Discussion.....106

6.1 Si- and F-doped DLC coatings.....106

6.1.1 Contact angle and surface energy of DLC coated samples.....106

6.1.2 Bacterial adhesion assays.....107

6.1.2.1 Effects of contact time on bacterial adhesion ·····107

6.1.2.2 Effect of flow rate on bacterial adhesion ·····111

6.1.2.3 Effect of interaction energy on bacterial adhesion ·····112

6.1.3 Bacterial adhesion assays with QCM-D system 115

6.1.3.1 Frequency curve (Δf) and dissipation factor curve (ΔD) measured by QCM-D system ·····115

6.1.3.2 Analysis of measurement data ·····117

6.1.3.4 EDLVO modelling and QCM-D measurements ·····124

6.1.4 Electrochemical corrosion test.....127

6.1.4.1 Open circuit potential ·····127

6.1.4.2 Potentiodynamic polarization test ·····130

6.1.4.3 Breakdown potential (E_b) and protection potential (E_p) ·····137

6.1.4.4 Effect of corrosion electrolyte ·····141

6.2 Influence of surface micro/nanostructure on bacterial adhesion.....142

6.2.1 Interaction energy between bacteria and surfaces.....142

6.2.1.1 Interaction energy between rod bacteria and flat surface ·····142

6.2.1.2 Interaction energy between rod bacteria and nanocube array surface 144

6.2.2 Surface topography by SEM 147

6.2.3 Contact angle.....149

6.2.4 Effect of micro-nanostructure on bacterial adhesion 151

6.2.5 Impact on the attachment mode of bacteria 153

6.2.6 Encrustation test in sterile urine.....157

7. Conclusions and future work 163

7.1 Conclusions.....163

7.2 Further work.....166

Reference.....168

DECLARATION

I hereby declare that this thesis is completed on my own, it contains no materials previously published or written by another person and it has not previously been accepted for a higher degree at University of Dundee or any other education institution.

Signature:

Date:

CERTIFICATE

This is to certify that Dawei Ren has done his research under my supervision and that he has fulfilled the conditions of Ordinance 39 of the University of Dundee, so that he is qualified to submit for the Degree of Doctor of Philosophy.

Signature:

Date :

ACKNOWLEDGEMENTS

First and foremost I want to thank my supervisor Dr. Qi Zhao for his expert guidance and great support in my research and life during these past four years. I appreciate all his contributions of time, ideas and funding to make my Ph.D. experience productive and stimulating. And it has been an honor to be his Ph.D. student.

I would like to thank Xueju Su, Wei Song, Yang Kuang, Chenghuo Shang and Markus Pakleppa for their help and advices in my research and to the other staffs of the Division of Mechanical Engineering and Mechatronics at the University of Dundee as well. As seniors and friends, they shared their very valuable experience with me.

I also wish to acknowledge Mr. David O'Connor and Bandwidth Foundry International Pty Ltd, University of Sydney, for their technical Support, Dr A. Bendavid, CSIRO Materials Science and Engineering, Australia for his help in preparation of doped DLC coatings, and also Martin Kieranshis, University of Dundee for his help on using SEM.

Finally, I would like to express my thanks to my family for their great support on finance and mental. I can not achieve this without their loves and encouragement.

Dawei Ren

ABSTRACT

The development of biomaterials mainly focuses on the improvement of their biocompatibility. The aim of this research was to develop a range of DLC coatings and micro-nanostructured surfaces with anti-bacterial properties for biomedical applications. In this study a DLC coating and Si- and F- doped DLC coatings with various Si and F contents were prepared by a radio frequency plasma-enhanced chemical vapor deposition (rf-PECVD) technology. Under water contact angle method was used to characterize the surface properties of these DLC type coatings, and bacterial adhesion assess were performed by fluorescence microscopy to evaluate their anti-bacterial ability. The results showed that the DLC coatings can effectively decrease the bacterial adhesion, which reduced the bacterial adhesion by 65%, compared with uncoated stainless steel. The extended DLVO theory was used to explain the bacterial adhesion mechanism. Quartz Crystal Microbalance technology (QCM-D), which is a simple, efficient, reliable, real time and information-rich method for measuring bacterial adhesion and related assesses, was used to measure and record the bacterial adhesion process with time. The frequency change curves and dissipation factor change curves of bacterial adhesion onto the coatings were obtained. The electrochemical corrosion tests showed that the doped DLC coatings has excellent anti-corrosion properties and can protect stainless steel from corrosion.

In this study the effects of material topography on bacterial adhesion were investigated

both theoretically and experimentally. The interaction energies between bacteria (*E.coli*) and micro-nanostructure were computed by extended DLVO theory. The results showed that 350nm scale surface structure has the highest interaction energy and should be able to minimize the bacterial adhesion. To verify this finding, a series of surface micro/nano-structures (350-1000nm) were produced on PDMS samples by a soft lithography method. The bacterial adhesion assays were performed with the micro/nano-structured PDMS surfaces. The bacterial adhesion results were consistent with our theoretical prediction. In addition the sterile urine encrustation experiments were also performed with the micro/nano-structured PDMS surfaces. The experimental showed that the micro-nano-structured surfaces significantly reduced or delay the urine encrustation formation on the surfaces.

1. Introduction

1.1. Biomaterials

Biomaterials are essentially the materials that can be used and adapted for health and medical applications. Biomaterial is a new research field, but its application and development have a rather long history. Wood, glass and gold were used as the original biomaterial by Chinese, Romans and Aztec at more than 2000 years ago. But the developments of biomaterials were very slow, until the last century, the invention of synthetic plastics opened a new era for the application of biomaterials. But the "biomaterials", as a science or subject, was still not raised or created. The early records should be the Clemson University biomaterials symposia in late 1960s and early 1970s. The scientific success of these symposia led to the formation of Society for Biomaterials in 1975, which can be taken as the starting point of modern biomaterials. (Ratner BD *et al.*, 2012) After that, related research rapidly progress, with the discoveries, developments and inventions on materials and theories, biomaterials has become a scientific discipline, which involves material science and other related fields, like medicine, molecular biology and mechanics. Biomaterials are very important in biomedical engineering and will affect or determine the design, manufacture, performance and maintenance of all medical devices and implants. Improving the biomaterials on their abilities can help the medical devices solve existing problems and reach better performance. So, the main purpose of this section is to get a general

knowledge of the common biomaterials. This review of the common biomaterials includes the properties, applications and features, which are very helpful for choosing the direction and beginning-point of this research. In the review, metallic and polymeric biomaterials showed their distinguishing features with the widest applications, but also have some weaknesses and limitations. So, my research mainly focused on these two types of biomaterials, and stainless steel and polydimethylsiloxane (PDMS) were chosen as the representative study objects.

1.1.1. Metals and alloys

Metals are defined as the solid state materials with metallic bond, and the mixtures or solid solution of different metals and other elements are alloys. Metallic materials have very important and wide applications in biomaterials fields from surgical instruments to different implants. Nearly half of the total 3.6 million orthopedic operations per year in the U.S. involve metallic implants. For the metals in biomedical applications, the most important properties are mechanical strength and chemical inertia. The typical metallic biomaterials include stainless steel, aluminum or titanium alloy and so on, but only the special high class kind of these materials can be used as biomaterials.

Stainless steel is a group of steel alloys with at least 10.5% chromium content by mass and was firstly invented by Lecon Guillet in 1904. Then in 1926, Strauss developed the 18Cr18Ni stainless steel, which is corrosion resistant because containing about 2-4%Mo and low carbon content (0.08%). After several improvements, in 1952, the

type 316 stainless steels, with contains about 2% Mo, were developed out and showed a better performance. 316L stainless steel is predominantly iron (60-65%) alloyed with major amount of chromium (17-19%) and nickel (12-14%), plus minor amount of nitrogen, manganese, molybdenum, phosphorous, silicon and sulfur, and the "L" means the low carbon content at about 0.030%. The surface oxide layer of Cr_2O_3 is the feature and advantage of 316L stainless steel, this layer with silicon and nickel can effectively improve the stability and anti-corrosion ability of stainless steel, while the low carbon content can decrease the formation of carbides, such as $Cr_{23}C_6$. 316L (grade 2) is the most common metallic biomaterials, so it was chosen as the subject in my research of metallic biomaterial improvement.

Titanium-based alloys are another group of widely used metallic biomaterials, among them CP titanium (ASTM F67) and extra-low interstitial (ELI) Ti-6Al-4V (ASTM F136) are the most common two for implants. The former is a high purity metal with 98.8-99.6% titanium, while the latter is a complex ternary alloy with Ti-Al and Ti-V phases. These titanium-based materials have trusted mechanical stability (the yield strength can be 485-1034 MPa and fatigue endurance limit can reach 300-689 MPa at 10^7 cycles) and chemical inertness. Then ASTM F75 is the representative of cobalt-based alloys, whose main feature is their outstanding corrosion resistance in chloride environment. (Ratner BD *et al.*, 2012)

Generally speaking, metallic biomaterials have high hardness, high strength, high

density, good electrical and thermal conductivity and relatively high cost. For these reasons, metals are extensively used as the biomaterials of the long-term repeated use devices or implants, which are required to be able to withstand certain mechanical forces. The present applications include common surgical instruments, joint replacement, bone plate, dental fixation and so on. (Tathe A *et al.* 2010)

1.1.2. Polymeric materials

Polymeric materials have wide applications on medical devices and implantations for their diversity of performance and high plasticity. Polymer usually is a long-chin molecule composed of many repeated subunits, known as monomers. Polymer is a huge family consists of wide variety of nature and artificial materials, from common industrial materials, like synthetic plastics or rubber, to deoxyribonucleic acid (DNA)-the genetic material of living creature, the polymer undoubtedly plays an important role in our daily life. As long-chain molecules, the changes on both the quantity and kind of the monomers can dramatically affect the molecular structure of polymers thereby affect the properties of materials. Selecting the biomaterials having properties can most closely match the requirements for certain application is the main task of biomedical engineers, and the varied properties of polymers can offer a great possibility, so there are wide applications of polymer as biomaterials on medical devices. The evaluation and selection of polymers should base on their mechanical properties, thermal properties and also surface characteristics, among them, fatigue

behavior and glass transition temperature should be especially concerned. Homopolymers are the most common type for biomedical purposes and are composed of a single kind of monomer. Typical homopolymers include PMMA, PE, PP, PTFE, PVC, and PDMS and so on. PMMA, known as the trade name of Plexiglas, is a hydrophobic, tough and highly transparent glassy material, whose applications are mainly on intraocular lenses and hard contact lenses. PE and PP are wildly use as the materials on catheters and acetabular components for its toughness, high-density and good chemical resistance. (Ratner BD *et al.*, 2012) PVC is a reliable polymer for long-term use. It was also found that, in some cases, synthetic polymers can achieve better bond with natural tissue. Examples include the bonding of heparin protein on the surface of polymers (silicone, urethane rubbers, etc.) can prevent blood clotting, and thereby decrease the thrombus.(Lakes RS, 2007) Generally speaking, polymers are cheap biomaterials, which can meet most mechanical and chemical requirements, so are preferred to be applied as the material of short-term or disposable devices.

Polydimethylsiloxanes (PDMS), or silicones, are a class of flexible synthetic polymers with repeating units of silicon and oxygen. The simultaneous presence of different groups attached to the silicon-oxygen backbone make PDMS can be used as fluids, emulsions, compounds, resins, and elastomers in numerous applications. The stability, low toxicity and the wide variety of mechanical (or viscous) properties of PDMS make these materials well suited for use in personal care, pharmaceutical, and medical device applications, like finger joints, blood vessels, heart valves, breast implants, outer ears,

catheters and so on.(van Dyke ME *et al.*, 2003; Ratner BD *et al.*, 2012; Rosato DV, 1983) Furthermore, PDMS samples used for tests are relatively easy to be manufactured, prepared and modified in laboratory conditions, so PDMS was used as the typical polymeric biomaterial in my research, which we tried to improve for medical applications.

1.1.3. Ceramic materials and bioactive glasses

Ceramic materials and glasses are very traditional and classic biomaterials. These materials are widely used as restorative materials in dentistry and orthopedics, for having very similar mechanical, chemical and even surface properties to the tooth and bone. In these applications, ceramics, glasses and glass-ceramics are generally used to repair or replace skeletal tissues, so the stable attachment of surrounding connective tissue is the key factor. Al_2O_3 bioceramics is a nearly inert crystalline ceramics having high Al_2O_3 content (>99.7%), high density, outstanding corrosion resistance, satisfactory biocompatibility, low coefficients of friction and high wear resistance.(McMillan PW, 1979; Hulbert S, 1993) Especially the last three features make this material a reliable choice for long-term implants in orthopedic surgery. Clinical applications of Al_2O_3 bioceramics and ZrO_2 bioceramics include knee prostheses, bone screws, ossicular bone substitutes, segmental bone replacements and blade. There are some research showed that, on the artificial hip joint and some other similar implants, ceramics material has more advantages and higher clinical success

rates than alloy materials.(Hench LL *et al*, 1993) Porous ceramics, hydroxyapatite as a representative, is another featured ceramic material. It has weaker mechanical properties, but the pores can help bone cells grow into these structures, thereby improve the coordination between implants and surrounding tissue. So, porous ceramics is an ideal functional material for the non-load-bearing implants.(Sopyana I *et al*,2007) Bioactive glasses has lower SiO_2 content (<60 mol.%, normally 45 wt.%), high NaO_2 and CaO content and high CaO/P_2O_5 ratio (normally 5:1), it is a material can bond to soft tissue as well as bone. Its common characteristic is that a biologically active layer will form on the surface after implantation, and this layer develops into the bonding interface between materials and tissues.(Wilson J *et al*, 1981) The successful clinical application of bioactive glasses is in middle-ear surgery. Ceramic materials and bioactive glasses are reliable biomaterials but with relatively high technology and price, so suit for being the materials of long-term or functional implants.

1.2. Biocompatibility and corrosion

For all biomaterials and medical devices for applications in humans, their biocompatibilities are significant issues. Biocompatibility is usually mentioned within biomaterials science, but there are still uncertainties about the actual meaning and mechanisms. The representative definition is the ability of a material to perform normally with an appropriate host response in a specific application, which were raised during the 2nd Consensus Conference in Liverpool.(Elshahawy W, 2011) From the

perspective of pathology, tissue responses, environmental impacts and material aging will be inevitably initiated when biomaterials or medical devices are implanted into living tissues. The tissue responses include blood-material interactions, acute/chronic inflammation, foreign body reaction and fibrosis/fibrous capsule development, and the environmental impacts include corrosion, degradation, stress, blockade and so on. All of these factors are closely related to the properties of biomaterials. So it is necessary to evaluate the biological responses and reliabilities of biomaterials or medical devices, thereby predict and determine that whether they can perform as intended and present no significant harm to the users. (Anderson JM, 2001)

Government agencies, i.e. FDA, and regulatory bodies, i.e. ASTM, ISO, USP, summarized the guidelines and standards to normalize assessments of the biocompatibility of biomaterials or medical devices. The evaluation aspects include materials, intended additives, process contaminants and residues, leachable substances, degradation and also properties of the final products. In order to facilitate the selection of appropriate tests, the medical devices and their biomaterials can be categorized by the tissue contact and contact duration of the medical devices, as shown in Table 1.1. And assessments about specific biological properties, like sensitization, immune response, toxicity, hemcompatibility, degradation and so on, should be selected according to the categories of materials and devices. (Chapekar MS, 1996; Langone JJ, 1999)

Tissue contact	
Surface devices	Skin, Mucosal membranes, Breached or compromised surfaces
External communicating devices	Blood path, Tissue/bone/dentin communicating, Circulating blood
Implant devices	Tissue/bone, Blood
Contact duration	
Limited	≤24h
Prolonged	＞24h &＜30 days
Permanent	＞30days

Table 1.1 Classification of biomaterials on tissue contact and contact duration.

By reading related statistical reports and guidelines, it can be found that, for most biomaterials (especially metallic and polymeric biomaterials), the existing and potential problems, including infections, corrosions and encrustation, are frequently mentioned and always draw researcher's special attentions. In other words, these issues are the main challenges for the applications of metallic and polymeric biomaterials, and the attempts of improving biomaterials should mainly focus on these issues. And in this part, we briefly discussed these problems of biomaterials from their causes, symptoms and affects, which are the important background knowledge of improving stainless steel, PDMS and other biomaterials.

1.2.1 Infection

Patients have been plagued by the infections and related complications for thousands of years, with the medical progress, although the serious infection can be effectively

avoided, some local infections still appear during today's treatments. The common infections mainly are health care-associated infection and device-associated infection. Health care-associated infections (HCAIs) are infections that patients acquire while receiving treatment for medical or surgical conditions and are very common adverse event during care delivery.(Bates DW, 2009) The related scientific literatures published in 131 nationals from 1995 to 2010 were summarized in World Health Organization's authoritative report in 2011. In this period of time, the HCAIs prevalence in high-income countries ranged from 3.5%-12%, while that date in Low- and middle-income countries can reach 5.7% to 19.1%.(Allegranzi B, 2011) While, device-associated infections (DAIs) are the infections in patients with devices (i.e., central line, ventilator, or indwelling urinary catheter) that were in use within the 48-hour period before onset of infections. The reports from International Nosocomial Infection Control Consortium (INICC) and CDC National Healthcare Safety Network (NHSN) illustrated that average rates of 6.95 catheter-associated bloodstream infections (CLABs)/1000 CL-days, 5.08 ventilator-associated pneumonia (VAP)/1000 ventilator-days, and 8.08 catheter-associated urinary tract infections (CAUTIs)/1000 urinary catheter-days in Medical-surgical ICUs, Coronary ICUs, Pediatric ICUs and Neonatal ICUs.(Rosenthal VD, 2008) Infections are major problems for patient safety and their impacts can lead to prolonged hospital stay, increased resistance of microorganisms to antimicrobial agents, a massive additional financial and mental burden for health system, patients and their families, and even excess deaths.（Burke JP，2003; Allegranzi B, 2011）Related investigations illustrated that the top 10 risk

factors of nosocomial infections include patient age (>60 years), cancer, long-term hospitalization (>4 weeks), indwelling catheter, tracheotomy, application of immunosuppressant, vascular catheterization, mechanical ventilation, prolonged use of antibiotics (>2 weeks) and adoption of more than two antibiotics. It can be found that four of these top10 factors are device related factors. So comparatively speaking, device-associated infections (DAIs) are more frequent and serious, and declining these infections is one of the main objectives when developing biomaterials. Following is an introduction of common device-associated infections.

1.2.1.1. Pin tract infections

External fixation is a common surgical treatment, where pins or wires are inserted into the bone through small skin incisions and are held together with an externally applied metal or carbon fiber frame, its aim is stabilizing bone and soft tissues at a distance from the operative focus.(Shirai T *et al*, 2009; Schalamon J *et al*, 2007) The pin tract connects the internal environment and external environment, and has relatively weaker immune ability, so pin-tract infection (PTI) is the most frequent complication during external fixation. In related literature, the infection rate can reach 2–30% (Shabtai L *et al*, 2013; De BastianiG *et al*, 1984; Keating JF *et al*, 1991) and 75% screw tips are cultured positive for infection at removal. (Mahan J *et al.*, 1991) There are also evidences illustrate that the rate of pin tract infection increases with the length of insert period and external fixation duration.(Antoci V *et al*, 2008; Respet P *et al*, 1987) Pin

tract infections can decrease the stability of the pin–bone interface, and the deeper and more serious infections may even cause osteomyelitis. The common causes of these implant-associated infections are Staphylococcus aureus (*S. aureus*) and Staphylococcus epidermidis (*S. epidermidis*).(Parameswaran AD, 2003; Antoci V *et al*, 2008; Fitzgerald RH Jr, 1995; Barth E *et al.*, 1989; Gristina AG *et al.*, 1985) Clinically, the common treatments of pin-tract infections include pin site care and clean (with saline, hydrogen peroxide, povidone iodine, or octenidine dihydrochloride) or even removing the infected devices. Good postoperative nursing can decrease pin tract infections, but once the pin begin to loose, the pin-tract infections will be difficult to avoid, even with good medical conditions. So, adopting new metal materials with better mechanical properties and corrosion resistance should be able to effectively decrease the pin loosening or deformation, and thereby reduce the pin tract infections.

1.2.1.2. Catheter-related bloodstream infections

Catheter-related bloodstream infection (CRBSI) is defined as the presence of nosocomial bacteremia originating from blood related catheter.(Sitges-Serra A *et al.*,1999) Overall, CRBSI occurs in 3% to 16% of catheterizations. Its affects and related complications are reflected in many aspects, the serious complications, like septicemia, are significant causes of morbidity and mortality. Of approximately 250000 CR-BSI occurring every year hospital-wide in the USA, about 28 000 lead to deaths in ICU patients, with an annual cost of up to US$ 2.3 billion.(O'Grady NP *et al.* 2011)

Even relative milder infection will still increase the main symptoms or delay the recovery, additional length of stay for per CRBSI episode varied between 4 and 14 days. Among the common medical devices, central venous catheterization most frequently cause catheter-related bloodstream infection, so in most research, central venous catheter related infection is discussed as the representative of CRBSI. Central venous catheter (CVC) is a kind of catheters placed into a large vein in the neck (internal jugular vein), chest (subclavian vein or axillary vein) or groin (femoral vein). The usages of CVC are very wide and include central venous pressure measurement, dialysis tubing and short & long term intravenous infusion. CVC infections are commonly caused by colonization of the catheter tip during insertion, contamination during routine use and infection source within the body. Many necessary precautions are taken for these three infection source, but according to the report from Raad II, almost all central venous catheters are adhered with microorganism biofilm to different extents. The biofilm is commonly composed of *Staphylococcus epidermidis*, *S. aureus*, *Candida albicans*, *P. aeruginosa* and *K. pneumonia*. (Esposito S *et al.*, 2013; Elliott TS *et al.*, 1997; Raad II *et al.*, 1992) Once the catheter-related bloodstream infections are diagnosed by spiking fever, malaise feel or rigors, the related catheters may have to be sealed by antibiotic or removed to prevent further endocarditis and septic. Prevention methods should aim at avoiding extra/endoluminal infections, so aseptic insertion condition and appropriate maintenance are necessary. Also, the material and mechanical factors are critical factors to determine the incidence of catheter-related infections. (Shah H *et al.* 2013; Mahan J *et al.* 1991)

1.2.1.3. Catheter-associated urinary tract infection

Urinary catheters are inserted in more than 5 million patients in acute-care hospitals and extended-care facilities every year to help the patients losing urinate ability, the recent surveys showed that use of urinary catheter can reach 17.5% of patients in 66 European hospitals having a catheter and 23.6% in 183 US hospitals. (Zarb P, *et al.*, 2012; Magill SS, *et al.*, 2014) And catheter-associated urinary tract infection (CAUTI) is also the most common nosocomial infection, 70–80% of these infections are attributable to use of an indwelling urethral catheter.（Zarb P, *et al.*, 2012; Magill SS, *et al.*, 2014; Warren JW，1991）Thus, the prevention of infections attributable to urethral catheter is an important goal of improving related biomaterials.

The microorganisms for catheter-associated urinary tract infection are *Escherichia coli*, *Klebsiella, Enterobacter, Proteus, Citrobacter, Pseudomonas aeruginosa, enterococci* and *staphylococci*, most of which are antibiotic-resistant pathogens. By extraluminal and intraluminal ways, these microorganisms can develop in up to 25% of patients requiring a urinary catheter for > 7 days, with a daily risk of about 5%.（Maki DG *et al.*, 2001; Kunin CM *et al.*, 1966; Stark RP *et al.*, 1984）Extraluminal contamination usually comes by insertion or capillary action, while intraluminal contamination is caused by contamination of urine in the collection bag or failure of closed drainage. The complexity of microorganism components and infection route is the main reason

leading to the high incidence of CAUTI. The infection affecting lower urinary tract can cause a simple cystitis, and that affecting the upper urinary tract may lead to pyelonephritis. The common symptoms of catheter-associated urinary tract infection, including pain, urgency, dysuria and fever, are relatively easy to be diagnosed and treated. But the adverse consequences, like local and systemic morbidity, even secondary bloodstream infection, are more serious and will increase the patients' pain and health care costs. In related statistics, the most catheter-associated urinary tract infection cases will add $500 to $1,000 acute-care hospitalization burden. (Evelyn L *et al.*, 2014; Nicolle LE, 2014; Patton JP *et al.*, 1991) Since the individual urethral catheter has relatively sample insertion/removal operation, the catheter will be replaced once the infection is diagnosed, but the pain during replacement process is great, especially for the males and elderly patients. In addition, the biofilm inside the catheter can also aggravate the encrustations in urinary catheter. (Stickler DJ *et al.*, 2010.) Encrustation of catheters is the formation of crystal on the lumen and is a very common complication for urethral catheter. The encrustation will block the flow of urine or result a renal stone, thereby affect the normal use of the catheter and even worse the patient's condition. Encrustation formation in urine involves a series of factors, e.g. temperature, PH, urine components, and the urinary tract infection also plays a very significant role. (Yates A, 2008) So, improving the materials of urinary catheters can decrease catheter-associated urinary tract infection and also reduce the encrustation in catheters.

1.2.1.4. Other device-associated infections

Except the above examples, the other devices are also troubled with the associated infections. For the long term implants, like artificial hip prostheses, artificial joints and prosthetic heart valves, roughly 1-10% may develop an infection after the operation, and because the complex surgery and significant implant position, the consequences of deep infections are very serious. (Darouiche RO, 2007; Fitzgerald RH Jr, 1989; Buchholz HW *et al*., 1981) More than 60,000 valve replacements are performed annually in the United States. And in different reports, 34-72.1% patients get infective endocarditis with a persistently high in-hospital mortality rate at approximately 15%–20%. (Illingworth BL et al., 2000; Murdoch DR *et al.*, 2009; Lee JH *et al.*, 2009) As the important rescue measures of respiratory tract obstruction and acute respiratory failure, tracheotomy tube and breathing assistor are also the sources of related respiratory system infections. The indwelling time extension and irregularities of aseptic operation of remaining tracheal intubation can increase the chance of infections. The remaining tracheal intubation directly connects the bronchus and external environment, as the first defense against infection, nasal meatus and oropharynx lose their functions, the biofilm and pathogens on the device can directly develop into lower respiratory tract thereby worsen the infections. The infection rate of oxygen humidifier bottle and its tube can reach 64.3%-73.9%, that of intubation can also be more than 60%, and these infections can lead to pneumonia or septicemia.

1.2.2 Urinary encrustation

A wide variety of polymer materials, like the silicone, polyurethane and polyethylene, are used as the material of medical catheters, including urinary catheter. Urinary encrustation is a common problem of long-term indwelling ureteral stents and urinary catheter. Encrustation is a result of the ionic components in the urine crystallizing out onto the surface of the biomaterials and becoming incorporated into a bacterial biofilm layer, and may arise as a result of alkalization of urine.(Stickler DJ, 2014) Furthermore, encrustation and urinary tract infections are closely related and can enhance each other, urinary encrustation can develop with or without urinary infection, but urinary infection can accelerate the catheter encrustation formation. The biofilm is made up of *Proteus spp* and *staphylococci* can produce urease, which precipitates ammonium magnesium phosphate and calcium phosphate crystals (Malic S *et al.*, 2011; Hedelin H *et al.*, 1991), the main ingredients of encrustation, the viscous biofilm matrix can also help large crystals gather and adhere in the catheter. At the same time, the catheter encrustation will also provide good adhesion and growth base for bacteria, thereby worse the infection.(Choong S *et al.*, 2001) Patients have a high tendency to catheter encrustations, and there is not much can be done to improve the situation except frequent washouts. Encrustation and dysfunction of urethral catheters or ureteric stents will result in painful hydronephrosis, which may lead to irreversible renal damage.(Shaw GL *et al.*, 2005) The damage caused by ammonia released during urease activity can also be a serious problem in patients with indwelling catheters, and

the remedies are unsatisfactory. These problems are costly to the health service, based on clinical statistics, encrustation and infection are two major complications of indwelling urinary devices, the cost of these complications amount to £1 billion per year in Western Europe and a similar amount in North America.(Choong S *et al.*, 2001) More than 50% patients with long-term indwelling catheters suffer the recurrent blockage caused by encrustation, so long term indwelling catheters are not recommended in clinical treatment. (Stickler DJ, 2014; Kohler-Ockmore J *et al.*, 1996) For these reasons, there are wide needs for the polymeric biomaterials (like PDMS) having capability of preventing or reducing encrustation.

1.2.3 Corrosion

Corrosion of biomaterials used on medical devices and implants is the process of altering or destroying such materials in interaction with in vivo environment. All kinds of biomaterials are subjected to the aggressiveness in their working environments, and in a certain period of time, the biomaterials shall suffer different degrees of corrosions or chemically degradations. And the failures of implants or devices due to the corrosion of their metallic materials are very frequent and severe. In related survey about the causes for failures of stainless steel implants, about 25% of the failures are attributed to corrosion attack, which is the second high. (Sivakumar M *et al.*, 1995) So, the corrosions of metallic biomaterials have remained as one of the most challenging clinical problems. And in this section, I investigated the corrosions of metallic

biomaterials about their types, features, mechanisms and so on, these are very necessary in the research and evaluation of improving 316L stainless steel on corrosion resistance.

1.2.3.1 Corrosion of biomaterials in biological environment.

Compared with the in vitro environments, the biological environment has its particularities for metallic corrosions. First of all, blood and other body fluid contain very complex organic and inorganic constituents. The aqueous medium in the human body consists of various anions (chloride, phosphate, and bicarbonate ions) and cations (Na^+, K^+, Ca^{2+} and Mg^{2+} etc.). Most of the implant corrosions in the body fluids take place via electrochemical reactions, so the ionic-rich environment is conducive to the occurrence and development of corrosions. Secondly, the pH of aqueous medium in vivo also has strong influence on the corrosion of biomaterial. Human body normally maintains the pH value slightly higher than 7.0, so the in vivo environment is slightly alkaline and has the balance between the concentrations of anions and cations. But, because of the accidents, diseases, infections and other factors, the PH value may change from 3 to 9, after surgery the pH surrounding the implant usually reduces to a value about 5.3-5.6, so the acid or base in vivo environment will lead to the acceleration of the corrosion of biomaterials. Therefore, the biological molecules and the metabolism of tissue cells can also disturb the equilibrium of the corrosion reactions of the biomaterials. The local excess cations in the solution may be caused by

binding, transfer and consumption of the ions by biological molecules, like proteins. In addition, the presence of bacteria seems to enhance corrosion by absorbing the hydrogen, which presents in the vicinity of the implant and acts as the corrosion inhibitor. (Manivasagam G, 2010) So, in human body, the medical implants have to face very severe and complex corrosion environment.

1.2.3.2 Marine Corrosion

The metal corrosion in natural environment mainly includes atmospheric corrosion, soil corrosion and marine corrosion, among them, marine corrosion is most significant, and has some similarities with the corrosion in biological environment. Marine environment involves different factors, like seawater composition, temperature, marine organisms and tidal etc., can strongly influence the corrosion of materials. (Francis R *et al.*, 2012) Seawater has the features of high salinity, conductive and biological activity, the concentration of dissolved oxygen in surface seawater nearly reaches the saturation and the PH is about 8.5, so seawater is typical corrosive electrolyte solution. Seawater contains various dissolved salts (mainly NaCl), the salinity, which usually represented by salt content or chlorinity, is an important index for describing the property of seawater. The mean salinity of seawater is about 35, Table 1.2 is the concentrations of the main dissolved substances in the seawater (salt content=35), so 3.5wt%NaCl solution can be used as the seawater substitute in most corrosion tests in laboratory.

ions	concentration(g/L)	ions	concentration(g/L)
Cl^-	19.34	Br^-	0.06
Na^+	10.73	SO_4^{2-}	2.71
Mg^{2+}	1.29	HCO_3^-	0.14
Ca^{2+}	0.41	B^-	0.004
K^+	0.40	F^-	0.001
Sr^{2+}	0.008		

Table 1.2 Concentration of dissolved substances in seawater (salt content=35). (Bai XD, 2005)

The conductivity of seawater is about 4×10^{-2}S/cm, which is much higher than the conductivities of river water (2×10^{-2}S/cm) and rainwater (1×10^{-2}S/cm), so the marine corrosions of metal are not only microcell corrosion function but also macrocell corrosion function (like galvanic corrosion effects).(Francis R *et al.*, 2012) The dissolved oxygen in seawater is another important factor of marine corrosion, its concentrations varies typically from 5 mg/L to 10 mg/L in different temperature. As the oxidant of most corrosion processes, the sufficient oxygen molecular will promote the corrosion of materials. Furthermore, other factors, like the propagation of marine microorganisms, the change of pH, tide and so on, can also affect the marine corrosion in different extents. Marine corrosion generally accords with the basic law of electrochemical corrosion, but also has its own characteristics. Primarily, because of the high chloride ions concentration can hinder and break the passivation process of metals, most metals (like iron, zinc and copper) have very week anodic-polarization

block, only a few kinds of metals, like titanium, zirconium, can remain passive state in seawater. Secondly, the main cathode reaction is depolarization process of oxygen: O_2+ H_2O+4e→4OH^-. And, the secondary reaction is hydrogen evolution reaction: 2H^++2e→H_2, hydrogen evolution corrosion can take place on the metals like aluminum, zinc and platinum.(Zhen HD *et al.*, 2012) The corrosion rates of steel materials are mainly controlled by the cathode depolarization process of oxygen, which is affected by the content and diffusion rate of dissolved oxygen. So the increase of dissolved oxygen content can raise the corrosion rate. Other factor is the temperature, although the increase of seawater temperature will lower the dissolved oxygen content, it also simultaneously accelerates the diffusion rate thereby eventually increase the corrosion rate. Furthermore, as seawater having high conductivity, there is low electrical resistance in corrosion process, the contact or approach of different metals will lead significant galvanic corrosion, the range of corrosion action is also wider. Lastly, localized corrosion is more severe, the flow of seawater tends to lead erosion corrosion and cavitation corrosion. (Francis R *et al.*, 2012; LaQue F L, 1975)

1.2.3.3 Corrosion and associated problem of 316L stainless steel in biological environment

Although the electrochemical corrosion mechanism is the fundamental mechanism of corrosion, the corrosions of 316L stainless steel and other metallic biomaterials are usually the results of the synergy of different several corrosion forms or types of

corrosion. In order to develop more effective anti-corrosion strategies for different biomaterials and applications, the effects of different types of corrosion should be considered comprehensively and pertinently. Furthermore, in the anti-corrosion tests of biomaterials (316L stainless steel in my research), the knowledge of corrosion forms can made my evaluation and analysis more targeted and reliable. For 316L stainless steel and other metallic biomaterials the main corrosion forms include following types:

(1) Uniform corrosion

In biological environment, all implanted metal and biomaterials have uniform corrosion in certain degree. The uniform corrosion, which is also referred as general corrosion, occurs on the whole implant surface and has relatively low corrosion rate, so the uniform corrosion is not a severe problem of biomaterials and implant, but the uniform corrosion products (mainly metal ions) have a large amount and will be absorbed by human tissue, thereby affect the biocompatibility of biomaterials.

(2) Pitting corrosion

Pitting corrosion or localized corrosion is the severe form can result in an extensive damage and also leach significant amounts of metal ions.(Kamachimudali U *et al.*, 2003) Pitting corrosion occurs on local area of the material surface is usually caused by the local break of the protective layer (passive film) on metal surface. The essence of pitting corrosion is the acceleration of the corrosion at the anode position in the micro-cell corrosion action. The usual performances of pitting corrosion are points and pits on material surface, which can be the source of metal fatigue and following crevice corrosion.

(3) Galvanic corrosion

In conductive solution (like blood, tissue fluid and soon), the corrosion action occurred between the two different kinds of metals is galvanic corrosion. The two metals and conductive solution can form an electrochemical corrosion circuit, the metal with lower electrochemical potential acts as the anode in corrosion process and is dissolved in the solution, while the cathode metal will not be corroded.

(4) Crevice corrosion

Crevice corrosion is the corrosion caused by the uneven distribution of chemical compositions in environment. The corrosion attack happens in a restricted area, often a narrow fissure with a width of normally only a few micrometers. (Wika SF, 2012) The supplements of dissolved oxygen (or other oxidizing agents) are difficult in these narrow fissure positions, the concentration gradients result in the oxygen concentration cell corrosion. For easily passivated metals, the oxide film on metal surface tends to dissolve for the shortage of oxygen in fissure, so these metals are more sensitive to crevice corrosion. Furthermore, the corrosion products are difficult to diffuse out of the fissure, its accumulation and hydrolysis action will lead a decrease of pH, thereby make the media more corrosive. Crevice corrosion usually occurs at the binding sites of different parts of implants (like bone plates and screws) and leads the loose or local deformation, which are significant factors of implant fail.

(5) Intergranular corrosion

Compared to the inner part of a given materials, grain boundaries or areas near grain boundaries are less corrosion resistant. Because of the different composition and

formation of carbides, the corrosive attack is localized at these areas. Intergranular corrosion will lead dramatically decrease of the material mechanical properties.

(6) Stress and fatigue corrosion

The break caused by the associative action of applied/ residual stress and corrosion is referred as stress corrosion, and the break leaded by cyclic stress and corrosion is fatigue corrosion. The stress corrosion cracking in biomedical implants can lead to the loss of structural integrity of the implanted device and its functions.(Manivasagam G, 2010) The failure analysis studied using scanning electron microscope (SEM) illustrated that the corrosion fatigue was promoted by the presence of intense localized corrosion and intergranular cracking.(Aksakal B et al., 2004) Stress and fatigue corrosion are complex and long-term process, improving the quality of material and adopting appropriate surface coating can reduce the corrosion affects.

As mentioned before, type 316L stainless steel is the extra-low carbon version of the 316 steel alloys and is the most commonly used implant material, because its remarkable corrosion resistance and efficiency-cost ratio.(Sivakumar M *et al.*, 1994) But the mechanical properties of 316L stainless steel is not outstanding, the hardness is relatively low (≤187 HV)，its surface is easy to be worn or scratched; Tensile strength, yield strength and fatigue strength of 316L stainless steel are also not high, so fracture, deformation and fatigue fail are common on the this material. These mechanical disadvantages and defects lead to the main types of corrosion of 316L stainless steel are pitting corrosion, crevice corrosion and fatigue corrosion. Survey of failed stainless

implants indicates that about 70% of failures in type 316L SS implants are associated with corrosion related to pitting and crevice attack, pit induced fatigue crack and stress-corrosion cracking.(Kamachimudali U et al., 2003) Furthermore, although the corrosion rate of 316L stainless steel is relatively low, the leaching of metallic ions is still an issue cannot be ignored. Cr, Mo and Ni are the most important and representative metal elements in stainless steel, which are the key elements of the corrosion resistance, but also have potential risks on patients' health. Among them, Ni^{2+} ion has relatively high toxicity and can decrease the biocompatibility. So, although having corrosion resistance, 316L stainless steel is still not thus satisfactory as the biomaterial for medical implants, and it is necessary to further improve its corrosion resistance. (AL-Mangour B *et al.*, 2013; Kamachimudali U *et al.*, 2003)

1.3. Improvements of biomaterials

This section is about the current strategies of improving biomaterials, which involve different physical, chemical and design methods. When developing new methods to help metallic biomaterial (316L stainless steel) and polymeric biomaterial (PDMS) perform better for biomedical applications, we can gain valuable experience and ideas from these examples. The improvements of biomaterial biocompatibility mainly focus on two issues, namely decreasing rejection and improving in vivo stability. Rejection includes serious foreign body responses, intense immune responses and other adverse tissue responses. In vivo stability means that, when contacting with tissues, organs and

body fluids, the materials can be less affected by the adverse changes, like corrosion, degradation, scaling and infections.

1.3.1. Improvements of rejection

As the most classic and basic strategy of avoiding rejection, inert biomaterial is always the first choice that will be considered and adopted by biomedical engineers. The inert biomaterials usually refer to those metal, polymer or ceramic materials, which are relatively stable, safe and reliable in internal environment. Inert biomaterials will be recognized as foreign agents by the host, but they can still remain essentially unchanged and tolerated due to their encapsulation in fibrous tissue. (Ratner BD *et al.*, 2012) This strategy is effective, but before the formation of fibrous tissue encapsulation, the materials still inevitably be affected by host responses. For example, inflammatory response can produce proteolytic enzymes and reactive oxygen species (ROS), which will corrode and damage the inert biomaterials. (Labow RS *et al.*, 2001) Since the fragments from mechanical damage and the ions from chemical degradation are not conducive to maintaining a good biocompatibility, high chemical and mechanical stability, corrosion resistance and low degradation are also the advantages of inert biomaterials. Application of titanium material is the most typical example of this strategy, titanium and titanium alloys are often used on artificial bones, joint replacements and dental implant. Some nickel-titanium alloy stents are usually coated with a thin carbon film to further enhance material inertness and blood compatibility,

and are used in treatment of cardiovascular disease. (Liu X *et al.*, 2004). Compared with stainless steel, titanium has higher strength, lower density, better wear resistance and better corrosion resistance. (Oldani C *et al.*, 2012) So, the devices or implants made by titanium or its alloy can often reach a higher success rate. But because of the high process technique and cost, titanium materials still cannot widely replace stainless steel and are just applied on important implants (or components).

Different with the above relatively passive strategy, surface modifications, attempting to guide the tissue interactions, are more active. This strategy is doping or coating certain substances on biomaterial surface according to specific needs. The aim is reducing the adhesion or activation of related cell or protein, or blocking signal substances, thereby the tissue responses can be prevented, declined or delayed. An application of this strategy is heparin coating (or heparinized biomaterials), which can inhibit the adhesion and aggregation of platelet on material of blood contacted device, effectively reduce blood clotting and thrombus. Other more complex modifications of this strategy mainly involve bioactive molecules, like adhesion sites, growth factors, anti-inflammatory mediators or drugs.(Boontheekul T *et al.*, 2003) The adhesion sites can promote cell-specific attachment, normally can help biomaterials imitate the tissue, thereby improve the biocompatibility. Furthermore, the abnormal or insufficient attachment between the foreign body giant cells (FDGC) and biomaterial is the inducement of foreign body recognition and response. While, arginine-glycine-aspartic acid (RGD) and proline-histidine-serine-arginine-asparagine (PHSRN) can help

biomaterial get a more normal attachment with FDGC, so decrease the body chronic inflammation and foreign body response caused by implants. The growth factor is a complex group, which composes of epidermal growth factor (EGF), fibroblast growth factor (FGF), granulocyte macrophage colony stimulating factor (GM-CSF) and so on. These factors can control the adhesion, migration, proliferation, and differentiation of fibroblasts, keratinocytes and endothelial cells in wound healing. (Barrientos S *et al.*, 2008) The appropriate growth factors can promote healing process, and decrease the possibility and period of rejection.

Another strategy for improving biocompatibility is the variation of roughness and surface topography. (Yim EK *et al.,* 2005; Fink J *et al.,* 2008) Extracellular matrixc (ECM) components in the nanometer scale can affect the adhesion, proliferation, migration and even gene expression of cell, so the roughness or pattern mimics these topographies can also affect the biocompatibility. The research from Chen S illustrated the different responses of macrophages to the biomaterials with different surface micro-nanostructures. In their experiments, the 0.25-2μm wide parallel gratings on material surface can dramatically affect the macrophage morphology and cytokine secretion. Macrophage is the main participant of foreign body reaction and an important assessment objective of biocompatibility.(Chen S *et al*., 2010) Previous in vitro studies (Bauer S *et al*., 2009) reported that the topography of TiO2 nanotubes improved osteoblast proliferation and adhesion compared to normal titanium surfaces. Alpaslan E' group compared bladder stents coated with surface nanotubes to normal

titanium bladder stents, and found that the 20 nm diameter nanotubular titanium stents enhanced human urothelial cell adhesion and growth up to 3 days in culture, and this formation of a monolayer of urothelial cells on the surface can permute injection of ureteral stents.(Alpaslan E *et al*., 2011) There are some other related research about topographic patterns' influence on fibroblasts (Schulte VA *et al.*, 2009), platelets (Smith B S, 2012), epithelial cells (Andersson AS *et al*., 2003), and endothelial cells (Dalby MJ *et al.*, 2002), but generally speaking, this strategy is still in the stage of laboratory research and has no practical application case.

1.3.2. Improvements of anti-infection ability

In this part, I attempted to clarify the approaches that are commonly used of anti-infection. At first, formation of biofilm on materials was studied. And then, the antifouling or bactericidal mechanisms and features of these strategies are briefly discussed and summarized.

1.3.2.1. Biofilm on materials

Since microorganisms broadly distribute in vitro and in vivo environments, the materials of medical devices will inevitably come into contact with the microorganisms. These microorganisms include bacteria, fungus, viruses and so on. The most clinical infections are caused by bacteria, which our research mainly focused on.

Once contacted with material, bacteria will begin adhering on the surface. Then though a series of phases, bacteria can firmly colonize on material surface and even grow and multiply further into biofilm. The following is the common growth process of bacteria on material surface.

(1) Deposit: When individual bacteria approach the materials, bacteria can temporarily stay or deposit surrounding the surface. At this stage, the bacteria are relatively separated, the deposition is reversible and not firm, and media flow or other environment changes can affect this process.

(2) Adhesion: Adhesion can also be referred as colonization, which means that the status of bacteria on materials transforms from reversible deposition to irreversible adhesion. At the beginning period of this stage, bacteria begin to produce extracellular matrix (ECM) to help them adhere, but bacteria are still relatively independent and can leave the material surface. When it comes to the end of this stage, bacteria will firmly and irreversibly adhere on material surface, so the difficulty of cleaning the bacteria is increasing.

(3) Propagation: After adhesion, bacteria will begin to grow, multiply and produce more ECM. The growth and multiplication situation of bacteria closely relate to material surface characteristics and surrounding environment. If the temperature, humidity and nutrition condition are bad, the growth and multiplication will be very slow, the bacteria may even turn into spore to against adverse environment. But as long as the conditions are appropriate, the bacteria will multiply rapidly. ECM is viscous matrix, so it is good adhesion base for follow-up bacteria, furthermore ECM also help

the co-aggregation between separated bacteria on material and finally form bacteria colonies. And in the colonies, just no more than 30% is bacteria, the other part is ECM.

(4) Biofilm formation: With the accumulation of bacteria and ECM, isolated colonies on material surface gradually gather and merge into a complex colony net. When the colony net continually develops to biofilm, its properties will dramatically change. The growth rate and reproduction rate decline, the bacterial density in biofilm remains stable or decrease slightly, but internal connections become much closer. The bacteria in biofilm have obvious physiological and morphological differences with individual free bacteria. Because of the protection of ECM, the bacteria in biofilm are generally not susceptible to the antibiotic, preservative and other chemicals, so are difficult to be destroyed by conventional drugs. Furthermore, ESM can provide relatively stable temperature, balanced pH and rich nutrition for internal bacteria, thereby help bacteria deal with dramatic external environment changes. The features and shapes of bacteria in the bottom layer of biofilm are not exactly same as those of bacteria in surface layer. Bacteria in bottom layer are less sensitive to external substance and have slower metabolism, and because of metabolites are difficult to be discharged, bacterial shape variation may also occur. While bacteria in surface layer are more similar to free bacteria, part of them may leave biofilm and once again become free bacteria.

Not all the bacteria can complete the whole growth process and form biofilm, the bacteria constantly grow, multiply and die during every stage. The periods of growth stages also depend on the bacterial specie, material and environment, and the effective

antibacterial methods are not alike in different stages. But generally speaking, once the bacterial biofilm form, it will very hard for conventional methods, like adopting conventional doses of antibiotics, to clean or limit these bacteria. So, preventing or delaying biofilm formation is the key factor for most antibacterial strategies.

Anti-bacterial materials are defined as the materials with the function of killing or inhibiting bacteria.(Tiller JC, *et al.* 2001) The history of anti-bacterial materials application is long. The drug immersed wrapping cloth on Egyptian mummy may be the earliest conscious use of anti-bacterial materials. In 1935, G.Domarkin treated the military uniform with quaternary ammonium salt to prevent wound infections, which can be viewed as the starting point of modern research and application of anti-bacterial materials. With the raise of people's living standards, there are wider demands and applications of anti-bacterial materials in the fields of medical health, building decoration, food packaging and daily necessities. By materials species, anti-bacterial materials can be divided into anti-bacterial plastic, anti-bacterial fiber, anti-bacterial ceramics, anti-bacterial steel and so on. But when it comes to anti-bacterial methods, the two main strategies are bacteriostatic strategy and anti-adhesion strategy.

1.3.2.2. Bacteriostatic strategy

This strategy is adding antibacterial agent (bacteriostat or bactericide) to the materials by coating, doping, surface modification or other methods to make materials can

inhibit bacterial growth or kill bacteria. The antibacterial materials act by either being toxic when coming into contact with the bacteria or by releasing an effective chemical or antibacterial agent from the surface.(Ivanova EP *et al.* 2011) So the key factor of this strategy is antibacterial agent, which includes inorganic antibacterial agent, organic antimicrobial agents, natural antibacterial agent and polymeric antimicrobial agents. Different agents have their features and are suit for different applications. The minimum inhibitory concentration (MIC) or minimum bactericidal concentration (MBC), antibacterial spectrum, antibacterial durability, weatherability, stability and safety, technology difficulty and price are the main feature factors of related evaluations and selections.

Inorganic antibacterial agent mainly uses metal, like silver, copper, zinc, titanium, or their ions to kill or inhibit bacteria, the main varieties are metal nanoparticles, metal oxides and phosphate. (Zhao L. *et al.* 2009; Kelly PJ. *et al*. 2009) These agents are heat-resistant, long-term, broad-spectrum antibacterial, low toxic and seldom to cause drug resistance, but are easy to discolor and hard to be applied on plastic materials. The antibacterial actions of most inorganic antibacterial agents and related anti-bacterial materials are passive and rely on dissolution and contact, which can be explained by the following two sides.

(1) Contact reaction mechanism: When contacted to bacteria cell, metal ions can break bacteria protein structure thereby cause bacteria death or dysfunction. The specific process is that anti-bacterial materials with inorganic antibacterial agents can

chronically and constantly release metal ions during the period of use, the negative charged cell membrane can attract these metal ions, and then metal ions will through cell membrane into bacteria and react with the hydrosulphonyl on bacteria protein:

$$\text{enzyme}<^{SH}_{SH} + 2Ag^{+} \rightarrow \text{enzyme}<^{SAg}_{SAg} + 2H^{+}$$

This reaction coagulates the protein and decreases the synthetase activity, which can affect the synthesis of DNA and lead bacteria die for lacking schizogamy ability. The metal ions can play the role even in very low concentration, and their anti-bacterial abilities are shown in following order:

$$Ag^{+} > Hg^{2+} > Cu^{2+} > Cd^{2+} > Cr^{2+} > Ni^{2+} > Pb^{2+} > Co^{2+} > Zn^{2+} > Fe^{2+}$$

Furthermore, highly charged silver ions (Ag^{3+}, Ag^{2+}) have very high reduction potential and produce atomic oxygen in surrounding space, thereby dramatically improve the anti-bacterial effects.

(2) Reactive oxygen species mechanism: The hypothesis of reactive oxygen species mechanism believes that the metal molecules or ions on materials act as the catalytic center. Catalytic center can absorb energy and activate nearby oxygen thereby produce hydroxyl group (-OH) and active oxygen ions (O_2^-), which have very strong redox ability, so can kill bacteria.

Compared with inorganic antibacterial agent, the application of organic antimicrobial agent are earlier and more mature. Organic antimicrobial agent is a huge group of different varieties of drugs and chemicals, typical examples include quaternary ammonium compounds (QACs), phenolic substances (PCP, PCP-Na, etc.), nitrile

substances (TBN, etc.) and so on. (Murata H. *et al.* 2007) The anti-bacterial mechanisms for different organic antimicrobial agents are also not the same, but are generally in the following sides.

(1) Reducing or eliminating the activity of metabolic enzyme in bacteria cell, thereby depress bacterial respiration.

(2) Hindering the biosynthesis of bacteria, namely interfering production of the necessities for bacteria's growth and survive.

(3)Destroying bacterial membrane or hindering membrane synthesis.

The anti-bacterial materials doped with organic antimicrobial agents usually have rapid and effective anti-bacterial effect, which is their most prominent advantage. But the disadvantages should not be ignored, the organic antimicrobial agents have high risk of causing drug resistance and decreasing biocompatibility, furthermore their heat resistances are low and many decomposition products are toxic. So this method is more suitable for the short-term used materials.

Natural antibacterial agents are usually got from animals and plants, the typical natural antibacterial agents include chitosan, sorbic acid, xanthorrhizol, hinokitiol and antimicrobial peptides.(Gao G *et al.* 2011) Natural antibacterial agents' most important features are safety and nontoxicity, but their heat resistance and antibacterial efficiency are very different. The relatively high production difficulty and price also limit their applications to a certain extent. So these materials with natural antibacterial agents are

widely used in food industry, daily necessities and medical health. Especially in body contacted materials and human security related fields, their advantages are unmatched.

Based on anti-bacterial mechanism of organic antimicrobial agents and natural antibacterial agents, researchers do the molecular design to develop the anti-bacterial polymers. Soluble pyridinium-type polymer was synthesized and found has antibacterial ability by Kawabata.(Kawabata N *et al.*, 1988) Pyridinium-type polymer was proved can catch bacteria by the absorption features of molecular chain, and kill the captured bacteria by electric charge on the molecular chain. Based on this achievement, pyridinium-type olefin material having similar anti-bacterial ability was developed.(Guangji Li *et al.*, 1996) Furthermore, PEI-based polymers (such as alkylated PEI), Polyvinylpyridine (PVP) based polymers (like alkylated PVP,benzyl PVP) and N-halamines (polymers with oxidative halogens) also have high antibacterial activity. (Beyth N. *et al*. 2008; Buffet-Bataillon S. *et al.* 2012; Kenawy ER. *et al.* 2007) Polymeric antimicrobial agents are long-term broad-spectrum antibacterial, safe and reliable, can overcome the disadvantages of organic antimicrobial agents and natural antibacterial agents (like low heat resistance and so on), this kind of antibacterial agents also have many different mechanical and biological properties.

There are also other anti-bacterial agents can be used on materials to improve the anti-bacterial ability, among them photocatalytic inorganic antibacterial agent is a special type. N-type semiconductor material, like TiO_2, ZnO, CdS, SnO_2, and ZrO_2,

can decompose bacteria under the effect of light or energy. So, applying these materials can made photocatalytic anti-bacterial materials. TiO_2 and ZnO_2 are the most common photocatalytic anti-bacterial substances, they will produce hydroxyl group ($HO\cdot$) and oxygen free radical (O_2^-) when in light condition, which can react with the bacteria's organic substance and rapidly kill bacteria. (Dastjerdi R *et al.* 2010; Wu J. *et al.* 2014) Photocatalytic anti-bacterial agents can show effect within 1 hour (about 24 hour for Ag type anti-bacterial agents), and because they play the role as catalyst, the anti-bacterial ability will not decline with time.

Generally speaking, bacteriostatic strategy is relatively simple and effective method for improving the antibacterial ability of materials. This strategy mainly aims at the propagation stage, bacteriostatic functions rely on contact and chemical reaction between anti-bacterial agents and bacteria cell, so it can effectively inhibit the bacterial colony formation. The bacteriostatic strategy also has revealed several shortcomings, anti-bacterial effects of this strategy are remarkable in beginning period, but bacteria can develop resistance against antibiotics and antibacterial agents.(Bridier A. *et al.* 2011) And the depletion of agents may lead to the concentration of the released agents may not be sufficient to maintain effective antibacterial activity (Warnes SL. *et al.* 2011), drug resistance and formation of biofilm may lead the strategy cannot reach the excepted anti-bacterial ability. In addition, the durability of the target surface may not be sufficient to maintain long-term antibacterial behavior.(Warnes SL. *et al.* 2011) Taking the silver coating as an example, the Ag added coating has strong antimicrobial

activity and can kill very majority of the bacterial adhered on the coating, thereby significantly decrease the infection in short term. But the further research found that, the dead bacterial layer can form on material surface and protect the live bacteria from the effect of silver ions, the bacterial biofilm can finally grow on the material surface. As a result, the silver-coated heat valves (Silzone valve) had to be withdrawn from markets and the silver-coated catheters were also not recommended for widespread use. (Cook G *et al.*, 2000) The bacteriostatic strategy has these inherent limitations, and many existing researches focused on this strategy, so in my research, I attempted to apply anti-adhesion strategy to improve the anti-infection ability of stainless steel and PDMS.

1.3.2.3. Anti-adhesion strategy

As mentioned before, bacterial adhesion on biomaterial surfaces and adjacent tissue is the initial motivation of related infections. The infection-resistant material of indwelling medical devices could be achieved by depositing a thin layer of coating or surface modification to reduce attachment of pathogenic bacteria. Although the mechanism of bacterial adhesion to the surface is not clear, it is accepted that the bacterial adhesion involves both initial physical interactions and further molecular-specific reactions. (Katsikogianni M *et al.*, 2004)

In molecular-specific reactions, the bacterial adhesion is directly related to protein

adsorption (Pavithra D *et al.*, 2008), the part on bacteria surface, like fimbrial, peptidoglycan, extracellular slime substance (ESS) and so on, can act as ligands, while the material surface and tissue cell act as the receptors. The specific binding between these ligands and receptors is the key factor and essence of irreversible bacterial adhesion. So, one of the anti-adhesion strategy is coating the biomaterial surface with certain substance, which can also be referred as anti-adhesive agent, to inhibit these specific bindings. The most of these anti-adhesive agent coatings are protein coatings and polymer coatings. When observing the adhesion of *Staphylococcus* on different medical catheter, Krinstinsson KG fond the serum treatment can effectively reduce the bacterial adhesion on the catheter. (Krinstinsson KG, 1989) Albumin coating was also reported can affect the bacterial adhesion, but there are different conclusions about its effects.(Subbaraman LN *et al.* 2011; Jansen B *et al.*, 1988) Unlike the bactericidal agents, the anti-adhesive agents coating will not cause the propagation and spread of resistant strains. But the disadvantages are also obvious, the differences of the specific bindings between different bacteria and different surfaces are large, so the narrow anti-adhesive spectrum and not outstanding stability lead to that this strategy still has no representative case.

Another anti-adhesion strategy focuses on physical interaction mechanism to reduce the capacity of bacteria to achieve the deposit and adhesion stages. Existing research illustrated that bacterial deposit and earlier adhesion on materials can still be taken as a reversible state, which is the result of the balance between attractive interaction and

repulsive interaction.(Rutter PR *et al.*, 1980) The main sources of attractive interaction include Van der Waals energy, Acid-Base energy and other specific interactions between bacteria and material surface, while the repulsive interaction are electrostatic repulsion and Brownian motion energy. Most of these interactions have strong relationship with bacterial characteristics and material surface properties. So, by changing material surface properties, we can weaken the interaction between bacteria and materials, thereby decrease bacterial adhesion and infections. Since the anti-bacterial mechanism is physical interaction but not chemical reaction, the components of coating will not be depleted. In addition, anti-adhesion strategy does not conflict with bacteriostatic strategy, the two methods can be adopted together to achieve a better anti-bacterial effect. This physical adhesion resistance strategy mainly relies on the surface properties of biomaterials, including chemical composition and reactivity, hydrophilicity and hydrophobicity, surface charge and surface topography. For having outstanding properties and broad applicability, many polymer films were developed into anti-adhesive coatings. Trimethylsilane (TMS) plasma nanocoatings were developed by Chen M's group using low temperature plasma coating technology on 316L stainless steel and grade5 titanium surface.(Ma Y *et al.*, 2012) Significant inhibition of *S. epidermidis* biofilm was observed on TMS plasma coated stainless steel and titanium, and it was also discovered that the bacteria cells on the TMS-coated surfaces were more susceptible to antibiotic treatment than their counterparts in biofilms on uncoated surfaces. The outstanding bacterial adhesion resistance could be attributed to the coating chemical inertness, low surface free energy, coating

smoothness and surface-bound CH_3 groups. Similarly, the Poly(l-lysine)-grafted-poly(ethylene glycol) (PLL-g-PEG) coating was also reported can decrease both the non-specific adsorption of blood cell and the adhesion of *S. aureus*. (Charnley M *et al.*, 2011; Harris LG *et al.*, 2004) Another method to achieve this adhesion resistance strategy mainly focuses on creating superhydrophobic surface on biomaterials via special polymer layers, in which case, the aqueous suspensions of bacteria have limited contact with the surface. A coating of nanostructured silica colloids and a low surface energy fluorinated silane xerogel was prepared and demonstrated can decrease the adhesion of *S. aureus* and *P. aeruginosa* by two orders of magnitude versus the control.(Privett BJ *et al.*, 2011) The superhydrophobic coatings were believed can serve as a physical and energetic barrier to protein adsorption and bacteria adhesion. Polymer brush coatings are another type of promising anti-adhesion coatings, which are formed by modifying polymer long-chains on biomaterial in a high density, the polymer long-chains are fixed to the surface and stretch out into the surrounding medium.(Busscher HJ *et al.*, 2010; Roosjen A et al., 2006) The typical polymer brush coatings are made of poly(ethylene oxide) (PEO), which are highly mobile and attain extremely large exclusion volume. The polymers used for brushes are usually hydrophilic, the medium can be attracted and absorbed by the brush layer to form a layer to repel the approaching proteins or bacteria and keep them away from the material surface at a distance, so the physical interaction between bacterial and biomaterial is low and the bacterial adhesion can be prevented. The higher density and longer chains of the polymer chains are more effective in prevention

of bacterial adhesion.(Bridges AW *et al.*, 2008; Roosjen A *et al.*, 2004)

Non-polymer coatings, like nickel–phosphorous (Ni–P) coatings, can also be developed into bacteria-resistant coating. Ni-P coatings have been widely used in the chemical, mechanical and electronic industries. Because the Ni-P coatings have low toxicity, high corrosion resistance and wear resistance, it can be applied on metallic biomaterials. Our group's previous research illustrate that other elements or molecules, like Ag, Cu, PTFE and TiO_2, can be doped into Ni-P coating to further improve anti-bacterial ability.(Zhao Q *et al.*, 2002,2013) In these researches, Ni-P coatings were prepared by electroless plating method, they have the advantages as follow. At first, Ni-P coating and related electroless plating can be used on more various materials. Unlike electroplating, which is just used for coating conductive materials, almost all metallic biomaterials and even some ceramic biomaterials, glasses or polymers can be the possible substrate for Ni-P coating and electroless plating. Secondly the coating is quite uniform on both thickness and coating components. The plating solution is very uniform, and the coating reaction is gentle, so there is no obvious edge effect. Then, Ni-P plating solution is safe and stable, electroless plating is easy to operate. Coating rate and thickness can be control by temperature and plating time. At last, the particles in Ni-P coating are in nanometer size, the coatings exhibit bright appearance. However, there are also some limitations. Although electroless plating Ni-P coating on polymer materials is possible, the cost and difficulty inevitably rise, while coating fastness and wear resistance will decrease. The plating solution has relatively complex components

and is not reusable. And there are high plating requirements on plating solution and equipments. The solution should be prepared by deionized water, which is a poor electrical conductor with high resistivity of 18.2 million ohm-cm (18.2 megohm). Plating tank should be kept clean to avoid metal particles accumulating on the plating tank walls.

Similarly, Diamond-like carbon (DLC) coating was applied as the anti-adhesion coatings to improve the stainless steel in our research. Diamond-like carbon (DLC) coating in fact is a group of materials with a wide range of atomic bond structure and properties depending on the preparation method (Sa ́nchez-Lo ́pez JC *et al.,* 2000). DLC can be used as a general term of amorphous carbon film group which can been divided into two types, namely, non-hydrogenated amorphous carbon (a-C) and hydrogenated amorphous carbon (a-C:H). The DLC film is mainly made up with the three-dimensional network of the mixture of the sp^3 and sp^2 carbon bonds. And for different crystal lattices (namely the different sp^3/ sp^2 ratios), the films can also be divided into amorphous carbon polymer, diamond-like carbon and graphite-like carbon. The common preparation methods of these DLC coatings include ion beam deposition, radio frequency plasma enhanced chemical vapor deposition (r.f.-PECVD), ion beam sputtering, magnetron sputtering technique and so on. (Zhang ZY *et al.* 2013; Grill A, 1993). Although the DLC coatings made by different methods have more or less differences in their compositions and properties, the DLC coatings' common properties such as the excellent thermal conductivity similar to metals, low friction surface, high

hardness, wear resistance and corrosion resistance make them stable and biocompatible, and can be wildly applied on the surface of surgical instruments, heart valves, artificial joints or stents.(Love CA *et al.* 2013; Hotta A *et al.* 2013) And the chemical stability of DLC coatings makes them possible to be doped with many other different elements for wider use. In my research, different DLC coatings were prepared on the surface of 316L stainless steel, their anti-bacterial ability were evaluated and the mechanism was also studied, and the results were published in 2013. (Ren DW *et al.* 2013)

The material surface topography is also found can influence the adhesion behavior of bacteria and cell, related reports involve stainless steel, dental ceramics, polymer and so on.(Truong VK *et al.*, 2010; Anselme K, 2000; Hilbert LR *et al.*, 2003; Hosoya N *et al.*, 2003) The responses of cell to material surface topography reflect in many respects, Fujita reported that the surface nanotopography can affect the shape and assembly of focal adhesions.(Fujita S *et al.*, 2009) The roughness, pattern size and pattern shape of surface topography were also found can affect the cell adhesion and spread on material surface to different extents (Dalby MJ *et al.*, 2004; Andersson AS *et al.*, 2003). Furthermore, the smallest feature size of surface topography that can be detected by the cells was found lower than 10nm.(Washburn NR, 2004) The role that material surface topographical features play in affecting bacterial adhesion has not been comprehensively characterized.(Whitehead KA *et al.*2005) The early studies were mainly about material surface roughness and its effects, many of them believed that surface roughness has less influence on bacterial adhesion than the surface chemical

composition, and the increase of surface roughness can assist bacterial adhesion.(Jeyachandran YL *et al.*, 2006, 2007) But, with the deepening of related research and the diversification of research subjects, researchers realized that surface roughness is not adequate to describing the surface topography,(Truong VK *et al.* 2010) so more attention was paid on the research about the effect of the specific pattern, size and depth of surface structure. (Crawford RJ *et al.*, 2012)

In this research, we tried to apply surface micro-nanostructure to improve PDMS material on its bacterial resistance, this idea was inspired by the applications of surface topography on anti-fouling. Applying material surface topography as an antifouling strategy is not any researcher's original innovation, but one comes from the observation and imitation of the creatures in nature. It was found that there are many natural surfaces can resist biofouling in the marine environments, this physical defense mechanisms used by marine organisms to defend against biological coverage range from the spicules of an echinoderm to the mechanical breaching of cetaceans. Figure 1.1-(A) and (B) show the surface of situation of two kinds of shark skins, *Spinner shark* skin and *Galapagos shark* skin with special scale patterns.(Bone Q *et al.*, 2009) The sizes of these rhombic and placoid scales are about 500μm, and the surface topography are formed with the ridges and grooves (about 100μm in width and 10μm in height). A similar regular ripple structure has been found on the periostractum of blue mussels shells (Figure 1.1-(C)), which are the effective antifouling surfaces, the ridges and grooves are 1-2μm wide and 1.5μm height. It is believed that the

combination of these physical topographic features and chemical mucosal coating contributes to the outstanding antifouling properties of these animals. (Magin CM *et al.*, 2010)

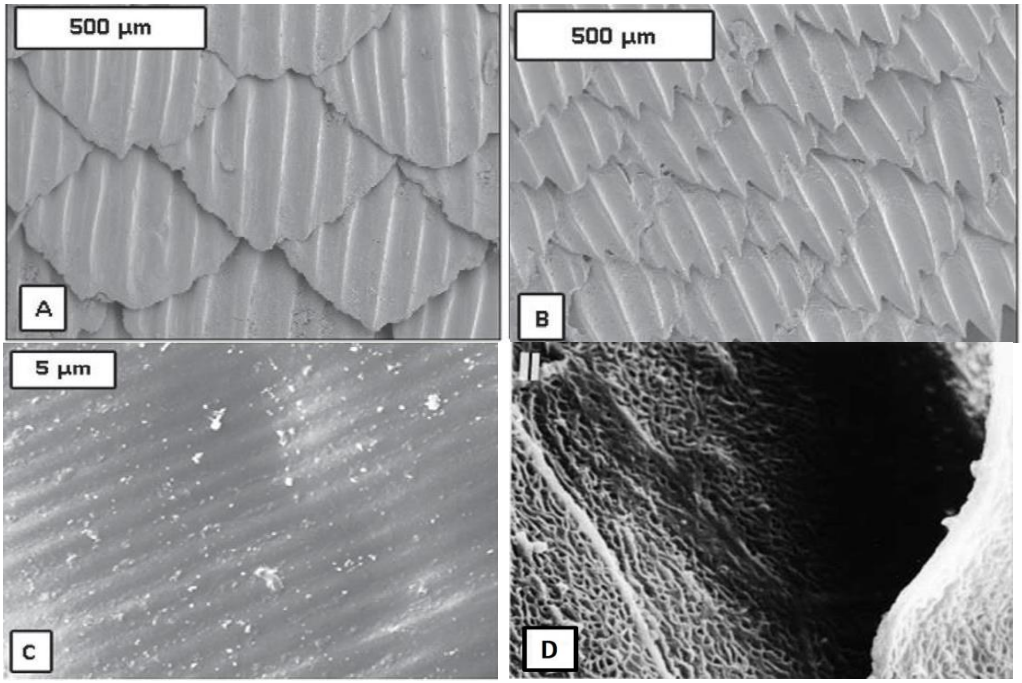

Figure 1.1 SEM of natural textural surfaces: (A) *Spinner* Shark skin; (B) *Galapagos* Shark skin; (C) *Mytilus edulis* mussel shell, (D) *Pilot* whale skin

Some biomimetic microstructured surfaces inspired by shark skin scales were designed and evaluated, and the barnacle settlement on the biomimetic microstructured surfaces was reduced by 95%, compared with flat surfaces.(Kesel A *et al.*, 2007) Brennan' group also designed and produced a range of anti-biofouling surfaces with Sharklet AF™ topographies inspired by the placoids of a shark on the polydimethylsiloxane (PDMS) substrates, which reduced cyprid settled by 97%.(Carmen ML *et al.*,2006; Schumacher JF *et al.*, 2007) Basded on a large number of motile spores settlement assays, they also summarized that the amount of microfouling spores adhered on unite area appear highly dependent upon the Engineered Roughness Index (ERI), which

encompasses three variables associated with the size, geometry, and spatial arrangement of the topographical features.(Schumacher JF *et al.*, 2007; Long CJ *et al.*, 2010)

$$\mathrm{ERI} = \frac{rdf}{f_D} \tag{1.1}$$

$$spores/mm^2 = -C_1 ERI + C_2 \tag{1.2}$$

Here, r is Wenzel's roughness factor, which refers to the ratio of the actual surface area to the projected planar surface. f_D is the depressed surface fraction, the ratio of the recessed surface area and the projected planar surface area. df is the degrees of freedom for movement across the surface, which is 1 or 2. C_1 and C_2 are constants related to the spore species. So, the microstructured surface with larger ERI index can display better resistance on marine biofouling.

Most biomimic anti-fouling surfaces are based on the microtextured surfaces which can reduce macrofouling (e.g. larvae, propagule, spores, barnacle etc), but they cannot effectively reduce the establishment of microbiofouling (bacteria and microalgae etc.). (Chambers LD *et al.*, 2006; Scardino AJ *et al.*, 2009) As the size of bacteria is about 0.5 μm, nano- or submicro-textured surfaces should be developed to effectively reduce initial bacterial adhesion. It was found that a pilot whale's skin has a specialized nanostructure that stops the buildup of micro-organisms. The whale's skin is made up of tiny pores 0.1 μm across surrounded by raised "nanoridges" (Figure 1.1-(D)) (Baum C *et al.*, 2002) So far a lot of experimental research work on the effect of surface nano-structures on bacterial adhesion has been performed. Anselme *et al.* gave a

detailed review on the influence of surface nano-structures on bacterial adhesion. However, the feature size, shape, the distance between nano-features and their organization have not been considered quantitatively.(Anselme K *et al.*, 2010) Moreover, the mechanisms regulating the bacterial response to nano-topography have not yet been addressed in the literatures. So in this research, we evaluated the anti-bacterial adhesion performance of different micro-nanostructure on PDMS surface, the effect of structure feature size on bacterial adhesion and its mechanism are the research focuses, which are very important in applying surface topography to improve polymeric biomaterials on anti-bacterial ability.

1.3.3. Improvement of urinary encrustation resistance

Most of the current strategies for the control of catheter encrustation are similar to the anti-bacterial strategies, which mainly involve to antimicrobial agent incorporation and prevention of bacterial adhesion.(Stickler DJ *et al.*, 2002, 2010) For antimicrobial agent incorporation, many applications, like catheters impregnated with antibacterial agents such as silver or nitrofurazole, have been produced. But there are still debates on whether this strategy can prevent infection and subsequent encrustation in long-term patients.(Wang R *et al.*, 2014 ; Schierholz JM *et al.*,2002) So prevention of bacterial adhesion is the more promising strategy and was adopted in my research. In fact, encrustation process is rather complex, except the microbial factors, it can also depend on contact time, the urine solute content, material chemical composition and

material surface physical properties.(Shaw GL *et al,*. 2005) There are also different attempts to improve the encrustation resistance of biomaterials. Heparin coating is believed can help ureteral stents effectively decrease the organic and inorganic deposits on it.(Riedl CR *et al.*, 2002) The surface property of polymer was also reported can affect the resistance of encrustation by David S Jones *et.al*. (Jones DS *et al.*, 2002) For material topography, L. C. Lai's research found that nanostructured titanium coating can offer superior encrustation resistance property than conventional titanium.(Lai L-C *et al.*, 2008) So, we studied the effects of material surface structure on urinary encrustation situation. Three-week in vitro urinary encrustation simulation tests were performed to evaluate the urinary encrustation situations.

1.3.4. Improvement of corrosion resistance

The most common methods to prevent corrosion in industry field include electrochemical metal protection, corrosion inhibitor protection and surface coating, but the former two methods are not suitable for medical devices and implants. There has been a constant attempt by engineers and scientists to reduce the failures of medical implants and biomaterials due to corrosion. At the product level, the appropriate selection of materials is the base of a good corrosion resistance. Furthermore, rational design is also very important, fewer parts and connections are conducive to reducing the crevice corrosion; the implants and related instruments are advised to be manufactured by the same material, and the implants made of two metals should be maintained no

contact to avoid the occurrence of galvanic corrosion. At material level, processing technique and surface modification are the main methods. Processing technique, like annealing, can increase the ductility and toughness of metallic material, thereby decrease the occurrence of stress and fatigue corrosion; decreasing the impurities (carbon, sulfur, phosphorus and so on) introduced during process can effectively impede the intergranular corrosion. The common surface modification method included chemical treatment, plasma ion implantation, plasma source ion implantation (PSII)), laser melting (LSM), laser alloying (LSA), laser nitration, ion implantation, and physical vapor deposition (PVD) and also surface texturing. The aims of these modifications include preparing surface coating, doping anti-corrosion elements or substances, improving surface passivation layer and improving surface topography. Among them surface coating is most reliable and effective. Zirconia films on 316L stainless-steel was prepared and showed outstanding corrosion resistance in simulated body fluid environment. (Sandhyarani M *et al.*, 2013; Balamurugan A *et al.*, 2003) In Fathi MH's reports, hydroxyapatite (HA) film, titanium (Ti) film, and a double-layer HA/Ti film on AISI 316L stainless steel were prepared and evaluated, these coatings were demonstrated can effectively raise the corrosion resistance and also inhibit nickel ion precipitation of stainless steel.(Fathi MH *et al.*, 2003) Aluminum oxide (Al_2O_3) coating prepared by sputter-deposited techniques was also believed can improve both the blood compatibility and corrosion resistance.(Tiwari SK *et al.*, 2011; Yuhta T *et al.*, 1994; Meinert K *et al.*,1996) From the perspective of material properties, DLC coatings should be able to help stainless steel against corrosion attack, so, in our research, we

also studied the effects of DLC type coatings on corrosion resistance.

1.4. Aim of study

1.4.1 Development and evaluation of doped diamond-like carbon (DLC) coatings

1) To prepare Si- and F-doped DLC coatings on 316L stainless steel surface.
2) To characterize the surface properties of the doped DLC coatings
3) To evaluate the anti-bacterial properties of the doped DLC coatings with selected bacteria that frequently cause medical related infections under both static and flow conditions.
4) To evaluate bacterial adhesion process with time using a Quartz Crystal Microbalance with Dissipation (QCM-D) system.
5) To explain anti-bacterial mechanisms of the coatings with the extended DLVO theory.
6) To evaluate anti-corrosion performance of the doped DLC coatings by an electrochemical corrosion system.

1.4.2 Development and evaluation of micro-nanostructured surfaces

1) To investigate the effect of surface micro/nano-structures on bacterial adhesion with the extended DLVO theory and to obtain optimum surface micro/nano-structures to prevent bacterial adhesion

2) To produce a series of micro/nano-structured patterns on PDMS samples by a soft lithography method.
3) To characterise the micro/nano-structured patterns with SEM
4) To evaluate anti-bacterial performance of the micro/nano-structured patterns and to compare with the theoretical prediction.
5) To evaluate anti-encrustation performance of the the micro/nano-structured patterns in sterile artificial urine and to investigate the effect of surface nano-structures on urinary encrustation formation.

2. Preparation of Doped DLC Coatings and Micro-nanostructured Surfaces

2.1. Preparation of DLC and Si-and F-doped DLC coatings

In this study, standard DLC coatings, Si-doped DLC coatings and F-doped DLC coatings were prepared on stainless steel plates by a radio frequency plasma-enhanced chemical vapor deposition (rf-PECVD) technology at CSIRO Materials Science and Engineering, Australia. The deposition system consisted of a plasma reactor equipped with rotary and turbo molecular pumps with controlled gas supply and pumping. A base pressure of $1x10^{-3}$Pa was attained in the chamber prior to deposition. Acetylene (C_2H_2), tetramethylsilane (TMS), CF_4 and argon (Ar), were used as process gases. The gases were introduced into the system through a gas distributor using mass flow controllers. The total pressure could be set independently of the gas flow by adjusting a throttle valve. Prior to deposition, the substrates were sputter cleaned in-situ for 5 min in argon plasma operated at 3.3 Pa with the argon flow rate set at 10 sccm (standard cubic centimeters per minute) at 200 W power. In order to improve the adhesion, a thin layer of hydrogenated amorphous silicon carbide (a-SiC:H) was first deposited onto the substrate using tetramethylsilane (TMS) as precursor. The interlayer deposition was performed at 3.3 Pa with the TMS flow rate set at 17 sccm at 200 W power for 2 min (approximately 50 nm thickness). The Si-doped DLC films were deposited using a mixture of C_2H_2 and TMS as precursors. The flow rate of C_2H_2 was kept constant at

100 sccm and the flow rate of TMS was varied between 0 and 20 sccm in order to obtain different silicon contents in the films. The deposition pressure and rf power were set at 6.6 Pa and 200 W respectively. Three Si doped DLC coatings with Si contents of 3.7, 9.7 and 19.2 % were produced. The films compositions were given by atomic percentages. The F-DLC coatings were deposited using a mixture of C_2H_2 and CF_4 as precursors. The flow rate of C_2H_2 was kept constant at 60 sccm and the flow rate of CF_4 was varied between 0 and 90 sccm in order to obtain different fluorine contents in the films. The deposition pressure was set at 6.6 Pa at an rf power of 200 W. Three F-doped DLC coatings with F contents of 6.5%, 20.7% and 39.2% were prepared. Standard DLC films were prepared and used as control sample. The surface composition of the deposited films was assessed by X-ray photoelectron spectroscopy (XPS) using a Specs 150 SAGE instrument operated with an Mg Kα X-ray source (Mg anode operated at 10 keV and 10 mA).

2.2. Preparation of PDMS samples with surface micro-nanostructure

2.2.1 Soft lithography techniques

With the strategy of "smaller bring new capability" become more and more promising, many practical micro-nanometer structure preparation techniques have been developed for microelectronics field or small system field (Qin D *et al.*, 2010). Among them,

photolithography is one of the most mature and widely used methods. Photolithography is a general term of many related techniques. The basic process includes 1) creating the geometrical patterns on a light-sensitive chemical "photoresist" layer on the substrate by exposure and development; 2) transferring the pattern to substrate by etching or ion implantation. As the different radiation sources, photolithography technology includes ultraviolet light (UV) photolithography, X-ray photolithography, e-beam writing and ion-beam wring and so on. Typically, the resolutions of photolithography methods are limited by the wavelength of the light used, and cannot surmount the so-called 100 nm barrier. Although the more advanced lithographic techniques, like deep ultraviolet light (DUV) photolithography, focused ion beam (FIB) writing, and proximal-probe lithography, can fabricate the pattern with the feature down to 50nm or even 30nm, but the high extra cost, high difficulty and risk of defects limit their applications.

Photolithography is the dominant technology in many fields, like microelectronics, but this technique also has some disadvantages for biological applications. Primarily, the substrates are commonly rigid material, like silicon wafer and metal layer, in order to work on other materials, the chromophores or add photosensitizers have to be attached, but neither type of the procedure is convenient. And photolithography is not an inexpensive technology, which is suitable for mass production but not laboratory tests (Rai-Choudhury P, 1997). Furthermore, photolithography also has high demand for facility and clean-room environment, but low tolerance for organic system and

chemicals. So, an alternative non-photolithographic set of microfabrication methods, soft lithography, has been developed.

Soft lithography was initially raised by Whitesides research group of Harvard University in 1990s (George MW *et al.*, 2009) and become more mature with continuous improvement. So far, soft lithography has bloom into a group of techniques, including microcontact printing(μCP) (Kane RS *et al.*, 1999), micromolding in capillaries(MIMIC) (Odom TW *et al.*, 2002), replica molding(REM) (Unger MA *et al.*, 2000), microtransfer molding(μTM)(Bailey RC *et al.*, 2000), solvent-assisted micromolding(SAMIM) (Truong TT *et al.*, 2007) and so on. The common feature of this series of techniques is using stamp or master to duplicate or transfer surface pattern structure. Whole process of soft lithography is made up of four main steps as shown in Figure 2.1, which includes designing of pattern, fabrication of master (motherboard), fabrication of stamp and subsequent operations(different for μCP, MIMIC, REM, μTM and SAMIM).

Compared with traditional photolithography and other micro-manufacture technology, soft lithography has its special advantages. Soft lithography can be applied on a wide range of materials, the most typical material is PDMS, and can also work on PU, epoxy, PMMA and even metal surface by adopting different operations. Soft lithography is low in capital cost and easy to learn, the same master can be repeatedly used to fabricate at least 20 samples. Furthermore, soft lithography can circumvent the

diffraction limitations and reach the higher limits to a resolution of about 30-60nm, and also provide access to quasi-three-dimensional structures and generate patterns or structures on nonplanar surfaces, which are very hard or impossible for projection photolithography. These advantages make soft lithography a low cost, reliable and large area suitable method for materials scientists, biologists and chemists to prepare 2D even 3D micro-nanometer surface structure.

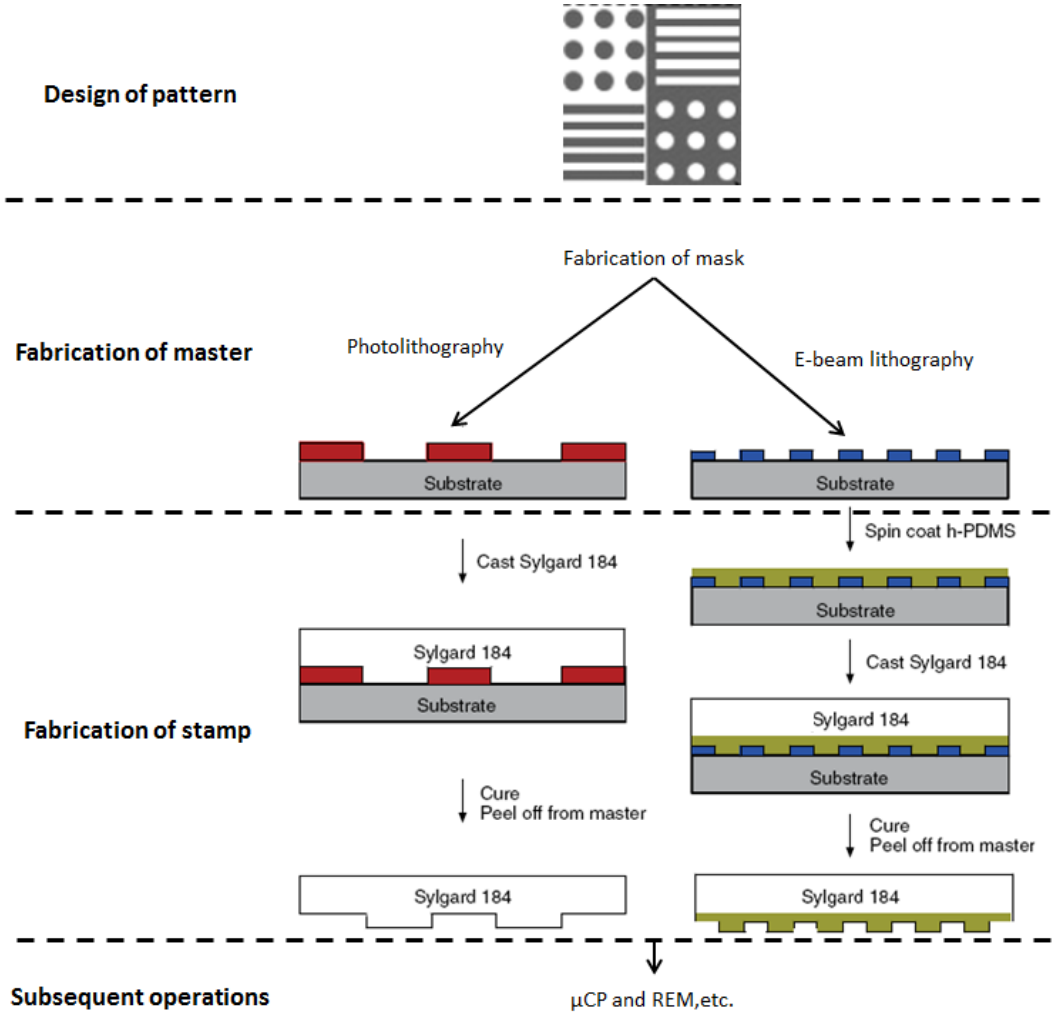

Figure 2.1. Schematic illustration of the process of soft lithography. The left panel is the fabrication of normal PDMS stamps, the right panel is about the h-/PDMS stamps, which having a thin layer of hard PDMS for small size features (<300nm).

2.2.2 Design of pattern

Generally speaking, pattern sizes (L), space width (D) and relief height (H) are important to describe most 3D pattern structures. L and D are decided by the pattern form, while H can affect the quality of the final protests, so should be considered and determined ahead by optimizing the aspect ratios, H/L and H/D, to prevent pairing and sagging of the elastomeric products (showed is Figure 2.2).

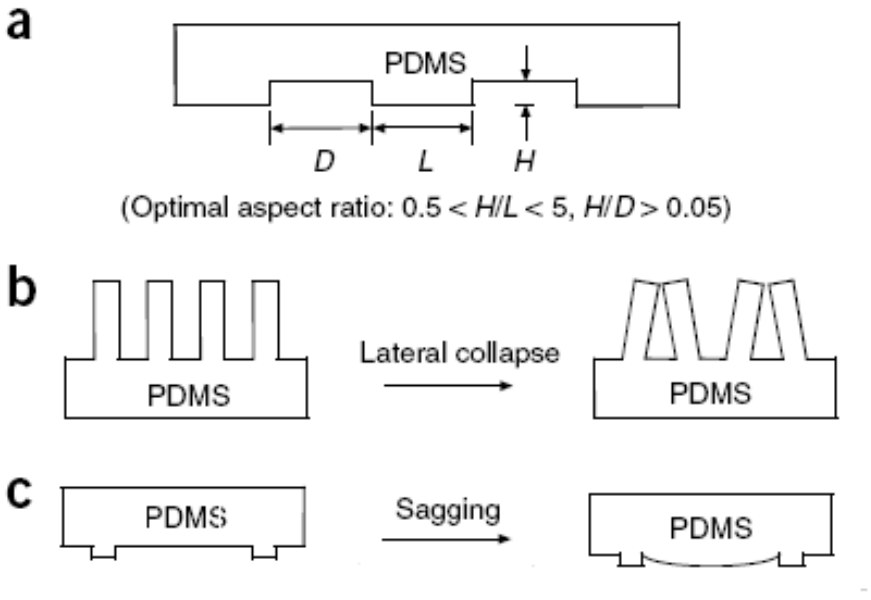

Figure 2.2 A: Schematic illustrations of surface pattern; B: lateral collapse of relief structures (or commonly known as 'pairing') with too large aspect ratios; C: sagging of recessed structures with too small aspect ratios.

CAD software was used to design the pattern. Figure 2.3 is about two pattern designs used in our research. Pattern A is an evenly spaced grid of squares， the side lengths of

square convex structures are L and their separation distances are also L; Pattern B is an offset grid arrangement, the side lengths of both square convex structure and square hollow are L. And the relief height of both pattern A and B are represented by H. And base on the analysis results in section 6.2, we tried to make four samples having the different pattern features of 1000nm, 500nm, 400nm and 350nm respectively. Table 2.1 illustrate the pattern design parameters and their SEM tests results. We did not forcibly try a pattern feature smaller than 300nm, because it is still expensive and unreliable when preparing structure under our current technical conditions.

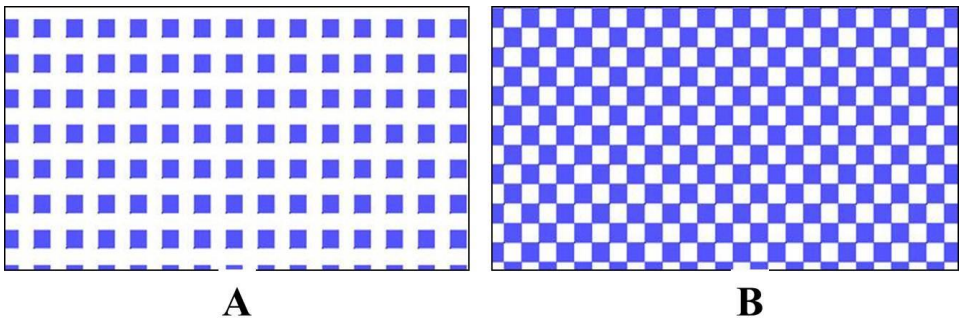

Figure 2.3 Design of the pattern: (A) Patern A and (B) Pattern B

	Sample	1000nm A	1000nm B	500nm A	500nm B	400nm A	400nmn B	350nm A	350nm B
Design data	L(nm)	1000	1000	500	500	400	400	350	350
	H(nm)	1000	1000	500	500	500	500	500	500
	H/L	1	1	1	1	0.8	0.8	0.7	0.7
SEM tests for L on samples (nm)		～995	～990	～680		～411	～395	～326	～329

Table 2.1 The pattern design parameters and SEM tests results.

2.2.3 Fabrication of master

The silicon masters were supplied by Bandwidth Foundry International Pty Ltd (BFI), a member of the Australian National Fabrication Facilities - Optofab Node (ANFF). BFI employed a Heidelberg DWL200 laser writer using a 4 mm write head to expose low reflective Chrome on soda lime reticules. The reticules were used in an ASML PAS5500/100 stepper with a 5:1 reduction ratio producing 1000 nm, 500 nm, 400 nm and 350 nm features on wafers. A 100 mm 1.0.0 silicon wafer coated with 1.2 μm thick SPR 660 positive photoresist, soft baked, was used as the substrate to form a mould for the PDMS castings. After exposure, the wafers were developed, hard baked and coated with a mold release, then the wafers can be used as silicon master (showed in Figure 2.4) in laboratory to prepare PDMS sample with the designed patterns.

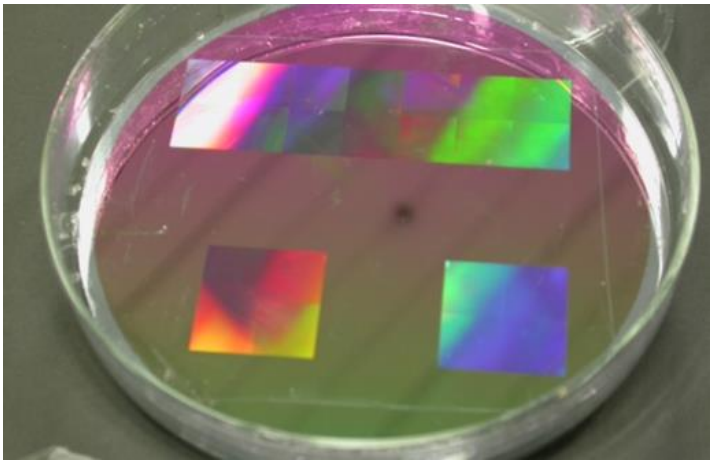

Figure 2.4 The silicon master for soft lithography.

2.2.4 Preparation of PDMS sample

Polydimethylsiloxane (PDMS) is a kind of polymer bio-materials. Because of the main molecular chain is spiral, the symmetry of this molecular structure leads the polarity of the silicon-oxygen bond can be offset by each other. Therefore, the solid-state PDMS is a hydrophobic material having low surface energy, non- toxicity, heat/cold resistance, chemical inert and biocompatible abilities. All these advantages make PDMS can be wildly used as material of contact lens and blood contact material on the artificial implant and interventional devices, like artificial heart, artificial bladder and artificial blood vessels. Simultaneously, PDMS is the most commonly used elastic material in soft lithography for the following features: (1) Outstanding thermal stability, very little deformation before and after curing. (2) Good flexibility, liquid state PDMS make a good contact with the complex patterned surface of silicon master. (3) Low adhesiveness. Cured PDMS samples are easy to be separated the from silicon master, which contributes to reduce defects.

The PDMS samples can be prepared by many methods, the thermal curing method was adopted in our research. Prior to use, the silicon masters were ultrasonic cleaned for 5 min in ethanol, rinsed thoroughly with deionized water and completely dried. PDMS (Sylgard 184 PDMS, Dow Corning Corporation, Ellsworth Adhesives) was mixed with its curing agent at the weight ratio of 10:1, after extensive mixing for about 20min, the mixture was ultrasonic degased and vacuum degased for 30 min to ensure fewer bubbles in liquid state PDMS. The PDMS were carefully poured onto the silicon masters, which had been previously fixed to the bottom of a small petri dish. For a

master of 100 mm in diameter, 15g Sylgard 184 resin and 1.5g of curing agent can be produced into PDMS film of roughly 3 mm thickness. The petri dish containing both silicon master and PDMS was placed in an incubator and the curving temperate was set at about 50℃ for a least 12h to ensure accomplishment of thermal curving. After that, PDMS film should be carefully peeled from the master and the nanometer structure was modified on the film surface. In general, a lower curving temperature is acceptable but will lead to a longer curing time; While higher temperature can save time but with the larger energy accumulated during the curing period between the PDMS film and silicon master. In this case it tends to be more difficult to separate them and increase the shrinkage of the casting. As a result it will harm the structure on both PDMS film and silicon master. Therefore, a curing temperature higher than 80℃ should be avoided when producing nanometer structures.

3. Characterization of Coatings and Micro-nanostructured Surfaces

3.1. Scanning electron microscope

Scanning electron microscope (SEM) can use electron beam scan the sample surface thereby get the information about the sample surface structure. SEM test can produce the 3-D high-resolution images of sample surface, so is widely used on the characterization of material surface. In this study, the Philips XL 30 Scanning Electron Microscope (SEM) in the Life Science College, University of Dundee was used for observing the topography of samples. The samples were cut into small pieces and then mounted on Al stubs using carbon adhesive tabs and coated with (15nm) Au/Pd using a Cressington 208HR sputter coater. The samples were examined in an atmosphere of up to 10-2 Pa of nitrogen gas with the resolution of 3.5 nm at 15kV.

3.2. Energy dispersive X-ray spectroscopy

Energy dispersive X-ray spectroscopy (EDXS) is an elemental analysis technology for sample surface. EDXS relies on the interaction of X-ray excitation and chemical components of sample surface. The theoretical basis of EDXS is that every element has its unique set of peaks on its X-ray spectrum. EDXS can provide the chemical components of material surface layer, and the content of every element is a relative

magnitude. EDXS spectra were acquired using a Phoenix EDAX X-ray microanalysis system embedded within a Philips XL 30 ESEM operating an accelerating voltage of 20 or 25 KV.

3.3. Contact angle method

The hydrophobicity is important in the research of material surface property, because it has strong relationship with the anti-adhesion ability or anti-fouling ability of materials. Contact angle is normally used to describe the material hydrophobicity. For a hydrophilic material, the droplet spreads on the solid surface, so the contact angle is small (θ_c <90°); for hydrophobic material, the contact angle is larger than 90°. More importantly, contact angle data are used for calculating material surface energy. The sessile drop method and captive bubble method were adopted to measure the contact angle in this research.

3.3.1 Sessile drop method

Sessile drop method is the most common method for measuring static contact angle. Dataphysics OCA-20 contact angle analyzer was used, and deionized water (W), Diiodomethane (DI) and ethylene glycol (EG) were taken as the test liquids. Before test, every sample was ultrasonically cleaned with alcohol and deionized water respectively for 15min, then dry the material surface completely. Test sample was

horizontally mounted on the test platform of contact angle analyzer, which can keep the sample at a proper test temperature (25℃ in our tests). Then drop a certain amount of test liquid through a syringe needle on the material surface, and take the image of droplet shape by analyzer video camera. The contact angle can be measured by the PC software. At least three repeat tests were made to reduce errors. In this study the contact angles of the three test liquids were measured for calculating surface free energy.

3.3.2 Captive bubble method

Captive bubble method is particularly suitable for hydrophilic material, on which liquids spread out and the static contact angle is small and difficult to be measured. Captive bubble method is initially applied on the measurement for soft contact lenses and hydrogels. In this research, this method was used to measure the underwater contact angle of the samples. As shown in the Figure 3.1, compared with the traditional sessile drop method, the U-shaped syringe needle and a water tank were used for the captive bubble method. Prior to contact angle measurement, the samples were ultrasonically cleaned in ethanol solution and in distilled water respectively for 15min. All measurements were made at 25℃. The Figure 3.1 is Dataphysics OCA-20 contact angle analyzer and U-shaped syringe needle for captive bubble measurement. The density less than water density, low solubility and chemical inertness (to protect the sample) are the basic rules of selecting the test substance. Three basic test substances

were selected in the captive bubble method, including air, n-octane and toluene.

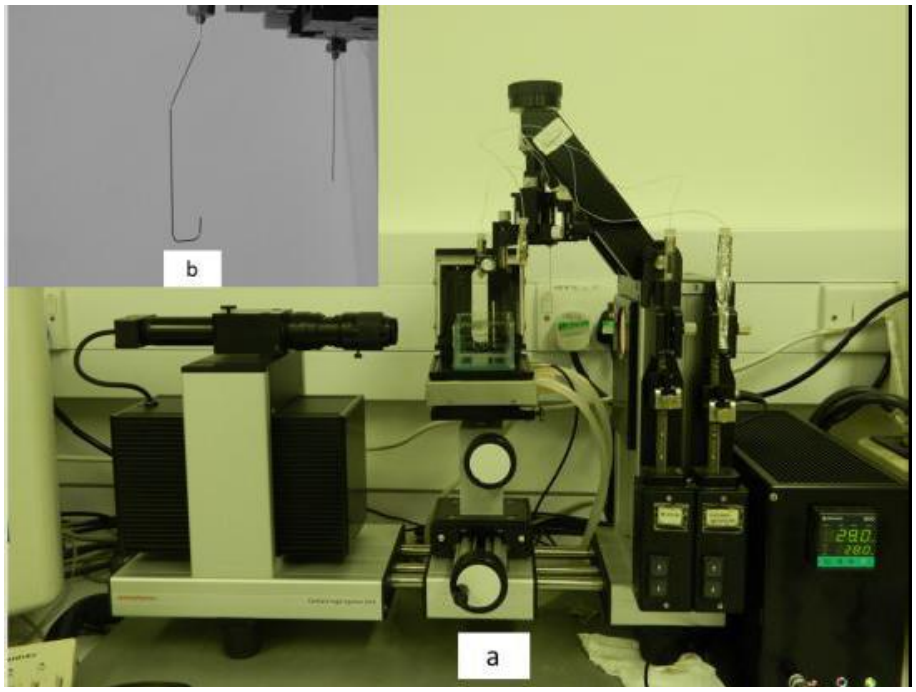

Figure 3.1 Equipment for captive bubble measurement (a) Dataphysics OCA-20 contact angle analyzer; (b) U-shaped syringe needle.

3.4. Surface energy

Surface energy quantifies the disruption of intermolecular bonds that occur when a surface is created, or be defined as the excess energy at the surface of a material compared to the bulk (Tadmor R, 2004). Surface energy can be calculated from contact angle data and the surface tension data of test liquids, which can be measured by a surface tension analyzer or obtained from published reports or text books. Surface tension analyzer and schematic diagram of measurement are shown in Figure 3.2.

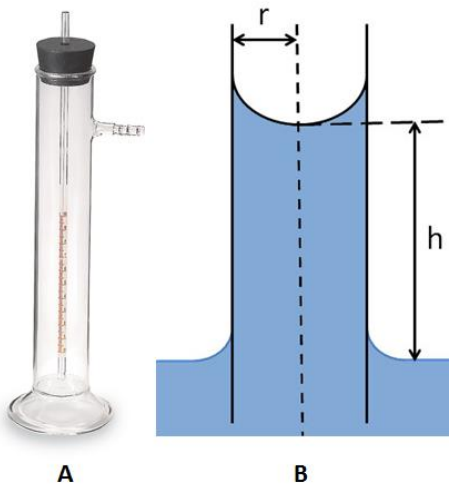

Figure 3.2 A: surface tension analyzer； B: schematic diagram of measurement.

$$\gamma = \frac{hr\rho g}{2} \tag{3.1}$$

γ is surface tension of liquid (dynes/cm), h is between menisci (cm), r is radius of capillary(cm), d is liquid density(g/cm^3), g is the gravitational acceleration (cm/s^2, ≈980cm/s^2).

3.2.1 Calculation of surface energy by sessile drop method

The mechanical equilibrium on solid-liquid-gas interface can be described by Thomas Young Equation, as shown in Figure 3.3 and equation (3.2). (Erbil HY, 2006)

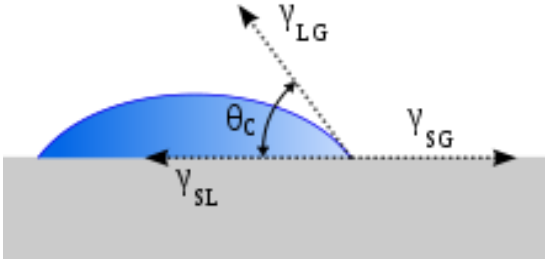

Figure 3.3 The basic principle of Thomas Young Equation.

$$\gamma_{LG}\cos\theta_c = \gamma_{SG} - \gamma_{SL} \tag{3.2}$$

θ_c is contact angle, γ_{LG} is the interfacial energy of the liquid/gas, γ_{SG} is the interfacial energy of the solid/gas, γ_{SL} is the interfacial energy of the solid/liquid interfaces.

Later in 1937, Bangham and Razouk showed that solid surface energy (γ_S) and liquid surface energy (γ_L) can be calculated from γ_{LG} and γ_{SG}.

$$\gamma_S - \gamma_{SG} \equiv \pi_{SG} \tag{3.3}$$

$$\gamma_L - \gamma_{LG} \equiv \pi_{LG} \tag{3.4}$$

π_{SG} is the equilibrium film (or spreading) pressure of gas adsorbate on the solid, and π_{LG} is equilibrium film pressure of gas adsorbate on the liquid, they can only be zero or positive value and usually be neglected in calculation.

$$\gamma_S = \gamma_{SG} \tag{3.5}$$

$$\gamma_L = \gamma_{LG} \tag{3.6}$$

$$\gamma_L \cos\theta = \gamma_S - \gamma_{SL} \tag{3.7}$$

There are many approaches to calculate the surface energy components, including Owens and Wendt Geometric Mean Approach, Wu Harmonic Mean Approach and Van oss Acid-Base Approach. In this research, the last one is adopted.

In 1986, Van Oss et al. raise that surface energy can be divided into Lifshitz-van der Waals apolar component γ^{LW} and Lewis acid-base polar component γ^{AB}.

$$\gamma^{TOT} = \gamma^{LW} + \gamma^{AB} \tag{3.8}$$

$$\gamma_{SL}{}^{LW} = (\sqrt{\gamma_S{}^{LW}} - \sqrt{\gamma_L{}^{LW}})^2 \tag{3.9}$$

$$\gamma_{SL}{}^{AB} = 2(\sqrt{\gamma_S{}^{+}} - \sqrt{\gamma_L{}^{+}})(\sqrt{\gamma_S{}^{-}} - \sqrt{\gamma_L{}^{-}}) \tag{3.10}$$

$$\gamma_{SL} = \gamma_{SL}{}^{LW} + \gamma_{SL}{}^{AB} = (\sqrt{\gamma_S{}^{LW}} - \sqrt{\gamma_L{}^{LW}})^2 + 2(\sqrt{\gamma_S{}^{+}} - \sqrt{\gamma_L{}^{+}})(\sqrt{\gamma_S{}^{-}} - \sqrt{\gamma_L{}^{-}}) \tag{3.11}$$

Combine the equations can get the final equation:

$$\gamma_L(1+\cos\theta) = 2(\sqrt{\gamma_S{}^{LW}\gamma_L{}^{LW}} + \sqrt{\gamma_S{}^{+}\gamma_L{}^{-}} + \sqrt{\gamma_S{}^{-}\gamma_L{}^{+}}) \tag{3.12}$$

In order to get the surface components of the materials, at least three test liquids with known surface tension components should be adopted, and two of which must be polar. The Table 3.1 is the values of surface tension components of the three test liquids.

Test substance	Temperature (℃)	γ^{LW} （mJ/m^2）	γ^{+} (mJ/m^2）	γ^{-} (mJ/m^2）	γ^{TOT} (mJ/m^2）
Water	25	21.8	25.5	25.5	72.8
Diiodomethane	25	50.8	0	0	50.8
Ethylene glycol	25	29.0	1.92	47.0	48.0

Table 3.1 The surface tension components of test liquids.

3.2.2 Calculation of surface energy by captive bubble method

For the calculation of surface energy for captive bubble method, the situation of the interface of air-water-sample, octane-water-sample and toluene-water-sample is described as the following equations

For air bubble:

$$\gamma_{\mathrm{wa}} \cos\theta_a = \gamma_{\mathrm{sw}} - \gamma_{\mathrm{sa}} \tag{3.13}$$

For n-octane bubble:

$$\gamma_{\mathrm{wo}} \cos\theta_o = \gamma_{\mathrm{sw}} - \gamma_{\mathrm{so}} \tag{3.14}$$

For toluene bubble:

$$\gamma_{\mathrm{wt}} \cos\theta_t = \gamma_{\mathrm{sw}} - \gamma_{\mathrm{st}} \tag{3.15}$$

Where γ_{sw} is the sample-water interfacial free energy, γ_{wa} , γ_{wo} and γ_{wt} are water-air, water-octane and water- toluene interfacial free energy,respectively. Similarly, γ_{sa} , γ_{so} and γ_{st} represent the sample- air, sample-octane and sample-toluene interfacial free energy respectively. They are illustrated in Figure 3.4.

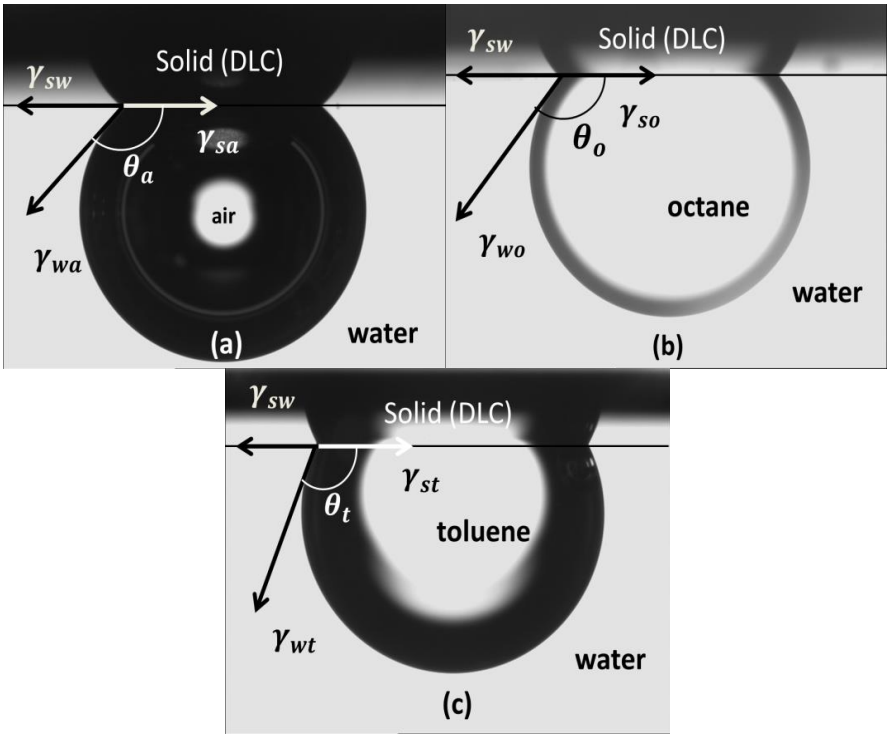

Figure 3.4 Contact angles and interfacial surface energies corresponding to the captive bubble method with the bubbles of (a) air, (b) n-octane and (c) toluene.

The interfacial free energy between material 1 and material 2 is given:

$$\gamma_{12} = \gamma_1 + \gamma_2 - 2(\sqrt{\gamma_1^{\mathrm{LW}}\gamma_2^{\mathrm{LW}}} + \sqrt{\gamma_1^{+}\gamma_2^{-}} + \sqrt{\gamma_1^{-}\gamma_2^{+}}) \tag{3.16}$$

Combine the above equations, we have:

$$\gamma_w(1-\cos\theta_a)=2(\sqrt{\gamma_s^{LW}\gamma_w^{LW}}+\sqrt{\gamma_s^{+}\gamma_w^{-}}+\sqrt{\gamma_s^{-}\gamma_w^{+}}) \tag{3.17}$$

$$\gamma_w(1-\cos\theta_o)-\gamma_o(1+\cos\theta_o)+2\cos\theta_o(\sqrt{\gamma_w^{LW}\gamma_o^{LW}}+\sqrt{\gamma_w^{+}\gamma_o^{-}}+\sqrt{\gamma_w^{-}\gamma_o^{+}})=$$
$$2(\sqrt{\gamma_s^{LW}\gamma_w^{LW}}+\sqrt{\gamma_s^{+}\gamma_w^{-}}+\sqrt{\gamma_s^{-}\gamma_w^{+}}-\sqrt{\gamma_s^{LW}\gamma_o^{LW}}-\sqrt{\gamma_s^{+}\gamma_o^{-}}-\sqrt{\gamma_s^{-}\gamma_o^{+}}) \tag{3.18}$$

$$\gamma_w(1-\cos\theta_t)-\gamma_t(1+\cos\theta_t)+2\cos\theta_t(\sqrt{\gamma_w^{LW}\gamma_t^{LW}}+\sqrt{\gamma_w^{+}\gamma_t^{-}}+\sqrt{\gamma_w^{-}\gamma_t^{+}})=$$
$$2(\sqrt{\gamma_s^{LW}\gamma_w^{LW}}+\sqrt{\gamma_s^{+}\gamma_w^{-}}+\sqrt{\gamma_s^{-}\gamma_w^{+}}-\sqrt{\gamma_s^{LW}\gamma_t^{LW}}-\sqrt{\gamma_s^{+}\gamma_t^{-}}-\sqrt{\gamma_s^{-}\gamma_t^{+}}) \tag{3.19}$$

Similarly, the surface free energy components parameters ($\gamma_S^{LW}, \gamma_S^{+}, \gamma_S^{-}$) of material can be calculated by the contact angles of at least three substances with known surface tension components ($\gamma_L^{LW}, \gamma_L^{+}, \gamma_L^{-}$). The surface energy components of test substance are given in Table 3.2

Test substance	Temperature (℃)	γ^{LW} (mJ/m^2)	γ^{+} (mJ/m^2)	γ^{-} (mJ/m^2)	γ^{TOT} (mJ/m^2)
water	25	21.8	25.5	25.5	72.8
n-octane	25	21.6	0	0	21.6
toluene	25	28.3	0	2.7	28.3

Table 3.2 Surface energy components of test substance in captive bubble method.(Van Oss CJ *et al*., 1988)

3.2.3 The surface energy and zeta potential of bacteria

The contact angles of the cells of bacteria were measured on the lawns of the bacteria deposited on membrane filters with pore diameter of 0.2μm by sessile drop method. Prior to contact angle measurement, the bacterial lawns were dried in the air to a certain state, indicated by stable water contact angles. Usually this state of drying of a

microbial lawn lasts for 30-60 minutes and indicates that only bound water is present on the surface. The zeta potentials of bacteria were referenced from existing reports (Liu, Y *et al.*, 2005). Table 3.3 is surface energy components and zeta potentials of *Klebsiella pneumonia* and *E. col*, which are necessary in further EDLVO theory.

	Temperature (℃)	γ^{LW} （mJ/m^2）	γ^+ （mJ/m^2）	γ^- （mJ/m^2）	φ （mv）
Klebsiella pneumonia.	25	35.5	1.93	37.89	-15.4
E.coli	25	27.2	4.7	7.9	-15.4

Table 3.3 Surface energy components and zeta potentials (φ) of *Klebsiella pneumonia* and *E. coli.*

4. Experiments and Methods

4.1. Bacterial adhesion assays

4.1.1. Bacterial culture

In this research, two bacterial strains were adopted to assay bacterial adhesion. *Escherichia coli* (commonly abbreviated *E. coli*, WT F1693, obtained from the Institute of Infection and Immunity, Nottingham University, UK.), is a Gram-negative, facultative anaerobic and rod-shaped bacterium. And *Klebsiella pneumonia* (ATCC 13883) was obtained from the Institute of Infection and Immunity, Nottingham University, UK.

E. coli is very common bacteria in clinical infections. *E. coli* related infections are mainly divided into intestinal infections and extraintestinal infections. Intestinal infections are mainly caused by food and can lead diarrhea. Extraintestinal infections are mainly caused by wound, surgery and organ inflammation. *E. coli* is the main causes of urinary tract infections (Campoccia D *et al.*, 2013). More than 90% urinary tract infections in non-hospitalized patients are involved by *E. coli*, other related infections include septicemia, peritonitis, pneumonia and so on. Furthermore, *E.coli* has strong relationship with the urine encrustation. Unlike the *Proteus mirabilis*, *E. coli* is usually not a producer of urease, which renders the urine more alkaline and

promotes the encrustation. But *E. coli* was found to strongly reduce urine citrate, which helps to decrease the crystallization in urine. Therefore *E. coli* can increase the rate of urease-induced encrustation in an in vitro model (Edin-Liljegren A *et al.*, 1995; Hedelin H *et al.*, 1990) and is a common bacterial strain used in urine encrustation related research (Stickler DJ *et al.*, 2002; Schierholz JM *et al.*,2002).

Klebsiella pneumonia is an opportunistic pathogen involved in outbreaks of nosocomial infections, such as bacteremia and sepsis, mainly in immunocompromised individuals. (Sahly H, 1997) It is not only the currently second most common cause of nosocomial Gram-negative bacteremia, but the most common species capable of producing extended-spectrum β-lactamases (ESBL), (Skogberg K *et al*, 2008; Yinnon AM *et al,*. 1996) so using bacteriostatic strategy is hard to reach the expected antibacterial effect. For this type of bacteria, adopting anti-adhesion strategy may be more effective and promising method.

4.1.2. Bacterial growth curve

The growth process of bacteria in bath culture can be described as four phases.

(1) Lag phase: After inoculation, there is a short process for bacteria to adapt the environment. Lag phase will last 1-4hours, and very few bacteria will multiply in this phase.

(2) Logarithmic phase (or exponential phage): In the phase, bacterial population has a

stable geometric growth, and the phase can range from hours to days. Bacteria in logarithmic phase have typical bacterial morphology, staining property and biological activity, so are the best objects for research.

(3) Stationary phase: In this phase, because nutrient consumption and toxic products accumulation, bacterial multiplication rate gradually declined and death rate begin to increase. The two rates tend to be equal, so the bacterial population is generally stable in this phase, but the bacterial activity may have large change, and metabolites, such as exotoxins, endotoxins, antibiotics and spore, are also produced.

(4) Decline phase: In the phase, bacterial multiplication rate steadily decrease, while dead bacterial significantly increase. Diastrophic decay and cell autolysis may occur. Bacterial physiological metabolic activity also tends to stagnate.

Figure 4.1 is the schematic diagram for typical bacterial growth curve and growth rate.

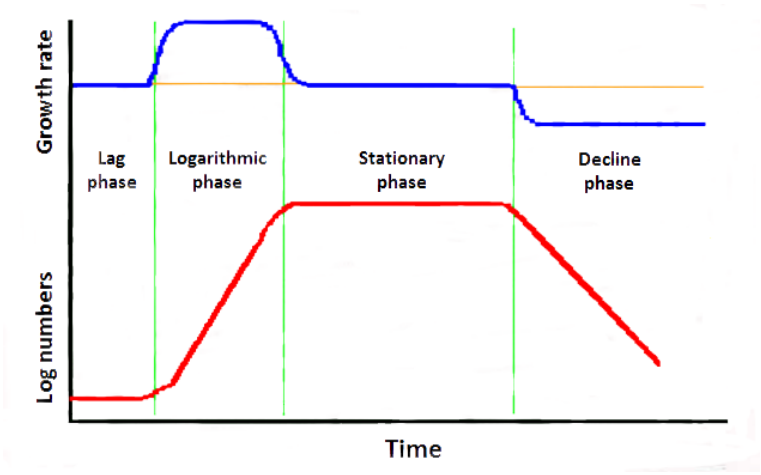

Figure 4.1 Typical bacterial growth curves.

The growth pattern of bacteria can help us control and select best bacterial suspension

for bacterial adhesion assays. Turbidimetric method was used to measure bacterial growth curve. The concentration of bacterial suspension is proportional to optical density (OD), so we can estimate bacterial suspension concentration by the OD of bacterial suspension. In this research, Biowave CO8000 Cell Density Meter was used for measuring OD of bacterial suspension. Figure 4.2 and Figure 4.3 are the growth curves and corresponding OD value in the logarithmic phase of *Klebsiella pneumonia* and *E.coli*.

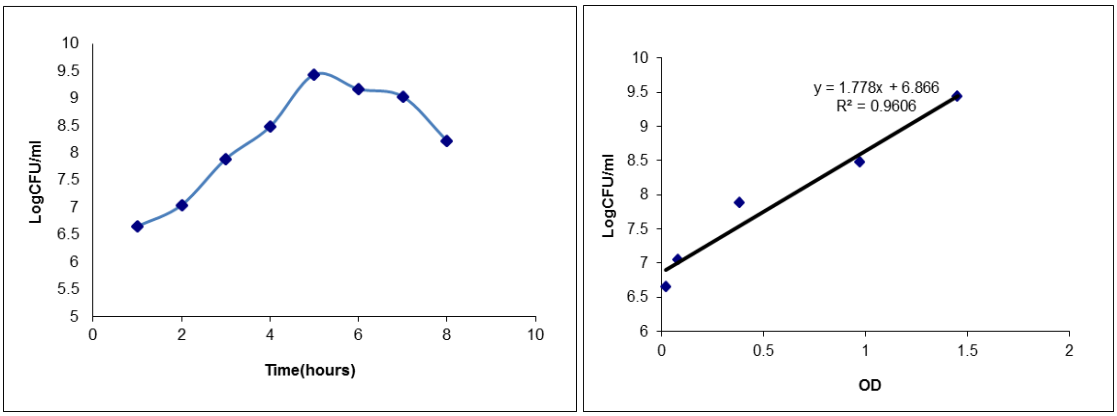

The 4.2 growth curve and corresponding OD value in logarithmic phase of *Klebsiella pneumonia*.

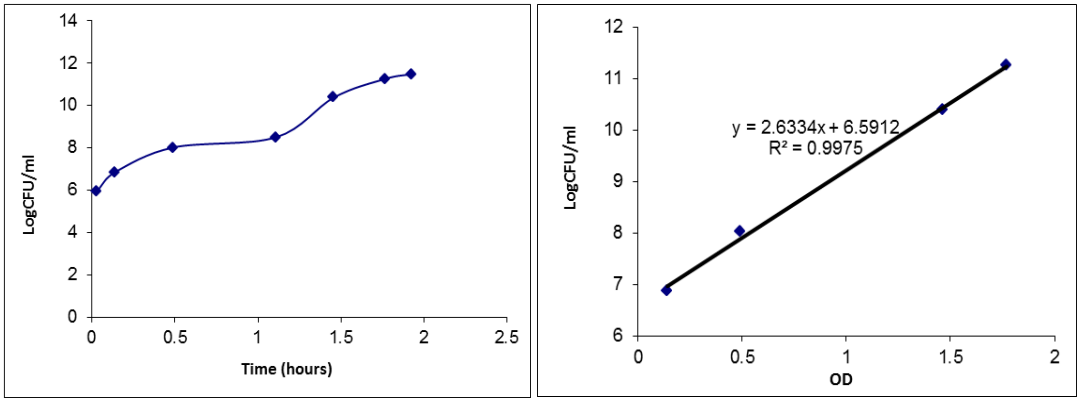

Figure 4.3 The growth curve and corresponding OD value in logarithmic phase of *E.coli.*

4.1.3. Bacterial suspension

The bacterial strain (in 500μL30% glycerol) can be kept in -20℃ refrigerator. After being thawed, bacterial strain was inoculated onto the tryptone soya agar (TSA) plates with a loop and located in the incubator to grow at 37 ℃ for about 12 hours. After that, one single colony should be transferred into 25 ml TSB and continually grow at 37 ℃ until the suspension density reached about 10^8 CFU /ml, at this generative grow phase, the bacterial morphology is relatively healthy and activity is good. Then, took appropriate amount of the suspension (10^8 CFU /ml) into the centrifuge tube, and centrifuged the suspension in centrifuge (Denley BR401 Refrigerated Centrifuge) for about 15 min to remove the supernatant TSB. Finally, diluted bacterial suspension into 10^6 CFU/ml, the bacteria in this suspension have good bacterial morphology and biological activity, which are important for following bacterial adhesion test.

4.1.4. Simulation of bacterial adhesion

Bacterial adhesion test is a comparative test under the same condition, test samples include original sample and modified samples. The different samples can be compared with each other, and the original sample is taken as the general standard of comparison. At first, the test samples should be autoclaved at 121 ℃ for 15 min, and then ultrasonically cleaned with the 75% ethanol solution and distilled water for 5 min respectively. Then, bacterial adhesion tests can be performed in static condition and fluid condition.

For bacterial adhesion test in static condition, all the samples were vertically placed in a glass tank and completely immersed into the bacterial suspension (10^6 CFU/ml). Then, tank should be placed in incubator at 37℃ to simulate in vivo environment. The adhesion period can range from 1-12hours, for a short adhesion time, comparison results are not obvious, while for a longer time, a great amount of bacteria begin to die for nutrient depletion.

For bacterial adhesion test in fluid condition，the samples were horizontally placed on the bottom of flow chamber. The flow chamber is made of PTFE, and sealed with silicon gasket and glass cover. The bacterial suspension was recalculated by peristaltic roller pump. The whole flow chamber system was placed in incubator at 37℃ during adhesion test period. The fluid flow should be relatively steady and uniform in flow chamber, in fluid mechanics, the Reynolds number is taken as a criterion for laminar flow.

$$R_e = \frac{DU\rho}{\mu} \tag{4.1}$$

R_e is the Reynolds number, ρ is fluid density (993.37kg/m^3 for water at 37 ℃)， μ is fluid viscosity (0.6947×10^{-3} Pa s for water at 37℃), U is average fluid velocity in chamber(m/s), D is equivalent hydraulic diameter

$$D = \frac{4dw}{2(d+w)} \tag{4.2}$$

$$U = \frac{Q}{dw} \tag{4.2}$$

d and w is the depth and width of chamber, Q is the fluid flow rate.

The chamber is 380mm (length) × 80mm (width) × 8mm (depth), fluid flow rate (Q) is about 0.75×10^{-6} m^3/s. The calculated Reynolds number (R_e) of the fluid in chamber is about 24.0, which is much smaller than 2000, so the fluid in chamber laminar flow.

And the shear stress is

$$\tau = \frac{6\mu Q}{d^2 w} \qquad (4.4)$$

τ is the wall shear stress, it is about 61.5 dynes/cm^2 for the fluid in the flow chamber. As the vascular wall shear stress range from 10-70 dynes/cm^2, and the mean shear stress is approximately 15 dynes/cm (Glagov S *et al*., 1988; Papaioannou TG *et al*., 2005), the bottom shear stress in flow chamber is similar to these values, so the fluid in chamber can simulate the in vivo situation to a certain extent.

4.1.5. Observation of bacterial adhesion and data statistics

After the simulation test of bacterial adhesion in static condition and fluid condition, the bacterial situation on sample can be observed and counted by plate count method and fluorescence microscope method.

4.1.5.1 Plate count method

Plant count method is the traditional method for determining bacterial number. The samples are taken out from tank or flow chamber after adhesion period, rinse the sample surface with distilled water (1-2ml, 37℃) and absorb the remaining liquid by filter paper, this can remove the remaining bacterial suspension on samples. Figure 4.4 shows the schematic diagram of the plate count method. Each sample was placed in a centrifuge tube or test-tube with 10 ml sterile PBS, ultrasonic cleaning for 15min to remove the adhered bacteria from sample surface to the PBS. Through triple dilution, the clear solution for every sample was dilated to the corresponding dilution series of 10^{0}, 10^{-1}, 10^{-2} and 10^{-3} dilutions. 0.1ml of each dilution was transferred to a TSA plate, spread inoculum over the surface evenly to separate the bacteria. After 24 hours incubation, the colonies can be counted under SC6 Digital Colony Counter. For every sample's dilution series, at least one countable plate with 30-300 colonies should be chose as the final result. The plate with fewer than 30 colonies is not statistically representative, while the plates with more than 300 colonies are not easy to count and may cause large errors. The count result divides dilute concentration and sample surface area can get the final adhesion density (CUF/cm^2) on every sample. Plate count method is mature and reliable, but will take relative long time, and only can count the alive bacteria.

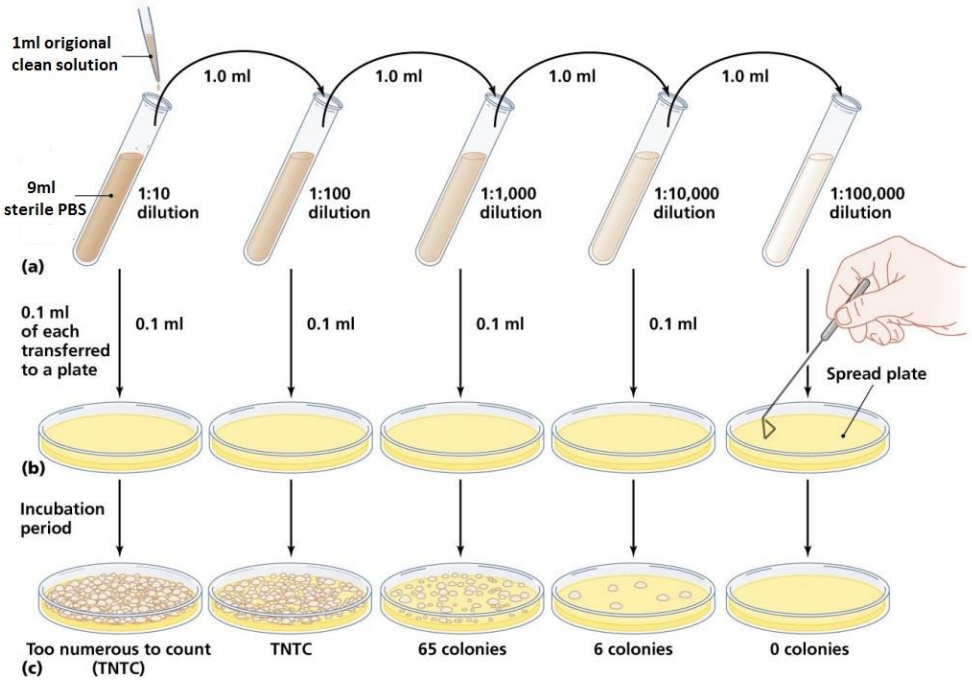

Figure 4.4 The schematic diagram for plate count method.

4.1.5.2 Fluorescence microscope method.

After the bacterial adhesion period, every sample was taken from suspension and rinsed by 5 ml sterile distilled water, then sucked off the big remaining droplets on the sample surface and dried the sample for about 15 min at 37℃. Next, the samples were stained with L13152 LIVE/DEAD® BacLight Bacterial Kits in dark for 15min, and then were observed under a fluorescence microscope. The Olympus X41 fluorescence microscope was used for bacteria count in this study. The microscope has different magnifications, but 400X and 1000X were mostly used in the tests. More than 8 microscope fields were selected randomly for each sample. Image Pro Plus was used to count and calculate the average adhered bacteria density on the sample surface.

Fluorescence microscope method is fast and reliable method, furthermore both alive and dead bacteria can be counted, so the evaluation is more comprehensive. In this research, most tests were performed by this fluorescence microscope method.

4.2. QCM-D method

As a very sensitive sensor, quartz resonators can response to a very tiny mass change in 10^{-6}-10^{-10} g, so the mass changes on the surface of the quartz resonators can be measured. The instrument based on this principle is called a quartz crystal microbalance (QCM), which is a new technology for the measurements of proteins, polymers, surfactants and cells in liquid.

4.2.1. QCM-D system and its principle

Figure 4.5 is the Q-sense D300 system, it includes four main parts, namely, measurement chamber, sensor crystal, electronic unit and PC software. The measurement chamber provides a controlled environment for the sensor crystal during measurements. It is connected with the electronic unit, and can drive sensor crystal, acquire data and control the temperature. There are two different measurement chambers, Axial Flow Chamber (QAFC 302) and the Window Chamber (QWiC 301), are available for different tests. Sensor crystals are the sensors of the system, and their surface can be modified by different methods, like spin coating, vapour deposition and

self-assembled monolayers, for different applications. Electronics unit (QE 301) is the core of the QCM system and can help whole system improve the accuracy. QSoft 301 and QTools are the software that used for measurement operation and data analysis respectively.

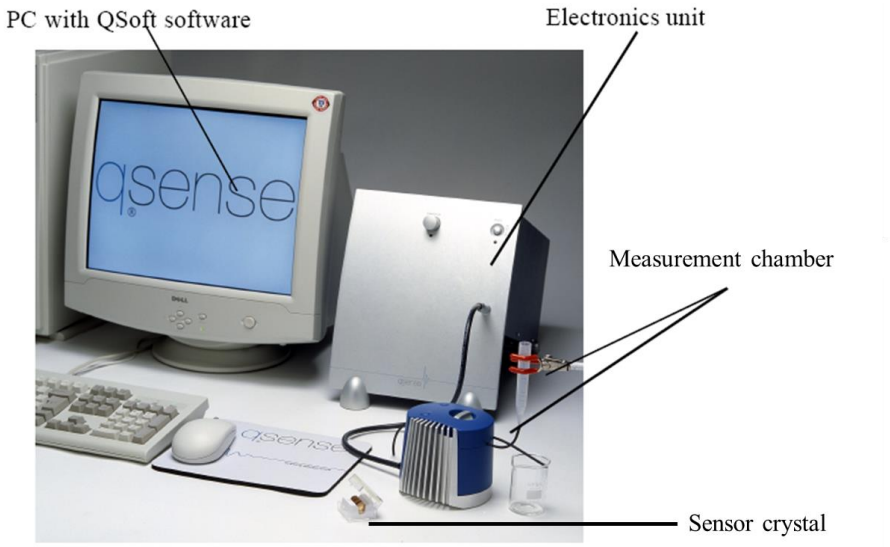

Figure 4.5 The Q-sense D300 system

The idea of quartz crystal microbalance (QCM) was raised early, and the early application was monitoring thin film deposition in vacuum systems at late 1950s. The principle of QCM system is based on the inverse piezoelectric effect of quartz, a QCM sensor consists of a thin (approximately 0.3 mm) quartz disc deposited with two electrodes, when electric field is applied to the electrodes, the quartz disc can mechanical deform. So the crystal can be made to oscillate at a frequency close to the crystal's resonant frequency f (usually in the MHz range) by applying an appropriate AC-field. The resonant frequency f of the crystal depends on the total oscillating mass and can be measured by QCM system. For theoretical rigid films on sensor face, its

mass can be calculated by Sauerbrey equation.

$$\Delta m = \frac{C\Delta f}{n} \tag{4.5}$$

$$h = \frac{\Delta m}{\rho} \tag{4.6}$$

Δm is the mass change on unit area, namely the film mass on unit area(g/cm^2); Δf is resonant frequency shift (Hz); C is a constant, for quartz crystal, it is about 17.7ng/Hz cm^2; And n = 1,3,5,7 is the overtone number. h is the film thickness and ρ is the effective density of the adhering layer.

In most situations the adsorbed film is not rigid but soft (viscoelastic), this mechanical property is reflected in the damping changes or energy dissipation (D) of oscillating crystal. Dissipation is determined from the time it takes for the oscillation to stop when the power is disconnected.

$$D = \frac{E_{lost}}{2\pi E_{stored}} \tag{4.7}$$

E_{lost} is the energy lost (dissipated) during one oscillation cycle and E_{stored} is the total energy stored in the oscillator. The dissipation can be automatically recorded by QCM-D system, can help software compute film viscosity and also improve measurement accuracy.

4.2.2. Measurement of bacterial adhesion by QCM-D system

Taking existing reports of QCM-D system application as references (Guntupalli R *et*

al., 2013; Saeki D *et al.*, 2014), the bacterial adhesion process on QCM-D system is shown as follow:

(1) Sensor crystals modification. Au and stainless steel are the most common sensor surface, and they can be suitable for most surface modifications. In our research, the surfaces of sensor crystals include gold, stainless steel, DLC coatings and Ni-P coatings. It should be noted that, during the surface modification process, the electrodes on sensor must be protected to ensure they can work properly.

(2) Sensor crystals cleaning and mounting. The most appropriate cleaning method depends on the coating surface and the properties of the sensor crystal itself. Rinse the crystal with deionized water and another appropriate liquid (alcohol), then chase liquid off the crystal with a flow of inert gas (nitrogen gas). After cleaning, the sensor crystal should be correctly mounted in the measurement chamber. The D-factors in air and water can be the good tools to check for proper cleaning and mounting of the crystal sensor. As shown in Table 4.1, a clean crystal sensor should have D-factor values in the indicated range.

Medium	D-factor at 5 MHz	D-factor at 15 MHz
Air	$25 \cdot 10^{-6}$ ($\pm 8 \cdot 10^{-6}$)	$10 \cdot 10^{-6}$ ($\pm 4 \cdot 10^{-6}$)
Water(25℃)	$315 \cdot 10^{-6}$ (±10%)	$180 \cdot 10^{-6}$ (±10%)

Table 4.1 Proper D-factor values for a clean and proper mounted crystal sensor in air and water.

(3) Calibration. Turn the control valve to “sensor” position, allow buffer liquid（PBS in

our tests）flow through the crystal sensor for certain time (2-5mins), record the f and D curve. When successful, f and D curve should be the stable baselines with a transient of less than 6Hz and 0.5 $\cdot 10^{-6}$ for 15MHz data (a transient of less than 2Hz and 0.3 $\cdot 10^{-6}$ for 5MHz data).

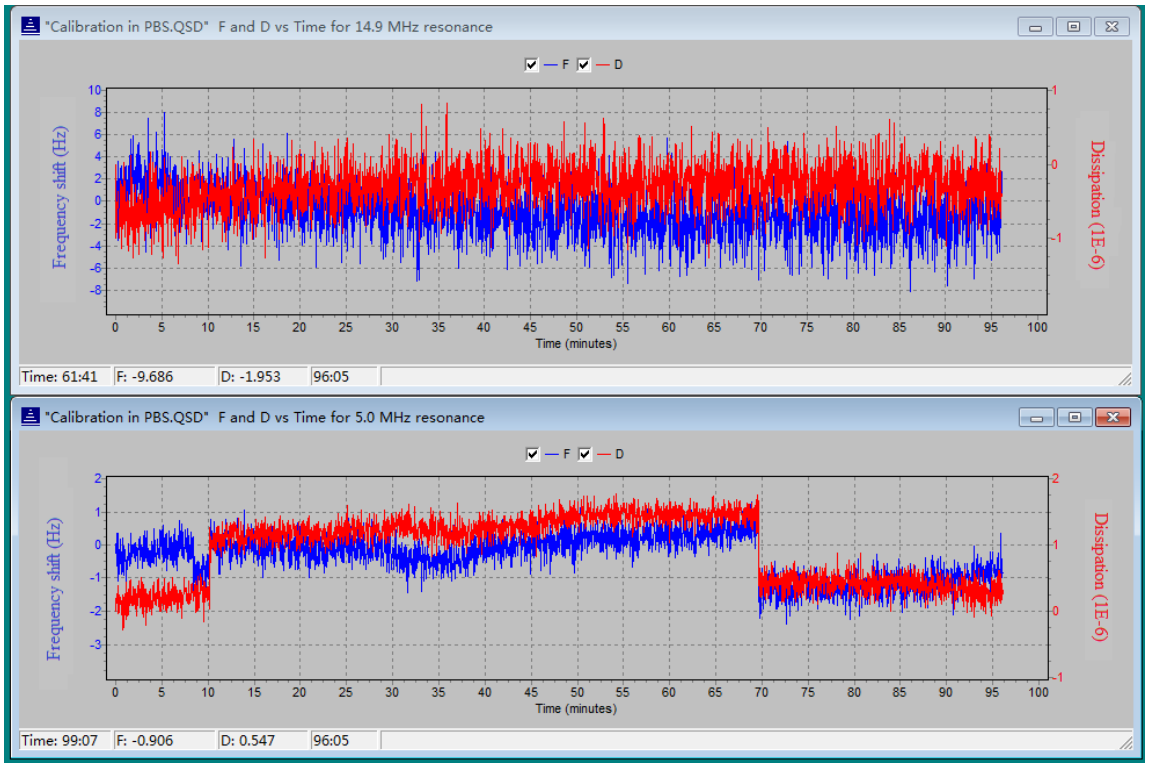

Figure 4.6 Typical stable baselines of DLC coated sensor in PBS buffer at 15.0MHz (the upper part) and 5.0MHz (the lower part).

Figure 4.6 is the typical stable baselines of DLC coated sensor in PBS buffer at 5.0MHz and 15.0MHz. The baseline is the original status of sensor in sterile PBS buffer, which is the “zero graduation line”of the microbalance system. Furthermore, the stable baselines indicates that there are no air bubble or impurities get into the sensor cell, the test system is stable during this test period, it is important to the real time measurement of QCM-D system.

(4)Measurement. After measuring in buffer liquid for 2-10mins and getting the stable baselines, the bacterial suspension should be pumped into the sample reservoir. It will take about 1 minute for bacterial suspension flow into sensor cell and contact with sample surface, and then the f change can be recognized on the PC screen. Figure 4.7 is the typical F and D curve measured by QCM-D system. (15MHz data for 10^6 CFU/ml *E.coil* suspension on stainless steel disk)

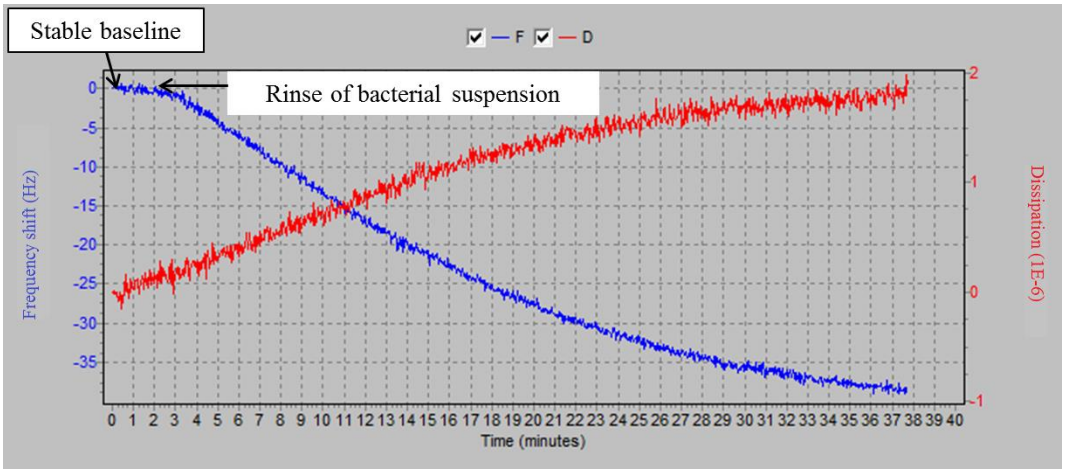

Figure 4.7 Typical F and D curve measured by QCM-D system. (15MHz data for 10^6 CFU/ml *E.coli* suspension on stainless steel disk)

(5) After Measurement. Clean the sensor crystal and chamber. Analysis the measurement results by Q-tools software.

4.3. Corrosion resistance test

The aims of anti-corrosion test include the study of corrosion mechanism, choice of biomaterials, durability assessment and reliability verification. Currently, the methods to evaluate the corrosion resistance of biomaterials can be divided into two main kinds,

namely, in vitro tests and animal in vivo tests. Animal in vivo tests are implanting implants into animal tissues, after the test period, the corrosion situation is evaluated by analyzing the implant surface situation and ion contents in animal tissues. This type of test can reflect the effect of the complex corrosion process in vivo environments to the maximum extent, the test results can provide integrated information including corrosion resistance, tissue responses and so on, but the long test period, complex test process and high test cost limit the application of animal in vivo tests. While, in vitro tests can evaluate material anti-corrosion ability by simulating the corrosion process in vitro environment. The common in vitro tests include electrochemical corrosion test, ion release rate test (AAS or ICP-AES), salt spray test and wear/fatigue corrosion test. For most in vitro tests, the test periods are relative short, methods are convenient, tests results are intuitionistic and theoretical analyses are mature. So, in vitro tests are widely used as the primary test methods to evaluate biomaterial corrosion resistance. In this research, electrochemical corrosion test was adopted to evaluate the corrosion resistance of DLC coating, Si/F doped DLC coatings and 316L stainless steel.

4.3.1. Electrochemical corrosion test

Electrochemical corrosion test system can simulate the electrochemical process of real corrosion, and the key of the test is measuring the material state in the electrochemical corrosion process. The typical metal electrochemical corrosion in conductive solution involves two half-reactions, the oxidation reaction at anode (anodic reaction) and

reduction reaction at cathode (cathodic reaction). In anodic reaction, metal (M) at anode position is oxidized from element state to ionic state (M^{n+}) with the generation of electrons ($n*e^-$). The metal ions dissolve in solution, therefore the anode is corroded. Simultaneously, the electrons move to cathode position and reduce the substance in solution. The reactions can be represented as,

Anodic reaction:

$$M \rightarrow M^{n+} + ne^- \tag{4.8}$$

Cathodic reaction:

$$O_2 + 4H^+ + 4e^- \rightarrow 2H_2O \text{ (neutral condition)} \tag{4.9}$$

$$O_2 + 2H_2O + 4e^2 \rightarrow 4OH^- \text{ (alkaline condition)} \tag{4.10}$$

$$2H^+ + 2e^- \rightarrow H_2 \text{ (acidic condition)} \tag{4.11}$$

The main measurement parameters of corrosion test are the electrode potential and corrosion current density, the former can illustrate the reaction trend on metal-electrolyte interface, and the latter is about the reaction rate. The electrochemical workstation used in our test is three-electrode system (showed in Figure 4.8), which is made up working electrode, reference electrode and auxiliary electrode. Working electrode and auxiliary electrode is the anode and cathode in corrosion reaction respectively, the potentials of electrodes can be measured by taking the reference electrode as standard. But, due to the decrease of reactant consent near electrode surface, the potentials of electrodes always change in reaction process. In order to solve the problem, potentiostat is used to keep the potential of working electrode (relative to reference electrode potential) at the set potential. Thus, the current-potential

relation can be measured and recorded to analysis the corrosion process.

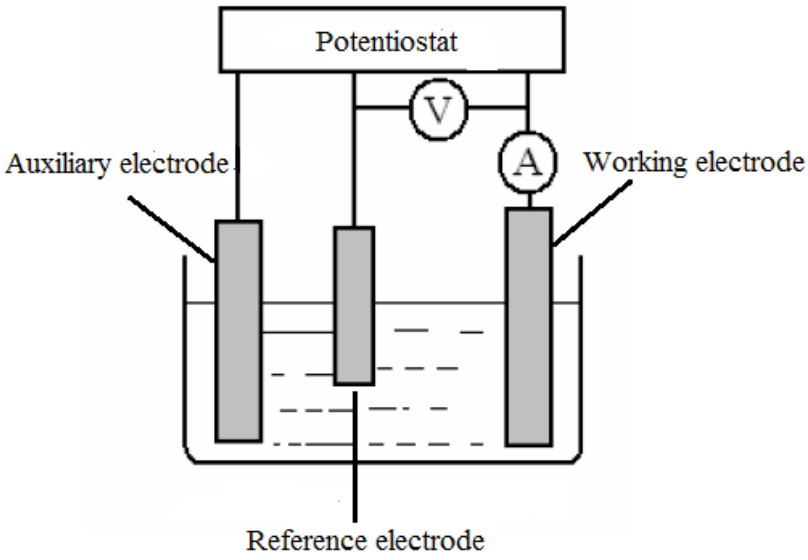

Figure 4.8 Three-electrode system for electrochemical workstation.

4.3.2. Test procedures

(1) Preparation and pretreatment of the working electrode

The aim of the preparation of working electrode is to make electrodes have the same (or similar) exposed area in solution, which is conducive to reducing systematic errors. The DLC coated sample, Si/F doped DLC coated samples and 316L stainless steel sample were cut into the same shape and size (radius 0.5cm round disk in this study). Wires were fasten on the non-test side of the sample with conductive adhesive (silver loaded epoxy adhesive), then the insulated epoxy resin was used to cover and seal the non-test side. This operation makes sure that, except for the test side, the rest part of samples cannot contact with the electrolyte in test process. Before tests, the samples

were ultrasonically cleaned in alcohol and deionized water for 15min respectively to remove organic and inorganic stains on the samples' surfaces.

(2) Set test system

A three-necked flask was used as the reaction vessel. 250 ml test electrolyte, namely PBS buffer and artificial seawater with the pH of 7.4 and 8.4 respectively was added Auxiliary electrode (Pt electrode) and working electrolyte were directly inserted into electrolyte through the bottlenecks, while reference electrode (calomel electrode) contacted with the electrolyte thought the electrolytic bridge structure. All the electrodes were connected to the potentiostat, which was controlled by PC and CorrTest software. The tests were performed at room temperature (about 25℃). The test started after 15min preheat of the system.

(3) Open circuit potential measurement and potentiodynamic polarization test

The samples were immersed in the electrolyte with no applied voltage; the open circuit potential of working electrode (E_o) was measured and recorded as a function of time. The tests last for about 2-3 hours, until the potential reached a stable value. The open circuit potential is the reflection of the stability of material surface, the higher open circuit potential indicates the presence of a stable passive film, whereas, the decline of the potential indicates the decrease of the stability of material surface or the break of the passive film.

After a stable open circuit potential of working electrode (varied in ±10 mv) was obtained, the potentiodynamic scan measurement started with an initial potential of 500mV below the open circuit potential at a scan rate of 0.5mV/S. In the anodic polarization phase, when the potential exceed a value, which is referred as the breakdown potential (E_b), the passive film is broke up, so the current density shows a dramatically increase. When the current density increases to a certain value ($0.5mA/cm^2$ for 316L stainless steel sample and $0.05mA/cm^2$ for DLC type samples), reverse the potential scan direction to check whether the materials have protection potential (E_p).

(4) Analysis measurement curves by CorrView software

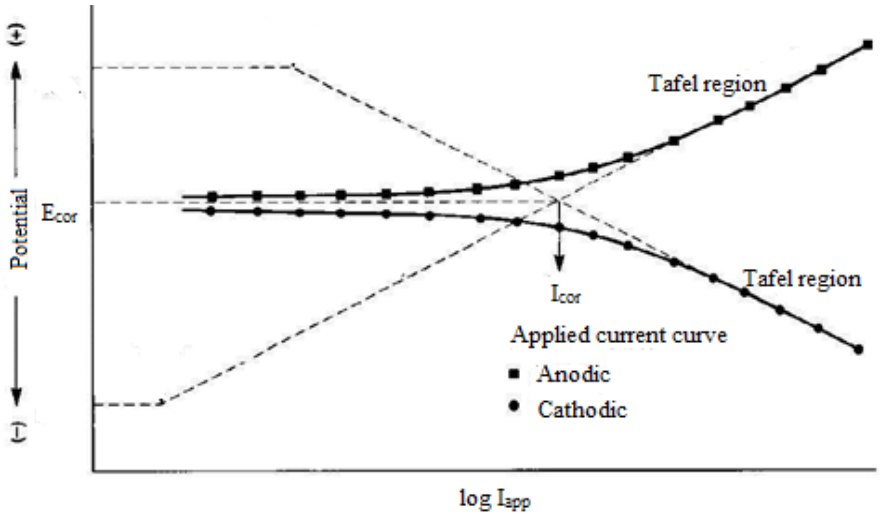

Figure 4.9 Typical Tafel extrapolation analysis of measured polarization curve.

The typical measured polarization curve is shown in Figu 4.9. The curve is made up of cathodic polarization curve and anodic polarization curve, when two curves intersect,

the potential is corrosion potential (E_{cor}). The corrosion current density is decided by Tafel extrapolation. In Tafel extrapolation, there are Tafel regions on both cathodic polarization curve and anodic polarization curve, intersection point of the two Tafel line extrapolations can determine the corrosion current density (I_{cor}).

4.4. Encrustation test

The components for preparing sterile artificial urine are listed in Table 4.2, which are based on the description by Lai et al (Lai L-C *et al.*, 2008). Solutions A and B were prepared separately to prevent brushite ($CaHPO_4 \cdot 2H_2O$) acidic precipitation. The two solutions were mixed by 1:1 to get artificial urine. This artificial urine is faintly acid with PH about 5.8, which is very close to the 4.8-8.0 (average value is 6.0) pH of human urine.

Components of solution A (g/L)		**Components of solution B (g/L)**	
KCl	1.6	Urea	25
NaCl	4.6	KH_2PO_4	2.8
NH_4Cl	1.0	Na_2SO_4	2.3
$MgCl_2 \cdot 6H_2O$	0.65	$Na_2C_2O_4$	0.2
$CaCl_2 \cdot 2H_2O$	0.65		
$Na_3C_6H_5O_7 \cdot 2H_2O$	0.65		

Table 4.2 Compositions of artificial urine

The PDMS samples were cut into the same size (2×7cm) and ultrasonically cleaned

with ethanol and deionized water for 15min. After dry, the mass of every sample was weighed by electronic balance. The back sides of samples, which have smooth surface, were attached to a glass slide, to ensure this side will not contact to the artificial urine. The samples were put in a tank with artificial urine and were completely immersed into the solution in 37℃ shaking incubator. After three weeks of exposure to artificial urine, the samples were taken out and rinsed with deionized water. After completely dry, the each sample was weighed again and the mass difference before and after the test was the mass of urine encrustation on the sample. The samples were kept in sealed petri dish for following SEM and EDXS test.

5. Modelling of Interaction Energy Between Bacteria and Surfaces

5.1 Extended DLVO theory

The Derjaguin–Landau–Verwey–Overbeek (DLVO) theory was first raised to explain and predict the coalescence and dispersion of colloidal particle in solution (Warren LJ, 1975; Xu Z *et al*., 1990). Then, extended DLVO (EDLVO) theory was raised by Van Oss CJ (Van Oss CJ, 1994) to analysis non-covalent interaction between biological and non-biosocial surfaces and particles. In this research, the EDLVO theory was used to analysis the interaction between bacteria and biomaterial surface. The principle interaction energies determining hetero-coagulation by the EDLVO theory include Lifshitz-van der Waals interaction component (E^{LW}), electrostatic double-layer component (E^{EL}), Lewis acid-base component (E^{AB}) and Brownian motion (E^{Br}). The total interaction energy (E^{TOT}) between a particle 1 and a solid surface 2 in liquid 3 can be written as the sum of these corresponding interaction terms:

$$E^{TOT} = E^{LW} + E^{EL} + E^{AB} + E^{Br} \tag{5.1}$$

5.1.1 Lifshitz-van der Waals interaction component (E^{LW})

Lifshitz-van der Waals interaction component is based on van der Waals forces, which is a general attractive interaction between neutral atoms and was first postulated by van der Waals in 1873. In Quantum Mechanics, Van der Waals forces can be divided into

dispersion force (or London force), orientation force, and induction force. Macroscopic approximation, raised by Hamaker in 1937, can calculate the interaction of two macro bodies. If body 1 is a sphere of radius R_1 and body 2 is a sphere of radius R_2 with center distance d in media 3, and A_{132} is the Hamaker constant, we have:

$$E^{LW}(d) = -\frac{A_{132}}{6}\left[\frac{2R_1R_2}{d^2-(R_1+R_2)^2} + \frac{2R_1R_2}{d^2-(R_1-R_2)^2} + \ln\frac{d^2-(R_1+R_2)^2}{d^2-(R_1-R_2)^2}\right] \tag{5.2}$$

In terms of the distance of closest approach of the spheres h=d- R_1-R_2,

$$E^{LW}(h) = -\frac{A_{132}\overline{R}}{12h}\left\{\frac{1}{1+\frac{h}{2(R_1+R_2)}} + \frac{\frac{h}{\overline{R}}}{1+\frac{h}{\overline{R}}+\frac{h^2}{4R_1R_2}} + \frac{2h}{\overline{R}}\ln\left[\frac{\frac{h}{\overline{R}}}{1+\frac{h}{\overline{R}}+\frac{h^2}{4R_1R_2}}\frac{1+\frac{h}{2(R_1+R_2)}}{}\right]\right\} \tag{5.3}$$

Here:
$$\overline{R} = \frac{2R_1R_2}{R_1+R_2} \tag{5.4}$$

If the distance between two bodies is rather small, h<<$\overline{R}$,

$$E^{LW}(h) = -\frac{A_{132}\overline{R}}{12h}\{1+\frac{h}{\overline{R}}[1-\frac{\overline{R}}{2(R_1+R_2)}]+2\frac{h}{\overline{R}}\ln\frac{h}{\overline{R}}+\cdots\} \tag{5.5}$$

So, when R_1=R, $R_2\to\infty$, the situation turns to a sphere and half-space or a thick flat

$$E^{LW}(h) = -\frac{A_{132}R}{6h}(1+\frac{h}{2R+h}+\frac{h}{R}\ln\frac{h}{2R+h}) \tag{5.6}$$

Furthermore, for two parallel cylinders, the LW interaction energy on per unit length:

$$E^{LW}_{unit}(h) = -\frac{A_{132}}{12\sqrt{2}h^{\frac{3}{2}}}\sqrt{\frac{R_1R_2}{R_1+R_2}} \tag{5.7}$$

For two crossed cylinders:

$$E^{LW}(\mathrm{h}) = -\frac{\sqrt{R_1R_2}A_{132}}{6h} \tag{5.8}$$

For two parallel flat surfaces, the LW interaction energy on per unit area:

$$E_{unit}^{LW}(h) = -\frac{A_{132}}{12\pi h^2} \tag{5.9}$$

As long as the Hamaker constant is known, most analyses can be simplified to these computing models, and the LW interaction energy can be calculated. Van Oss presented a simple method for the calculation of Hamaker constant based on the surface energy components materials in 1988:

$$A_{ii} = 24\pi h_o^2 \gamma_i^{LW} \tag{5.10}$$

γ_i^{LW} is the Lifshitz-van der Waals polar component of the surface energy, h_o is the minimum equilibrium distance between the two interacting bodies, it is about 0.157nm. (Van Oss CJ, 1988)

The Hamaker constant for interaction between particle 1 and surface 2 in medium 3 is:

$$A_{132} = (\sqrt{A_{11}} - \sqrt{A_{33}})(\sqrt{A_{22}} - \sqrt{A_{33}}) \tag{5.11}$$

For bacterial adhesion situation, the radius of bacteria (R) is about 0.5-2μm, while the effective distance of van der Waals interaction ranges from several angstroms to several hundred angstroms (Pinto F, 2008), so h<<R, the LW interaction energy between bacteria 1 and a flat solid surface 2 in water 3 can be calculated as:

$$E^{LW} = -\frac{24\pi h_o^2 (\sqrt{\gamma_1^{LW}} - \sqrt{\gamma_3^{LW}})(\sqrt{\gamma_2^{LW}} - \sqrt{\gamma_3^{LW}})R}{6h} \tag{5.12}$$

5.1.2 Lewis Acid–Base Interaction (E^{AB})

In aqueous media, the polar interactions mainly comprise the interactions between hydrogen-donors and hydrogen-acceptors. It is preferable to extend the concept of polar interactions more widely, and to define them to comprise all

electron-acceptor-electron-donor interactions, or lewis acid-base interactions, designated by the superscript AB (Van Oss CJ, 1994). Lewis Acid–Base Interaction (E^{AB}) may be up to two decimal orders of magnitude higher than E^{LW} and E^{EL}, and are commonly described as the components of the traditional DLVO energy balance. For bacterial adhesion, the Lewis acid–base interaction (E^{AB}) between bacteria 1 and flat surface 2 in water 3 can be calculated as:

$$E^{AB} = 2\pi R\lambda E_{h_0}^{AB}\sqrt{\frac{h_0 - h}{\lambda}} \tag{5.13}$$

$$E_{p(h_0)}^{\mathrm{AB}} = 2[\sqrt{\gamma_3^+}(\sqrt{\gamma_1^-} + \sqrt{\gamma_2^-} - \sqrt{\gamma_3^-}) + \sqrt{\gamma_3^-}(\sqrt{\gamma_1^+} + \sqrt{\gamma_2^+} - \sqrt{\gamma_3^+}) - \sqrt{\gamma_1^+\gamma_2^-} - \sqrt{\gamma_1^-\gamma_2^+}] \tag{5.14}$$

where λ (0.2-13nm) is the characteristic wavelength of the interaction. In this research, the value of λ for water is taken as 0.6 nm for water.

5.1.3 Electrostatic Double-Layer Interaction (E^{EL})

In aqueous media, very few biological macromolecules or particles can completely devoid surface electrical charge. The particles immersed in aqueous media will be with the same charge and repel each other. In the total interaction energy, Electrostatic Double-Layer Interaction energy (E^{EL}) is the main repulsion energy.

The Electrostatic Double-Layer Interaction (E^{EL}) between bacteria 1 and flat surface 2 in medium 3 can be described as:

$$E_{132}^{EL}(h) = \varepsilon\pi R(\varphi_1^{\,2} + \varphi_2^{\,2})[\ln(1 - e^{-2\kappa h}) + 2\frac{\varphi_1\varphi_2}{\varphi_1^{\,2} + \varphi_2^{\,2}}\ln(\frac{1 + e^{-\kappa h}}{1 - e^{-\kappa h}})] \tag{5.15}$$

In this equation, φ_1 and φ_2 are the zeta potentials of bacteria and the flat surface, respectively. $\varepsilon=\varepsilon_0\varepsilon_r$. ε_0 is relative dielectric permittivity of water (78.55 at 25℃), and ε is permittivity under vacuum (8.854×10^{-12} C/Vm). κ is Debye-Hŭckel length and also an estimation of the effective thickness of the electrical double layer($1/\kappa$ =1.1 nm).

5.1.4 Brownian motion component (E^{Br})

Among particles suspended or macromolecules dissolved in liquid media, Browmian movement always occurs at temperature higher than 0 ℃K. Brownian free energy (E^{Br}) is $1\frac{1}{2}KT$ with three degrees of freedom, K is Boltzmann's constant (1.3806×10-23 J/K) and T is the absolute temperature in degrees K. The bacterial adhesion model involves two degrees of freedom, so the Brownian free energy in calculation is 1KT,

$$E^{Br} = 0.414*10^{-20} J \qquad (5.16)$$

5.2 Surface integral method for ccalculating interaction energy

5.2.1 Interaction energy between spherical bacteria and flat surface

Based on the extended DLVO theory states, the total interaction energy per unit area (E_p^{TOT}) between a flat plate 1 and a flat plate 2 in water 3 consists of Lifshitz-van de Waals (E_p^{LW}) component, electrostatic force (E_p^{EL}) component and Lewis acid-base (E_p^{AB}) component, which is express as: (van Oss CJ, 1994; Hoek EMV *et al.*, 2006)

$$E_p^{TOT}(h) = E_p^{LW}(h) + E_p^{EL}(h) + E_p^{AB}(h) \tag{5.16}$$

$$E_p^{LW}(h) = -\frac{A_{132}}{12\pi h^2} \tag{5.17}$$

$$E_p^{EL}(h) = \varepsilon\varphi_1\varphi_2\{\frac{\varphi_1^{\ 2} + \varphi_2^{\ 2}}{2\varphi_1\varphi_2}[1 - \coth(\kappa h)] + \frac{1}{\sinh(\kappa h)}\} \tag{5.18}$$

$$E_p^{AB}(h) = E_{132(h_0)}^{AB} e^{\frac{h_0 - h}{\lambda}} \tag{5.19}$$

As has been defined in extended DLVO theory, h is the separation distance, h_0=0.157nm is the minimum equilibrium distance. And A_{132} is the Hamaker constant for the interaction between the plate 1 and the plate 2 in water 3, which can be calculated by surface energy components. φ_1 and φ_2 are the zeta potentials of the plate 1 and plate 2, respectively; ε is the electrical permittivity of solution, κ is the Debye-Hückel parameter (1/κ =1.1nm); and λ is the correlation length of the molecules of the liquid medium.

If the plate 1 is replaced by a spherical bacterium, for each interaction component, it can be obtained by integrating the above equations (5.17), (5.18) and (5.19), respectively over the hemisphere surface of the bacterium 1 facing to the flat plate 2:

$$E_{132}^{LW}(h) = -\int_0^{\frac{\pi}{2}} \frac{A_{132} \cdot 2\pi R^2}{12\pi[h + R(1 - \cos\theta)]^2} \sin\theta \cdot d\theta$$
$$= -\frac{A_{132}R}{6h} \cdot \frac{R}{R + h}$$
$$\approx -\frac{A_{132}R}{6h} \quad (R >> h) \tag{5.20}$$

$$E_{132}^{EL}(h)=\int_0^{\frac{\pi}{2}}\varepsilon\varphi_1\varphi_2\{\frac{\varphi_1^{\ 2}+\varphi_2^{\ 2}}{2\varphi_1\varphi_2}[1-\coth(\kappa(h+R(1-\cos\theta)))]+\frac{1}{\sinh[\kappa(h+R(1-\cos\theta))]}\}2\pi R^2\sin\theta\cdot d\theta$$

$$=\varepsilon\pi R(\varphi_1^{\ 2}+\varphi_2^{\ 2})[\ln(1-e^{-2\kappa h})+2\frac{\varphi_1\varphi_2}{\varphi_1^{\ 2}+\varphi_2^{\ 2}}\ln(\frac{1+e^{-\kappa h}}{1-e^{-\kappa h}})]$$

(5.21)

$$E_{132}^{AB}(h)=\int_0^{\frac{\pi}{2}}E_{132(h_0)}^{AB}e^{\frac{h_0-[R(1-\cos\theta)+h]}{\lambda}}2\pi R\sin\theta Rd\theta$$

$$=2\pi R\lambda E_{132(h_0)}^{AB}(e^{\frac{h_0-h}{\lambda}}-e^{\frac{h_0-h-R}{\lambda}})$$

$$\approx 2\pi R\lambda E_{132(h_0)}^{AB}e^{\frac{h_0-h}{\lambda}}\qquad (R>>\lambda)$$

(5.22)

These equations were calculated and simplified by Maple software. Assuming that R >> h and R >> λ, the equations can be simplified to the classical forms as described by extend DLVO theory, so the surface integral method is reliable in computing the interaction energy.

5.2.2 Interaction energy between rod bacteria (cylinder model) and flat surface

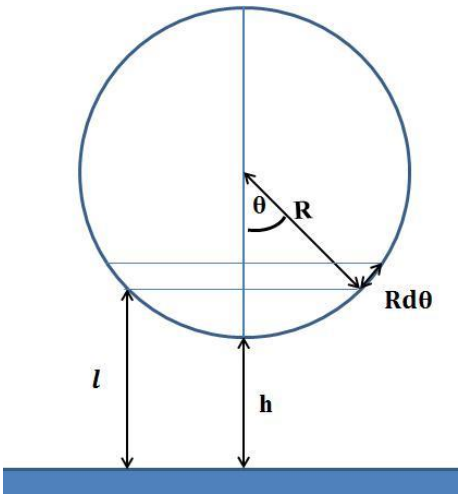

Figure 5.1 Schematic cross section of a cylinder to flat surface situation.

Figure 5.1 is the cross-section schematic diagram for a cylinder to flat surface situation, here, h is the separation distance (closest distance between the sphere surface and flat surface), l is the distance from any point on cylinder surface to the flat surface. The interaction energy for rod bacteria (cylinder model) to flat surface can be obtained by integrating the plate–plate (slip-slip) interaction energies over the cylinder surface.

$$E_{132}^{TOT}(h) = 2\int_0^{\frac{\pi}{2}} E_p^{TOT}(l) LRd\theta \tag{5.23}$$

Here, $l = R(1-\cos\theta)$, L is the length of cylinder,

$$E_{132}^{TOT}(h) = 2\int_0^{\frac{\pi}{2}} E_p^{TOT}(R(1-\cos\theta)) LRd\theta \tag{5.24}$$

$$E_{132}^{LW}(h) = 2\int_0^{\frac{\pi}{2}} -\frac{A_{132}}{12\pi[h+R(1-\cos\theta)]^2} RLd\theta \tag{5.25}$$

$$E_{132}^{EL}(h) = 2\int_0^{\frac{\pi}{2}} \varepsilon\varphi_1\varphi_2\{\frac{\varphi_1^{\ 2}+\varphi_2^{\ 2}}{2\varphi_1\varphi_2}[1-\coth(\kappa(h+R(1-\cos\theta)))] + \frac{1}{\sinh[\kappa(h+R(1-\cos\theta))]}\} LRd\theta$$

(5.26)

$$E_{132}^{AB}(h) = 2\int_0^{\frac{\pi}{2}} E_{132(h_0)}^{AB} e^{\frac{h_0-[R(1-\cos\theta)+h]}{\lambda}} LRd\theta \tag{5.27}$$

5.2.3 Interaction energy between rod bacteria (cylinder model) and nanocube array surface

In order to investigate the effect of surface nanostructures on bacterial adhesion, a nanocube array on PDMS substrate was designed. Figure5.2 shows schematic diagram and sectional view of the bacterial attachment situation on surface micro-nanostructure.

The edge length of the nanocubes was assumed to be “a” and the distance between the two adjacent nanocubes was also assumed to be “a”.

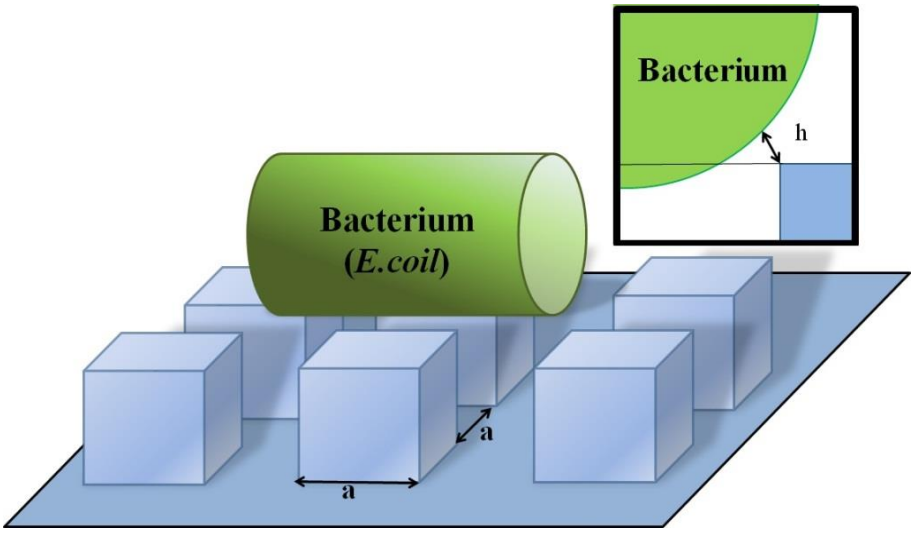

Figure 5.2 Schematic diagram for *E. coli* adhesion on a surface with a nanocube array

The interaction energies between the rod-shaped bacterium 1 and the nanocube array surface 2 in water 3 can be obtained by integrating the above equations (5.17), (5.18) and (5.19) over the surface of the cylindrical bacterium 1 with radius R and average effective length $\bar{L}$ ($=\frac{L}{2}$ for our pattern) facing to the nanocube array 2:

$$E_{132}^{LW}(h) = -\int_{\arcsin(\frac{a}{2R})}^{\frac{\pi}{2}} \frac{A_{132}RL}{12\pi[\sqrt{(R+h)^2-(\frac{a}{2})^2}-R\cos\theta]^2}d\theta - \int_0^{\arccos(\frac{\sqrt{(R+h)^2-(\frac{a}{2})^2}}{R})} \frac{A_{132}RL}{12\pi(\frac{a}{2}-R\sin\theta)^2}d\theta$$
$$-\int_0^{\frac{\pi}{2}} \frac{A_{132}RL}{12\pi[a+\sqrt{(R+h)^2-(\frac{a}{2})^2}-R\cos\theta]^2}d\theta$$

(6.21)

$$E_{132}^{EL}(h)=\int_{\arcsin(\frac{a}{2R})}^{\frac{\pi}{2}}\varepsilon\varphi_1\varphi_2\{\frac{\varphi_1^{\ 2}+\varphi_2^{\ 2}}{2\varphi_1\varphi_2}[1-\coth(\kappa(\sqrt{(R+h)^2-(\frac{a}{2})^2}-R\cos\theta))]+$$

$$\frac{1}{\sinh[\kappa(\sqrt{(R+h)^2-(\frac{a}{2})^2}-R\cos\theta)]}\}LRd\theta+$$

$$\int_0^{\arccos(\frac{\sqrt{(R+h)^2-(\frac{a}{2})^2}}{R})}\varepsilon\varphi_1\varphi_2\{\frac{\varphi_1^{\ 2}+\varphi_2^{\ 2}}{2\varphi_1\varphi_2}[1-\coth(\kappa(\frac{a}{2}-R\sin\theta))]+\frac{1}{\sinh[\kappa(\frac{a}{2}-R\sin\theta)]}\}LRd\theta+$$

$$\int_0^{\frac{\pi}{2}}\varepsilon\varphi_1\varphi_2\{\frac{\varphi_1^{\ 2}+\varphi_2^{\ 2}}{2\varphi_1\varphi_2}[1-\coth(\kappa(a+\sqrt{(R+h)^2-(\frac{a}{2})^2}-R\cos\theta))]+$$

$$\frac{1}{\sinh[\kappa(a+\sqrt{(R+h)^2-(\frac{a}{2})^2}-R\cos\theta)]}\}LRd\theta \tag{6.22}$$

$$E_{132}^{AB}(h)=\int_{\arcsin(\frac{a}{2R})}^{\frac{\pi}{2}}E_{132(h_0)}^{AB}e^{\frac{h_0-[\sqrt{(R+h)^2-(\frac{a}{2})^2}-R\cos\theta]}{\lambda}}LRd\theta+\int_0^{\arccos(\frac{\sqrt{(R+h)^2-(\frac{a}{2})^2}}{R})}E_{132(h_0)}^{AB}e^{\frac{h_0-(\frac{a}{2}-R\sin\theta)}{\lambda}}LRd\theta+$$

$$\int_0^{\frac{\pi}{2}}E_{132(h_0)}^{AB}e^{\frac{h_0-[a+\sqrt{(R+h)^2-(\frac{a}{2})^2}-R\cos\theta]}{\lambda}}LRd\theta$$

(6.23)

6. Results and Discussion

6.1 Si- and F-doped DLC coatings

6.1.1 Contact angle and surface energy of DLC coated samples

Sample	Contact angle and stand deviation (°)			Surface energy(mJ/m^2)				
	air	DI	EG	γ^{LW}	γ^{AB}	γ^{+}	γ^{-}	γ^{TOT}
DLC	60.4 ±1.6	35.2±2.0	47.0 ±6.00	41.9	1.8	0.04	21.0	43.7
DLC-3.7%Si	57.6±2.8	37.6 ±1.39	39.0 ±3.5	40.7	1.9	0.04	24.6	42.6
DLC-9.7%Si	58.1 ±3.6	39.6 ±3.9	37.5±2.2	39.8	3.4	0.12	23.4	43.1
DLC-19.2%Si	59.7 ±2.4	40.4±1.6	39.6 ±2.9	39.4	3.0	0.1	22.3	42.3
DLC-6.5%F	50.8 ±1.6	44.1±2.6	33.0 ±1.3	41.7	3.0	0.07	30.1	44.0
DLC-20.7%F	55.8 ±2.4	40.9 ±1.6	41.7 ±2.9	39.1	1.1	0.1	28.23	40.2
DLC-39.2%F	46.1 ±2.2	45 ±1.8	34.3±2.79	37	4.3	0.12	38.8	41.3
SS	70.2 ±5.2	30.6 ±4.0	51.9±10.7	43.9	2.1	0.1	10.2	45.9

Table 6.1 Contact angles by sessile drop method and surface energy of doped DLC coatings.

Sample	Contact angle and stand deviation (°)			Surface energy(mJ/m^2)				
	air	n-octane	toluene	γ^{LW}	γ^{AB}	γ^{+}	γ^{-}	γ^{TOT}
DLC	136.6 ±1.0	114 ±1.6	110.9 ±0.7	33.2	19.1	3.3	27.6	55.8
DLC-3.7%Si	135.7 ±1.9	117.2 ±2.0	108.0 ±1.6	29.0	25.4	7.6	21.3	54.5
DLC-9.7%Si	127.6 ±1.2	105.6 ±2.9	95.4 ±1.6	31.2	16.7	3.3	21.3	48.0
DLC-19.2%Si	133.5 ±2.0	115.7 ±0.5	113.9 ±1.5	28.1	19.7	3.3	29.5	48.0
DLC-6.5%F	130.4 ±1.2	110.3 ±1.7	106.4 ±1.0	29.8	16.2	2.4	27.5	46.4
DLC-20.7%F	124.7 ±2.4	104.6 ±2.0	94.8 ±2.9	28.8	15.1	2.6	22.2	44.2
DLC-39.2%F	128.1 ±1.4	111.9 ±0.8	109.6 ±1.3	25.7	16.4	2.3	29.4	42.4
SS	126.5 ±3.0	89.9 ±5.9	62.8 ±1.8	47.9	12.2	4.3	8.9	60.1

Table 6.2 Contact angles by captive bubble method and surface energy of doped DLC coatings.

Table 6.1 and Table 6.2 shows the contact angles and surface free energies of the doped DLC coatings measured by sessile drop method and captive bubble method respectively. For DLC and Si- and F- doped DLC coatings, the surface energies by captive bubble method methods generally agree to those by sessile drop method. While the γ^{AB} and γ^{+} components by captive bubble method are generally larger than those by sessile drop method, leading to the higher total surface energies (γ^{TOT}) by captive bubble method.

6.1.2 Bacterial adhesion assays

6.1.2.1 Effects of contact time on bacterial adhesion

Klebsiella pneumonia (ATCC 13883, obtained from the Institute of Infection and Immunity, Nottingham University, UK.) was used in this bacterial adhesion assays. The eight samples, three Si-doped DLC coatings, three F-doped DLC coatings, a standard DLC coating and a stainless steel 316 plate were used for bacterial adhesion tests. A series of bacterial adhesion assays with different contact times (1-12h) were performed in static condition to evaluate effect of contact time of bacterial adhesion situation on DLC coating samples. For each contact time, more than three repeated tests were performed to reduce the experimental error and to get the reliable results. Figure 6.1 and Figure 6.2 are the fluorescence microscopy photos and bacterial adhesion density on samples at different contact times. Figure 6.2 clearly shows that

for contact time shorter than 7 hours, the total bacteria densities (both dead and live bacteria densities) on the surfaces of stainless steel, DLC and Si/F doped DLC coatings increased rapidly with the contact time increasing until reached the maximum value at about 7hour and there were more live bacteria than dead bacteria. For a contact time longer than 7 hours, the bacteria densities decreased with contact time increasing. This was because some bacteria dead in bacterial suspension due to lack of nutrients.

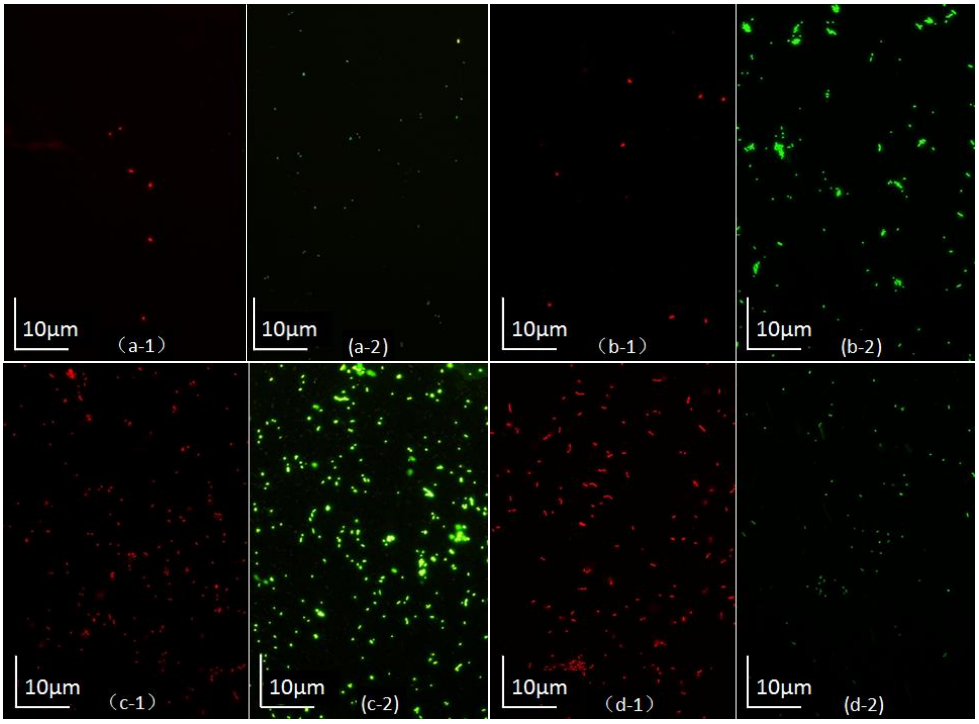

Figure 6.1 Bacterial attachment on DLC coatings at different time. (a-1)/(a-2) for dead/alive bacteria at 1h; (b-1)/(b-2) for dead/alive bacteria at 4h; (c-1)/(c-2) for dead/alive bacteria at 7h; (d-1)/(d-2) for dead/alive bacteria at 12 h.

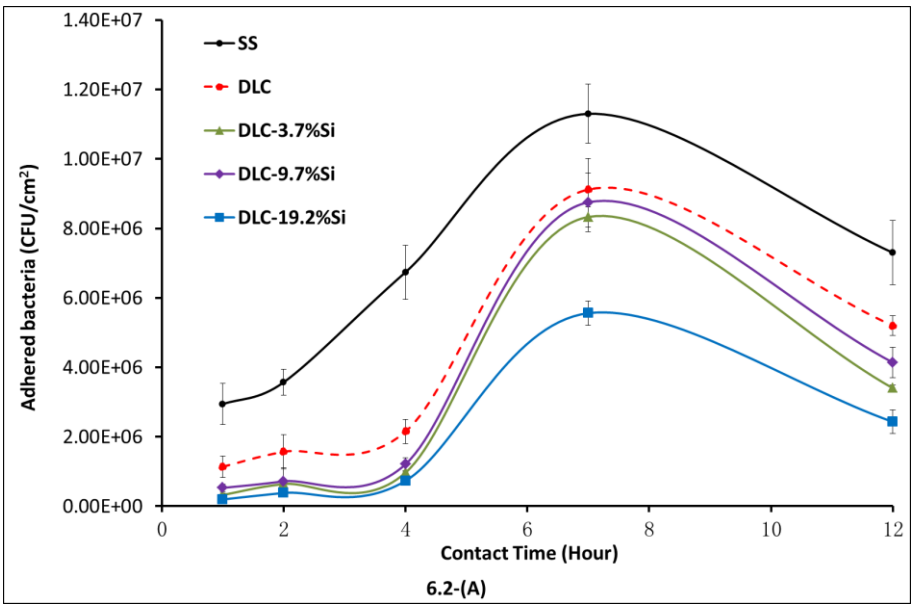

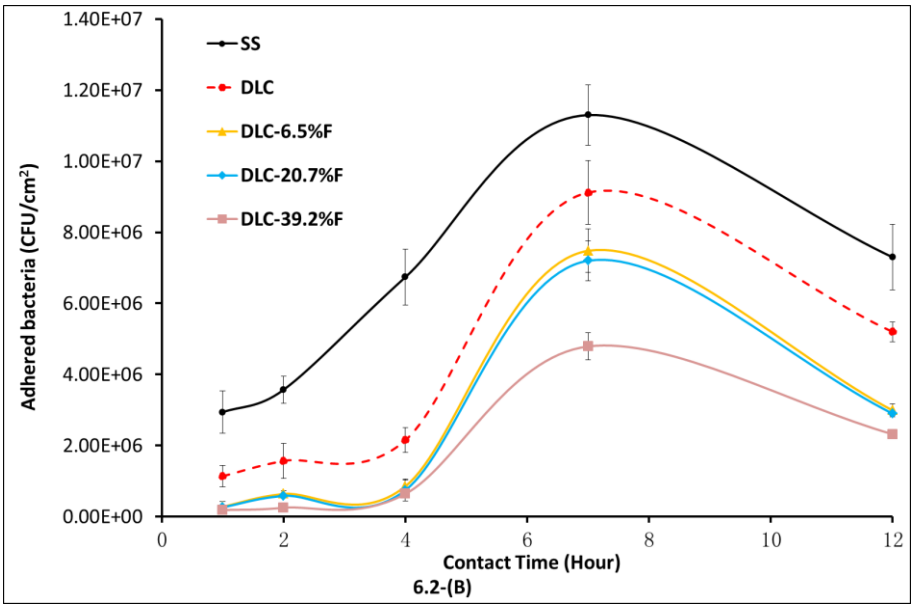

Figure 6.2 Effect of doped element contents in DLC coatings and contact time on the adhesion of *Klebsiella pneumoniae* in static condition. (A): Si-doped DLC coatings; (B): F-doped DLC coatings.

Bacterial adhesion assays were also performed under flow condition with the flow rate of about 0.75×10^{-6} m^3/s in a flow chamber for 1-12 hours, as shown in Figure 6.3. The similar results were obtained. That is, there existed maximum bacterial density at contact time of 7 hours.

Clearly all the DLC coatings performed better than stainless steel against bacterial adhesion under both static and flow conditions. The doped DLC coatings performed better than the standard DLC. The F-doped DLC coating with high F (39.2 at.%) performed best.

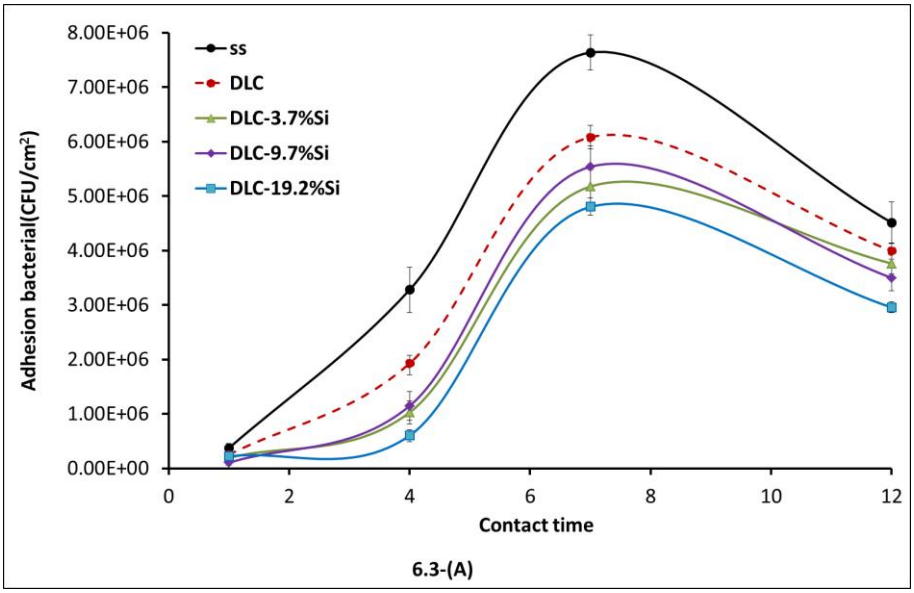

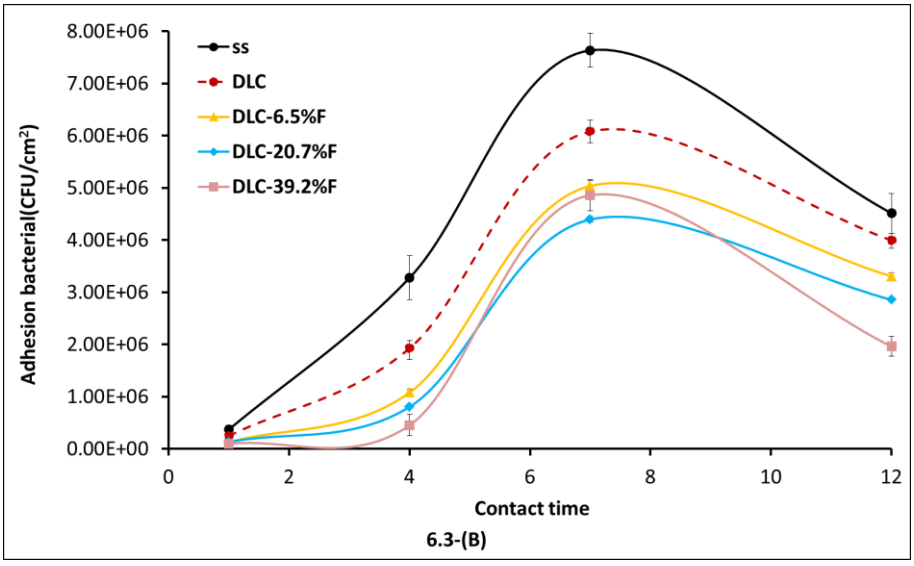

Figure 6.3 Effect of doped element contents in DLC coatings and contact time on the adhesion of *Klebsiella pneumoniae* in flow condition. (A): Si-doped DLC coatings; (B): F-doped DLC coatings.

6.1.2.2 Effect of flow rate on bacterial adhesion

Figure 6.4 and Figure 6.5 show that the bacterial adhesion densities in fluid condition were similar to those in static condition at contact time 4 hour. While at 7hour, the bacterial adhesion densities in flow condition were significant lower than those in static condition. These results indicate that the fluid can generate shearing stress which are help to decrease the bacterial adhesion, or the adhered bacterial can be removed by fluid flow.

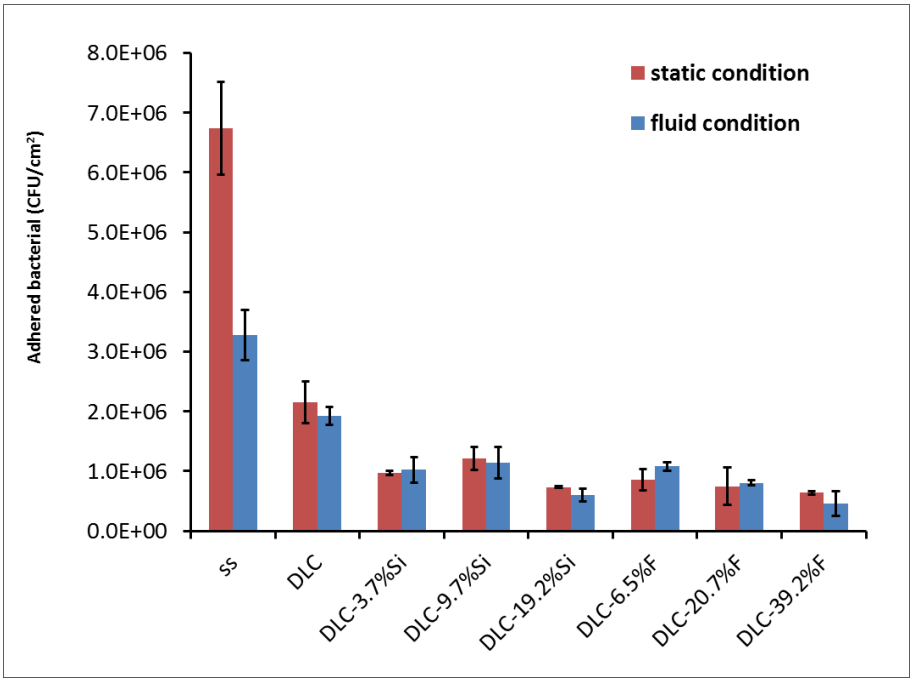

Figure 6.4 Bacterial adhesion densities in flow and static conditions at 4hour

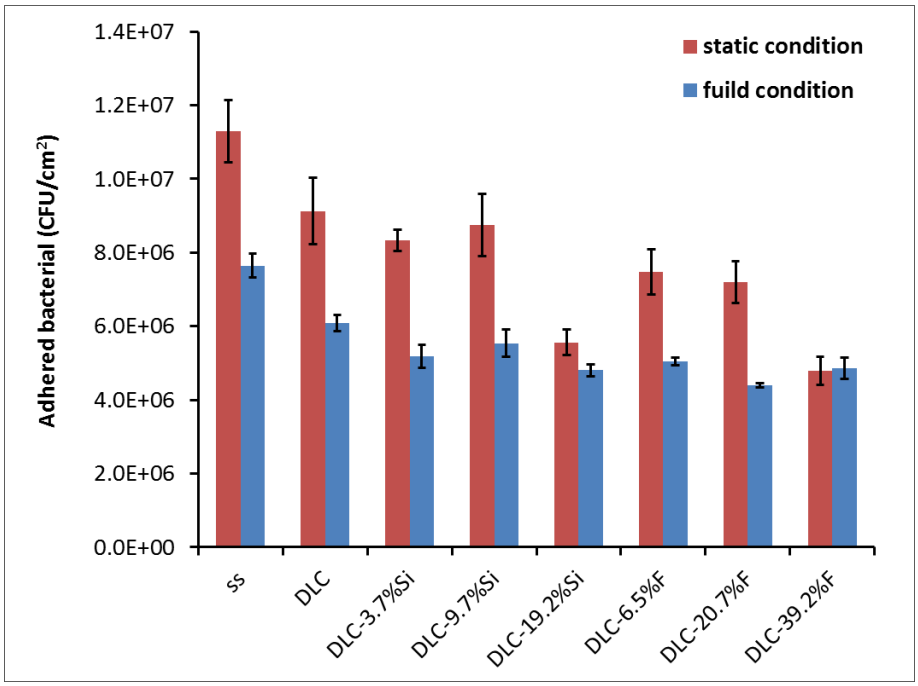

Figure 6.5 Bacterial adhesion densities in flow and static conditions at 7hour

6.1.2.3 Effect of interaction energy on bacterial adhesion

The interaction energies between the bacterium *Klebsiella pneumoniae* and the surfaces of stainless steel, DLC and Si/F doped DLC coatings were computed by EDLVO theory. Figure 6.6 and 6.7 show the interaction energy between the bacterium and the coatings as function of separation distance (h). According to the EDLVO theory, bacterial adhesion will decrease with the interaction energy increasing. Clearly the F-DLC coating with 39.2% F had the highest interaction energy; while the stainless steel (ss) had the lowest interaction energy. All the theoretical modeling results in Figures 6.6-6.7 are consistent with the experimental results in Figure 6.2.

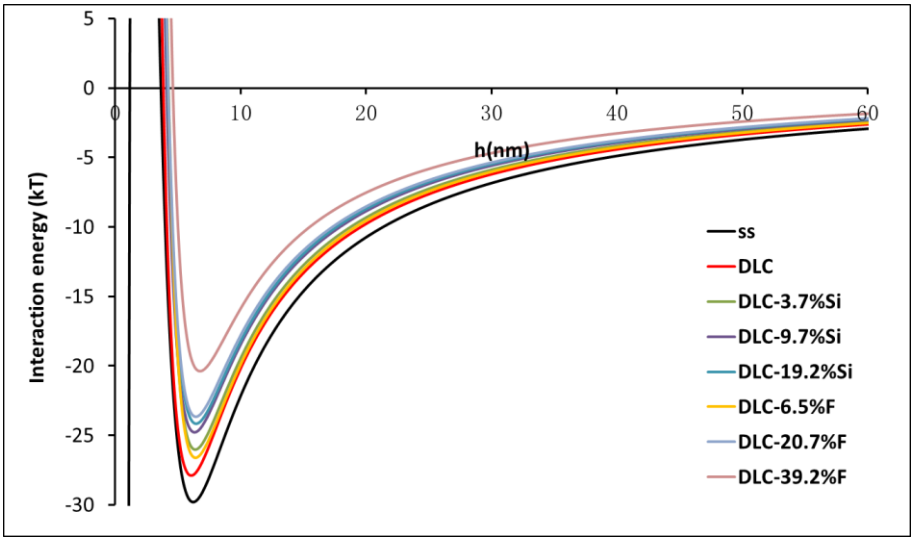

Figure 6.6 Interaction energy between the *Klebsiella pneumoniae* and the coatings as function of separation distance (h). (Surface energy from sessile drop method)

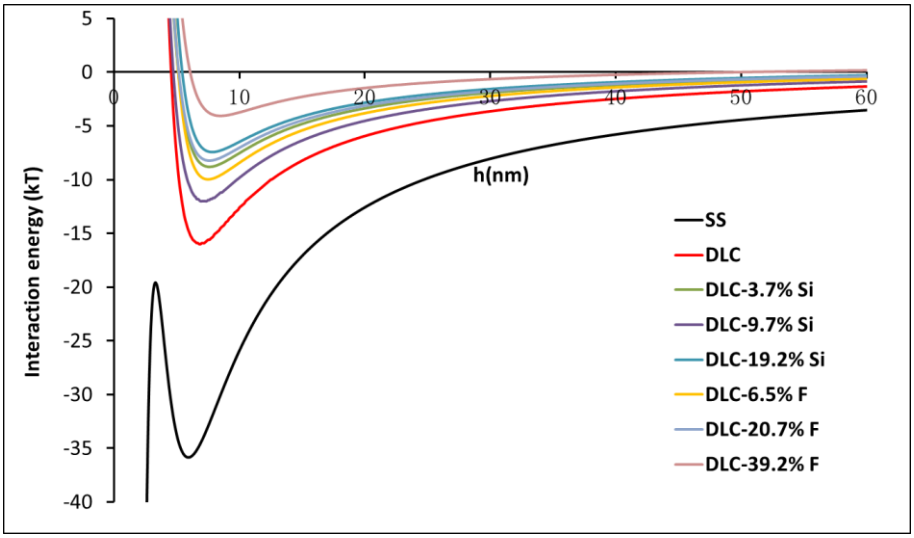

Figure 6.7 Interaction energy between the bacterium and the coatings as function of separation distance (h). (Surface energy from captive bubble method)

Figure 6.6 and 6.7 also show that the interaction energy reached minimum at separation distance = 7 nm. Figure 6.8 and Figure 6.9 show the relationship between bacterial adhesion and the interaction energy at separation distance = 7 nm at 3 different contact time. Clearly there are strong correlations between the interaction energy and the bacteria adhesion. The adhered bacteria (CFU/cm^2) decreased with the interaction

energy increasing, which is consistent with the EDLVO theory.

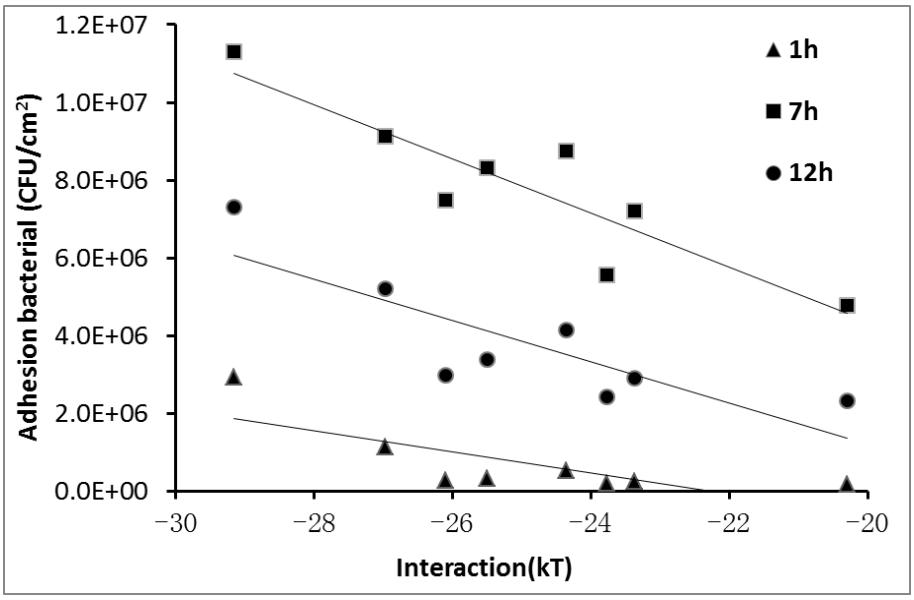

Figure 6.8 Relationship between bacterial adhesion and the interaction energy at 7nm separation distance for the coatings at different time (1hour, 7 hour and 12hour). (Surface energy from sessile drop method)

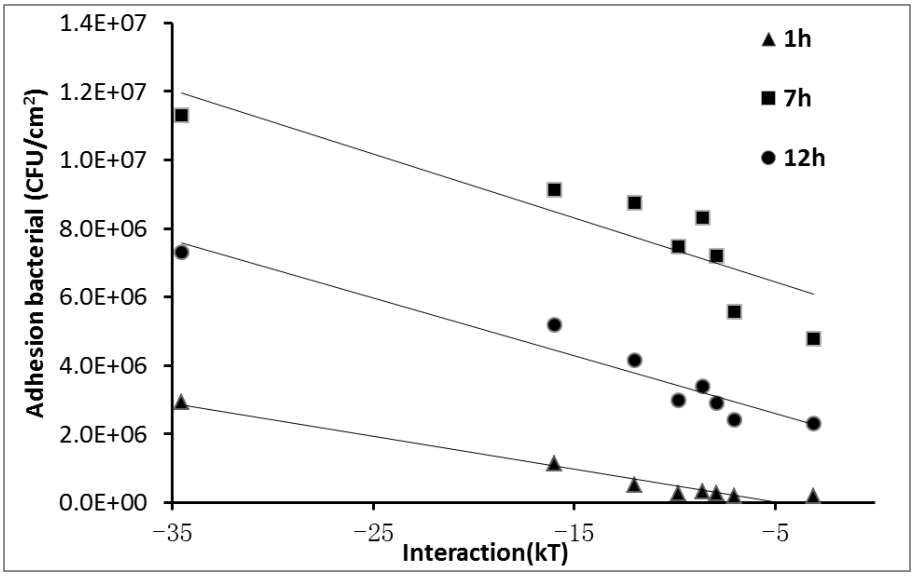

Figure 6.9 Relationship between bacterial adhesion and the interaction energy at 7nm separation distance for the coatings at different time (1hour, 7 hour and 12hour). (Surface energy from captive bubble method)

6.1.3 Bacterial adhesion assays with QCM-D system

6.1.3.1 Frequency curve (Δf) and dissipation factor curve (ΔD) measured by QCM-D system

Four crystal sensors with different surfaces (stainless steel, DLC coating, gold and Ni-P coating) were tested by QCM-D system in *E.coli* suspension. The Ni-P coated sensor was prepared by electroless plating method. When the Ni-P coating was exposed to buffer liquid (PBS), the f curve showed a steady raise of approximately +0.8Hz/min and cannot reach a stable baseline for long period of time. The drift was about -13nm/($cm^2 \times min$) when calculated with the Sauerbrey equation, which was much higher than the highest acceptable baseline drift (±0.015 Hz/min or ±0.15nm/($cm^2 \times min$). This resonant frequency response indicated a slow but significant surface material removal or dissolution from the Ni-P coating in buffer liquid. The fail of achieving a stable baseline caused the measurement of the Ni-P coated crystal sensor cannot get reliable results for analysis. While, for the crystal sensor coated with stainless steel, DLC and gold, relative stable baselines were achieved in 2-10min, and the following measurements were normal.

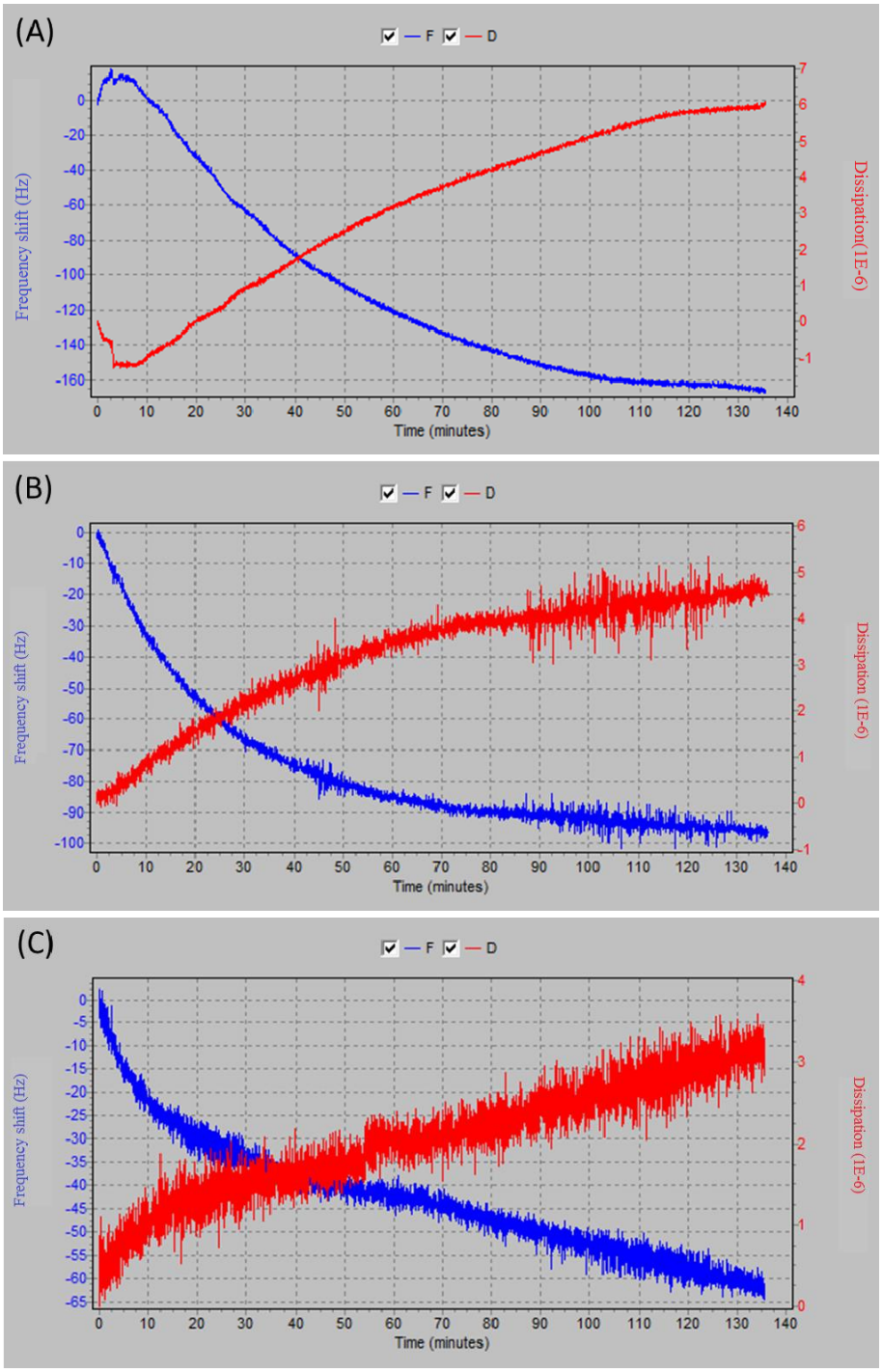

Figure 6.10 Frequency vs time by QCM-D system at 15.0 MHz in 10^6 CFU/ml *E.coli* suspensions; (A) Stainless steel surface; (B) DLC coating surface; (C) gold surface.

In these tests, the 3rd overtone crystal sensor resonance frequency (about 15MHz) was easily searched by the QCM-D system, and the relative stable measurement curves

were obtained. Therefore the measurements in this study were performed at the 3rd overtone frequency. As shown in Figure 6.10, the bacterial adhesion process with time on three different surfaces were successfully measured by the QCM-D system.

At the beginning of the test, the measured resonant frequency dramatically decreased. The decline slowed down with time after three hours. For the sensors with the 3 different coatings, the trends of frequency change were similar but the values of frequency varied from -65Hz to -160Hz. Compared with the changes of frequency (Δf), the changes of dissipation factor (ΔD) displayed the reverse trends. The dissipation factors on different sensors were similar and slightly increased with the bacterial adhesion time, and just increased about 4-6$\times 10^{-6}$ in three hours. As mentioned before, the reduced resonant frequency means the increase of the mass (e.g. bacterial mass) on sensor, and the dissipation factors are related to the property of adhered biofilm layer.

6.1.3.2 Analysis of measurement data

The Sauerbrey relation can be used to estimate the attached/removed mass (or thickness) when dissipation is comparatively small. But for a high dissipative system ($\Delta D > 10^{-7}/\Delta f$), the Sauerbrey equation may underestimate the attached mass (or thickness), so it is essential to verify the validity of the Sauerbrey relation (Olsson AL *et al.*,2009). In our measurements, the decrease of frequency (Δf) was in the range of

65-160Hz, while the changes of dissipation were lower than 6×10^{-6}, so the bacterial adhesion on the coated sensor surfaces was not in high dissipative system.

The Voight model is another method can be used to estimate the influence of dissipation values on Sauerbrey modeling. The adhered layer can be viewed as a Voight unite, which is represented by a purely viscous damper and purely elastic spring connected in parallel, as shown in the Figure 6.11.

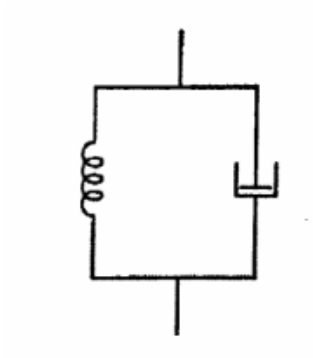

Figure 6.11 Schematic diagram of a Voight unite.(Voinova MV *et al.*, 1999)

In Voight model, shear viscosity η and modulus of shear elasticity E are introduced to describe the mechanical properties of the adhered layer. In QCM-D system, shear viscosity η and modulus of shear elasticity E can be calculated by the change of frequency (Δf) and the change of dissipation factor (ΔD) by QTools software, as shown in Figure 6.12. It can be seen that the shear viscosity η and shear elasticity E of bacterial layer on sensor surface were about $0.02N\cdot s/m^2$ and 8×10^4Pa.

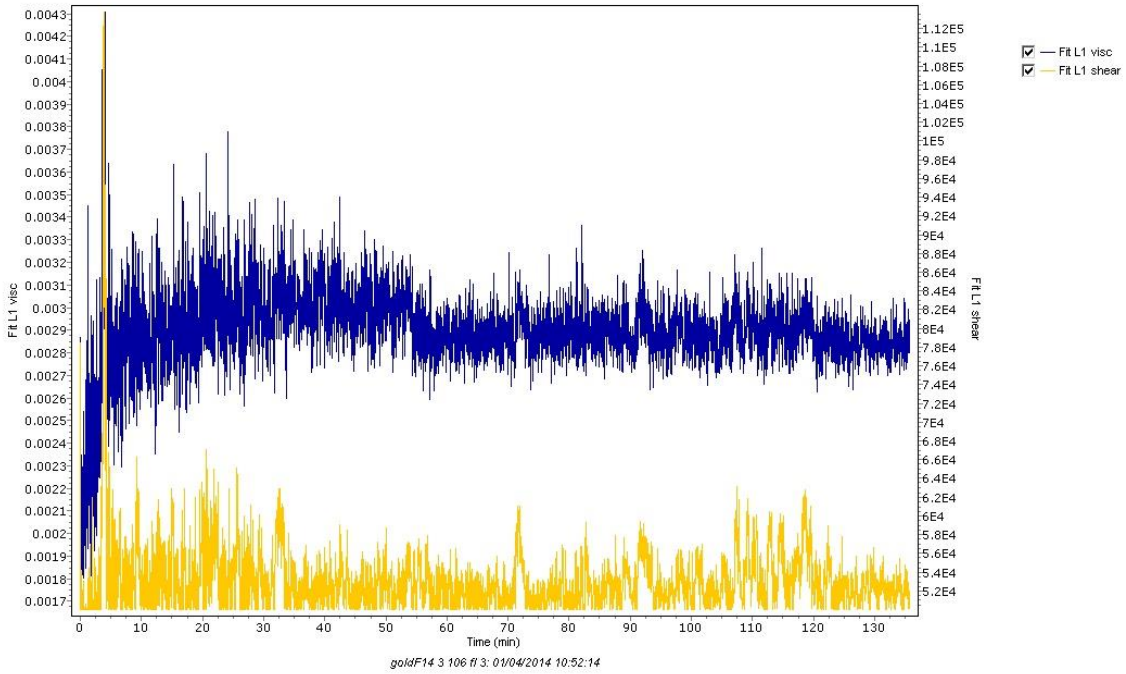

Figure 6.12 Shear viscosity η (blue curve) and modulus of shear elasticity E (yellow curve) of adhered bacterial layer calculated by QTools software.

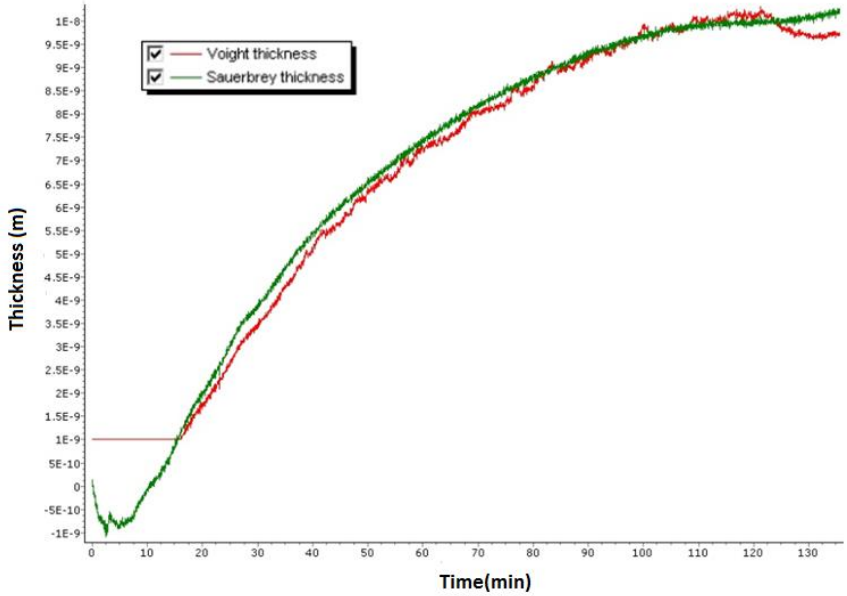

Figure 6.13 Adhesion thickness estimated with the Sauerbrey relation and Voigt relation by QTools modeling software. (The data from the measurements of 10^6 CFU/cm^2 *E.coli* adhesion on stainless steel surface at15.0 MHz, showed in Figure 6.10- (A)).

In Figure 6.13, the Sauerbrey thickness is compared with the Voight thickness from the bacterial adhesion measurement on stainless steel, which showed the largest change value of dissipation. It is clear that the two curves overlap nicely, which indicates the dissipation factors in bacterial adhesion process are relative low and the error induced by using the Sauerbrey relation in this case is negligible.

Furthermore, the study from Bing Wu believes that when the modulus of shear elasticity E is large, the Sauerbrey relation can be directly used for a thin film. For the film with $\eta = 10^{-2}$ N s/m^2 and E=10^4 Pa, Sauerbrey relation is effective when thickness less than 100nm. Similar views were also mentioned by Hook and Rodahl (Höök F *et al.*, 2001; Rodahl M *et al.*,1996). The experimental results meet the conditions of above conclusion, so using Sauerbrey relation to analysis the measurement results of bacterial adhesion is reliable.

Figure 6.14 shows the biofilm thickness of adhered *E.coli* on the 3 coated sensors, which was calculated from the measurement results using Sauerbrey relation.

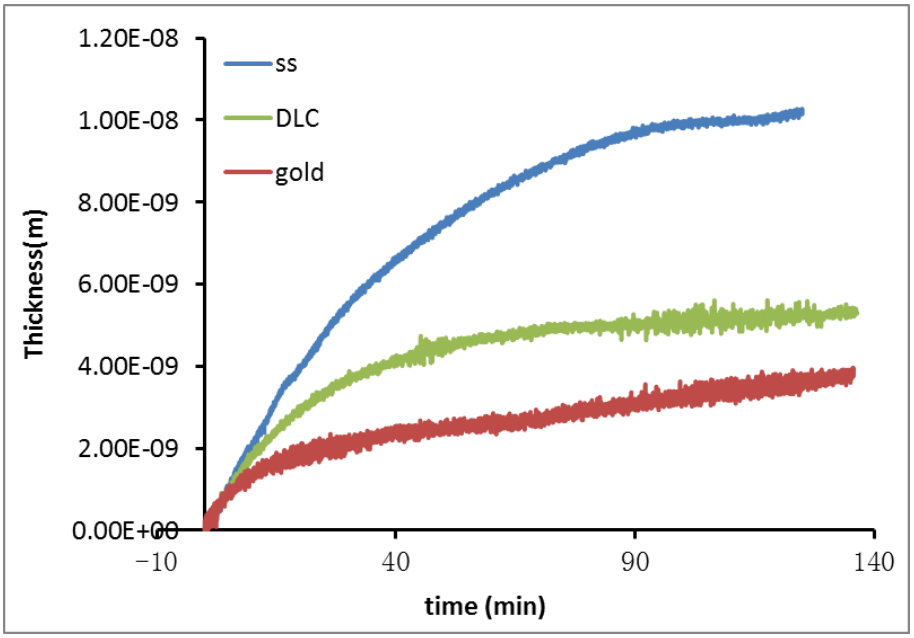

Figure 6.14 Thickness of adhered bacterial on 3 different coatings calculated from the measurement results with Sauerbrey relation.

The number of adhered bacteria (CFU/cm^2) can be calculated by

$$CFU/cm^2 = \frac{h}{\overline{V_B}} \tag{6.1}$$

where, h is the thickness of bacterial layer measured by QCM-D system. $\overline{V_B}$ is the mean cell volume of *E.coli* and is taken as 0.7 μm^3 (Kubitschek HE, 1990). The adhered bacterial surface densities on the coated sensors as a function of time are shown in Fig 6.15. The adhered bacteria increased with time increasing. The adhesion rates were relatively high at the beginning and then declined to stable. For the three different surfaces, the gold coating showed the lowest bacterial adhesion (about 5×10^5 CFU/cm^2). This result is similar to the conclusion in related reports, that gold exhibits better antibacterial activity than most other dental implant metals, like titanium, cobalt, vanadium, aluminum, chromium and iron (Berry CW *et al.*, 1992). The bacterial

adhesion on DLC coating was about 7×10^5 CFU/cm^2, which was just half of that on stainless steel surface, so the DLC coating is much better than stainless steel 316L in inhibiting bacterial adhesion.

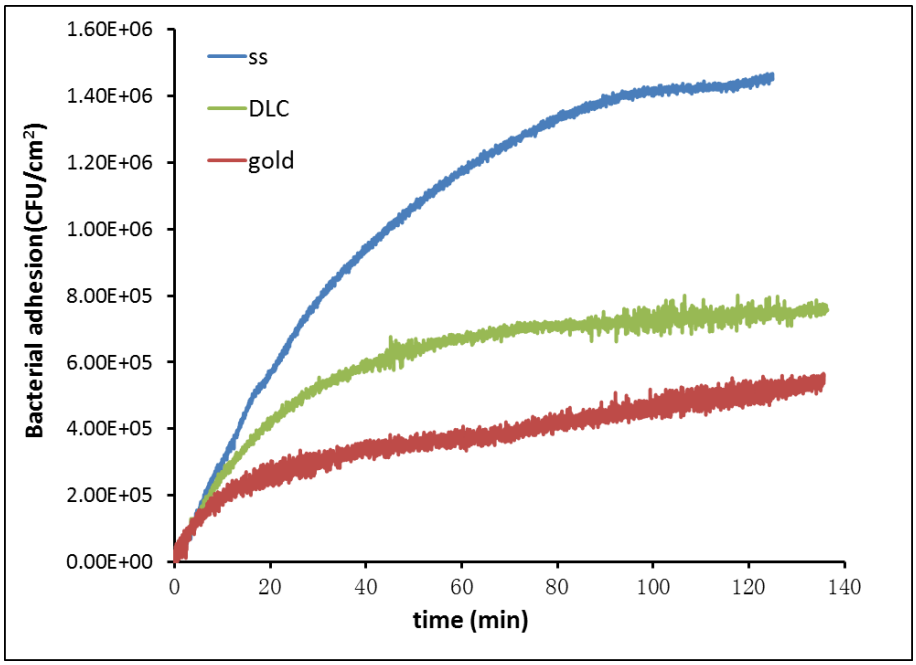

Figure 6.15 Bacterial adhesion density on the coatings.

In order to verify the accuracy of the measurement results of QCM-D method, the bacterial adhesion on the stainless steel coated sensor was also examined by fluorescence microscopy after the QCM-D test, as shown in Figure 6.16. The adhered bacteria on the stainless steel coated sensor were about 1.88×10^6 ($\pm10\%$) CFU/cm^2, was very close to the result measured by QCM-D method (1.42×10^6 CFU/cm^2). So QCM-D is a reasonable and reliable method for evaluating bacterial adhesion.

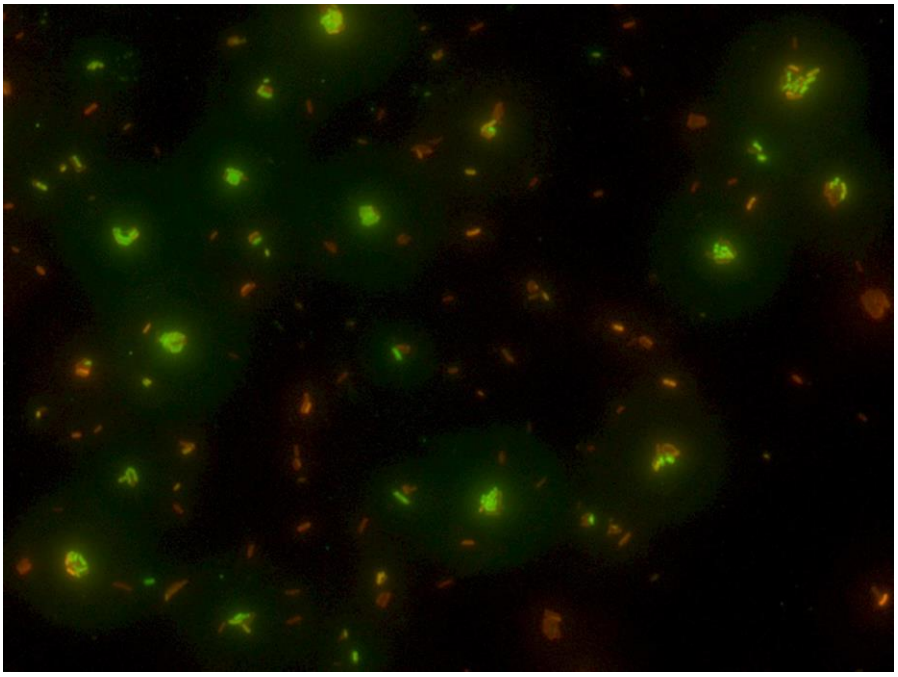

Figure 6.16 Fluorescence microscopy photo of bacterial adhesion on stainless steel coated sensor.

6.1.3.3 Effect of concentration of bacterial suspension on bacterial adhesion

Figure 6.17 shows the effect of bacterial concentration (*E.coli* suspensions:10^6 CFU/ml and 10^5 CFU/ml) on bacterial adhesion on DLC coated surface. Clearly more bacteria attached to the DLC coated sensor surface in the higher bacterial concentration.

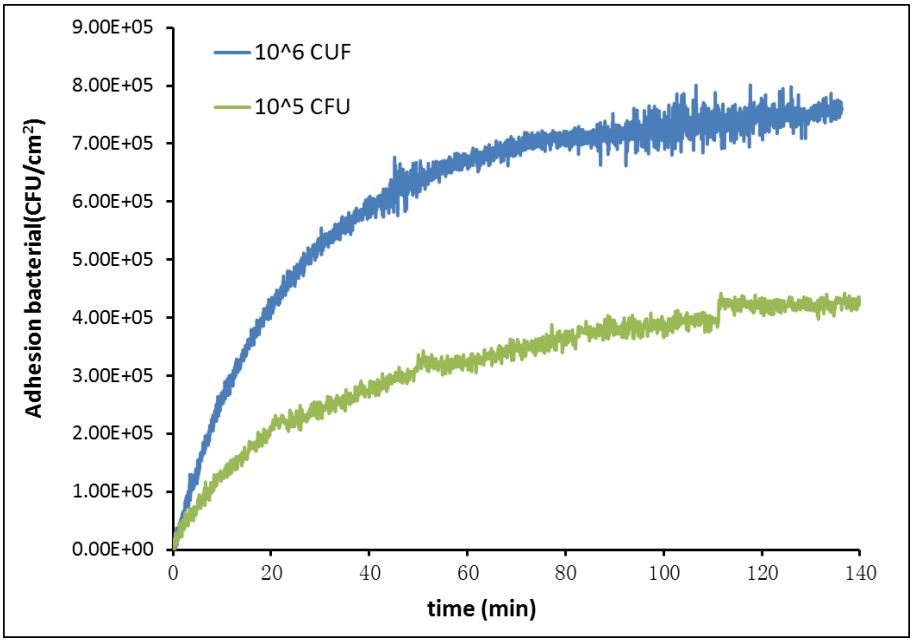

Figure 6.17 Effect of bacterial concentration (10^6 CFU/ml and 10^5 CFU/ml) on bacterial adhesion on DLC coated surface

6.1.3.4 EDLVO modelling and QCM-D measurements

In order to explain the bacterial adhesion behavior obtained by the QCM-D measurements, the interaction energy between the *E. coli* and the coated sensors with ss, DLC and gold was computed using the EDLVO theory. The surface energy components and the zeta potentials of the 3 coatings are given in Table 6.3. for EDLVO modeling. The characteristic wavelength of the interaction λ was taken as 0.6nm.

	γ^{LW} （mJ/m^2）	γ^{+} （mJ/m^2）	γ^{-} （mJ/m^2）	ζ （mv）
stainless steel	43.9	0.1	10	-40
DLC	41.9	0.04	21	-40
gold	32.3	0	40	-40

Table 6.3 Surface energy components and zeta potentials of the coatings

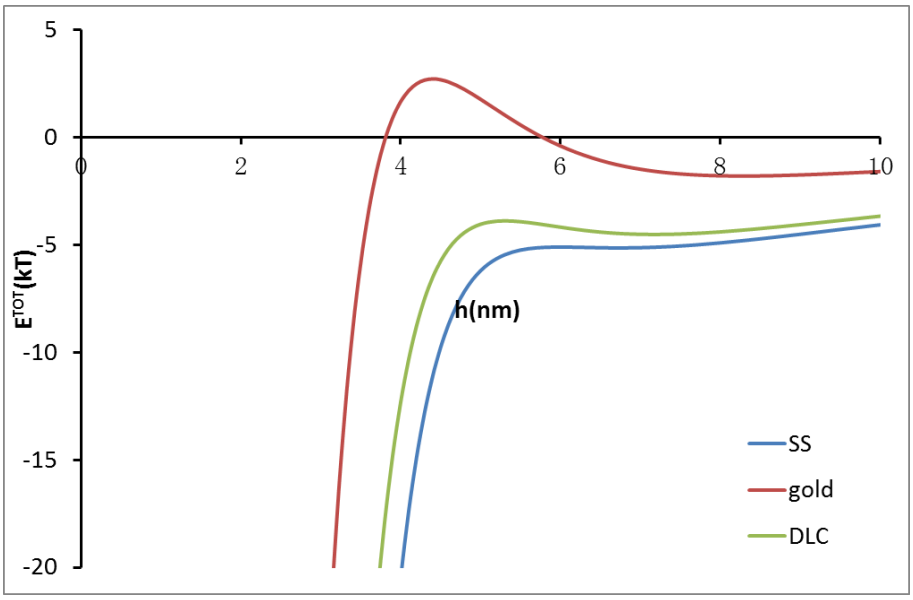

Figure 6.18 Interaction energy between *E. coli* and the coatings as function of separation distance (h)

Figure 6.18 shows interaction energy between the bacterium *E. coli* and the coatings (ss coating, DLC coating and gold coating) as function of separation distance (h). Clearly the total interaction energy changes in the following order: gold coating > DLC coating > stainless steel (ss) coating. According to the EDLVO theory that bacterial adhesion decreases with total interaction energy increasing, the numbers of adhered bacteria (or bacterial surface density) increases in the following order: gold coating < DLC coating < stainless steel (ss) coating. Therefore the modelling results with the EDLVO theory explain the experimental results shown in Figure 6.15.

Figure 6.18 also illustrates that the primary interaction energies is at the closest separation distance of 0.157 nm and the secondary interaction energies is at the separation distance of about 7nm. In order to further investigate the effect of total

interaction energy on bacterial adhesion, the interaction energy between *E.coli* and the coatings was computed at the separation distance 0.157 nm and 7 nm, respectively, as shown in Figure 6.19 and Figure 6.20. The results show that the the number of adhered bacteria on the 3 coated surfaces decreased with the increase of total interaction energies (E^{TOT}), which is consistent with the extended DLVO theory.

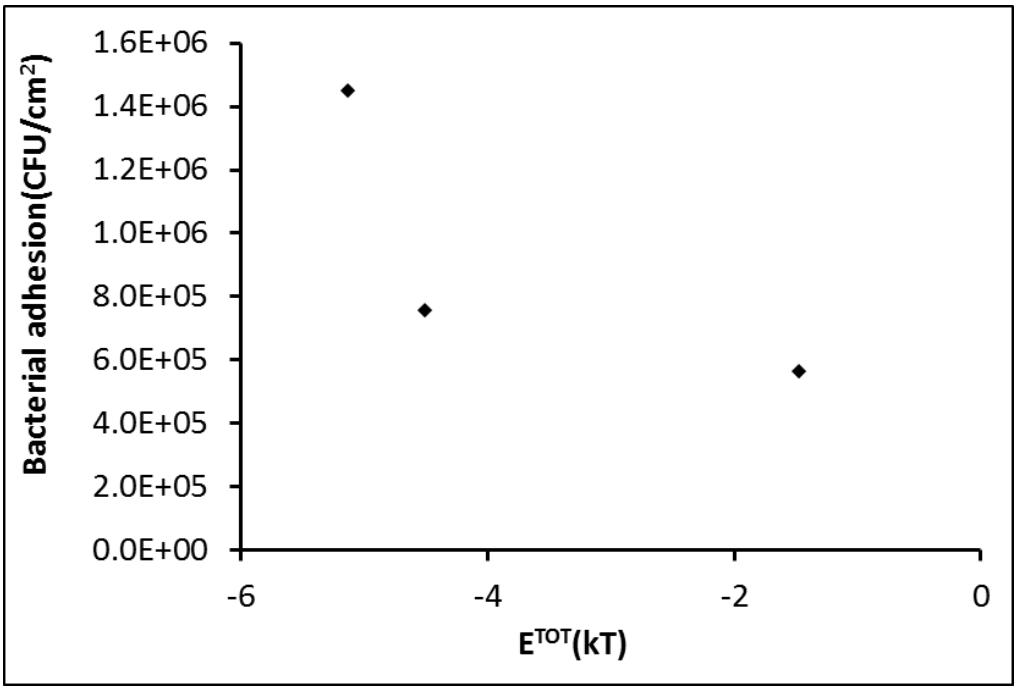

Figure 6.19 Effect of interaction energies on *E.coli* adhesion at H = 7 nm.

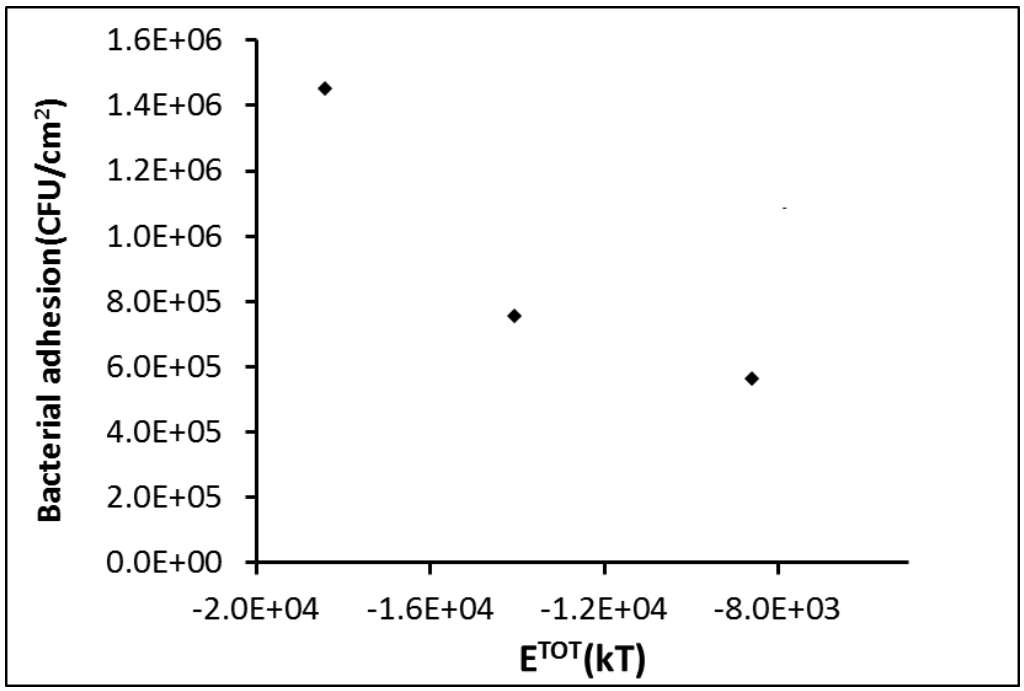

Figure 6.20 Effect of interaction energies on *E.coli* adhesion at H =H_0=0.157 nm.

6.1.4 Electrochemical corrosion test

The anti-corrosion performance of the Si-doped DLC coatings and F-doped DLC coatings was measured using the CS300 Electrochemistry Workstation. The anti-corrosion performance of standard DLC coating and stainless steel was also measured for comparison.

6.1.4.1 Open circuit potential

Figure 6.21 and Figure 6.22 are the open circuit potential curves of the coatings measured by the CS300 Electrochemistry Workstation. The open circuit potentials of the coatings varied in a relatively large range in the first 1 hour, and then the potential

values became stable at certain levels. For 316L stainless steel, its open circuit potentials in both PBS solution and 3.5 wt.% seawater decreased at first, and then stayed at about -227.7 mV and -93.5mV respectively. For the DLC coating, the open circuit potential in PBS solution raised to about -112.3 mV and then showed a very slight decreasing trend, while, its open circuit potential in seawater had an obvious decreasing trend from +100mV to about -93mV. The open circuit potentials of most Si doped DLC coatings increased and reached the values of -72mV and -19.2mV in PBS and seawater respectively. The open potential curves of F doped DLC coatings had the most dramatic increase trends, and the final stable values are also the highest, and are at about 26.6mV and 81.4mV in the two electrolytes. Therefore, compared with uncoated 316L stainless steel, the DLC coating and Si- and F- doped DLC coatings can effectively improve the surface electrochemical stability in both PBS and seawater.

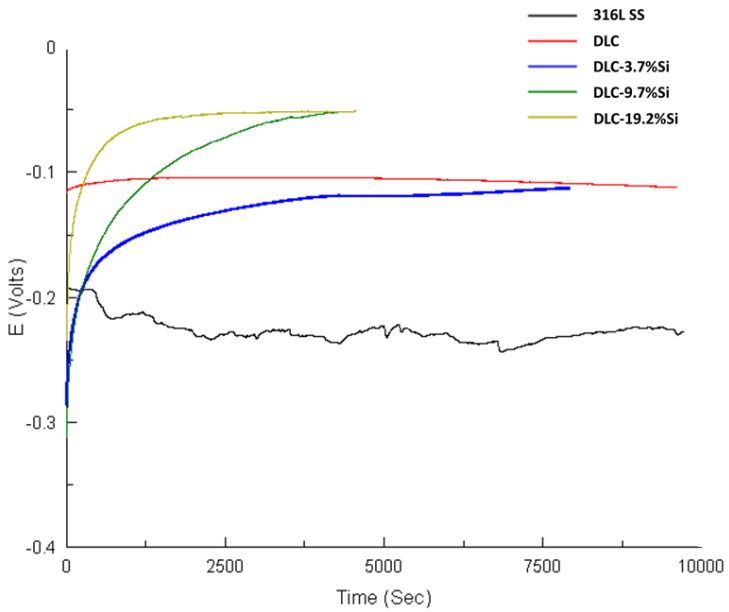

Figure 6.21-(A) Open circuit potential curves of Si doped DLC coatings, DLC coating and 316L stainless steel in PBS solution

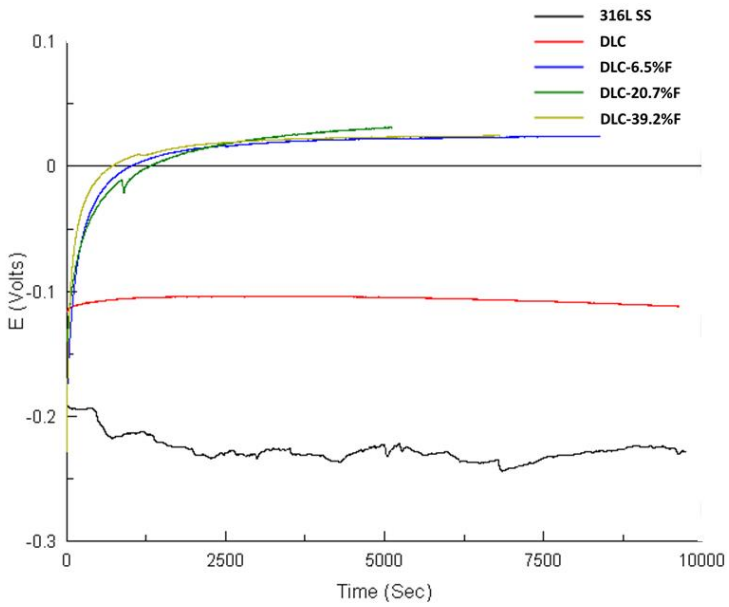

Figure 6.21-(B) Open circuit potential curves of F doped DLC coatings, DLC coating and 316L stainless steel in PBS solution

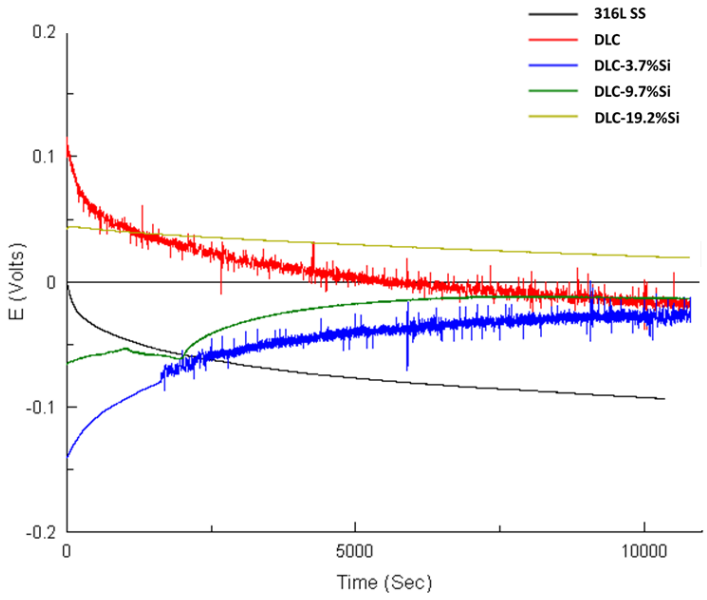

Figure 6.22-(A) Open circuit potential curves of Si doped DLC coatings, DLC coating and 316L stainless steel in 3.5 wt.% seasalt solution.

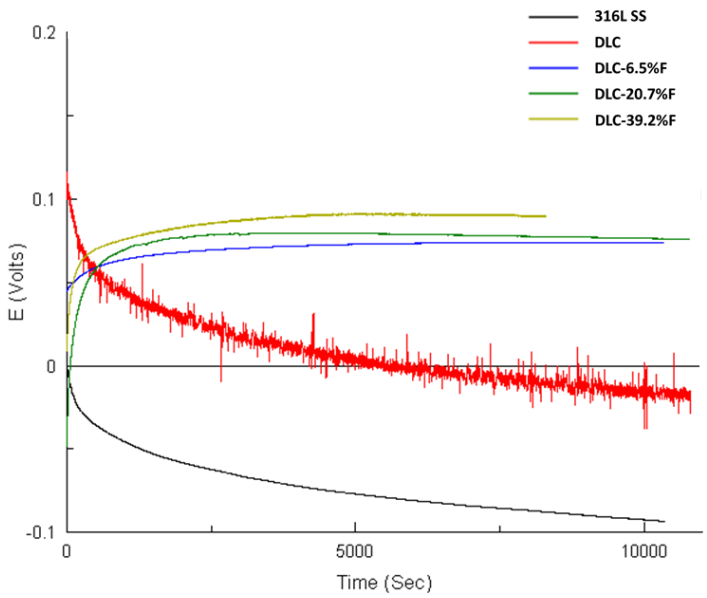

Figure 6.22-(B) Open circuit potential curves of F doped DLC coatings, DLC coating and 316L stainless steel in 3.5 wt.% seasalt solution.

6.1.4.2 Potentiodynamic polarization test

The potentiodynamic polarization curves of the coatings are shown in Figure 6.23 and Figure 6.24, and the analysis results by Corrview Software are listed in Table 6.3 and Table 6.4 respectively. Among the electrochemical parameters in the Tables, the corrosion current density (I_{corr}) is the most important in evaluating the corrosion resistance of materials, in addition to corrosion rate. The smaller corrosion current density (I_{corr}) indicates a better corrosion resistance of material, because the corrosion current is from the dissolution of metal caused by corrosion.

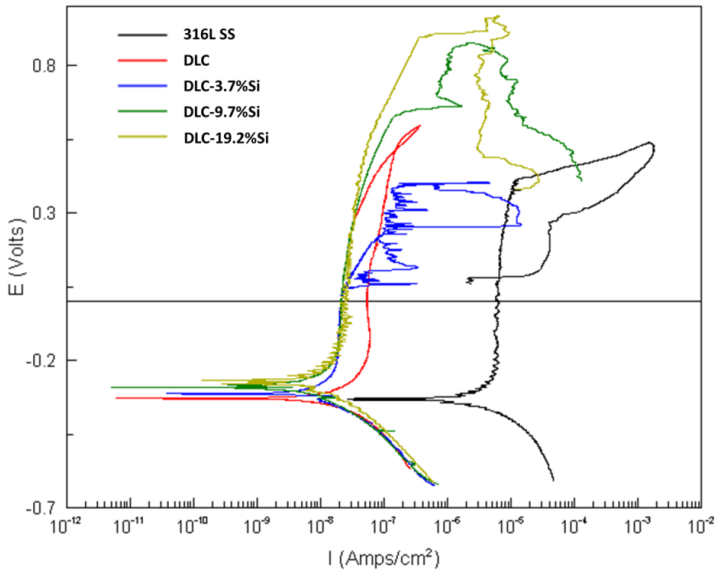

Figure 6.23-(A) Polarization curves of 316L stainless steel, DLC and Si doped DLC coatings in PBS.

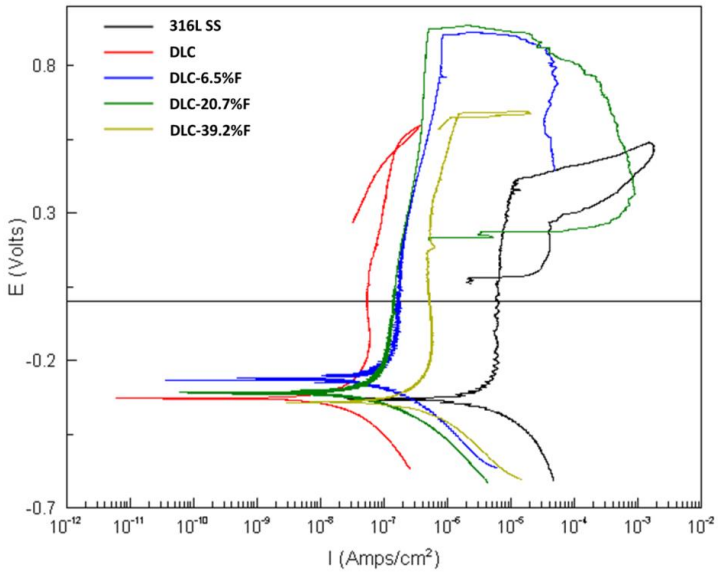

Figure 6.23-(B) Polarization curves of 316L stainless steel, DLC and F doped DLC coatings in PBS.

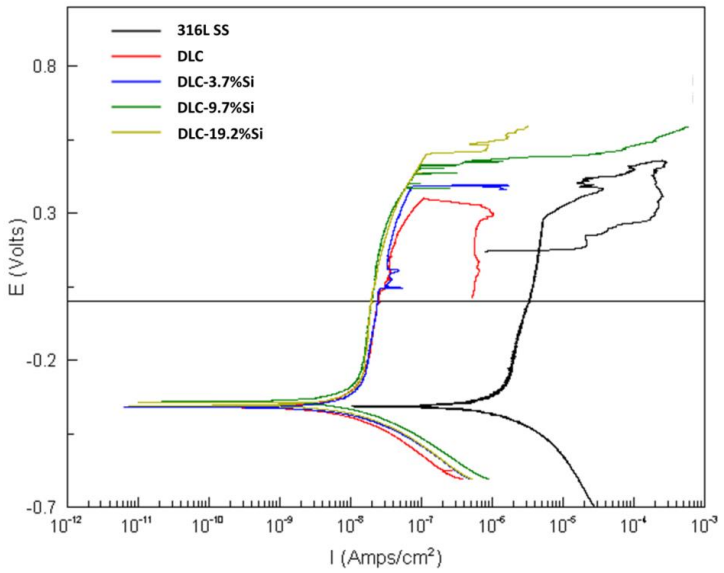

Figure 6.24-(A) Polarization curves of 316L stainless steel, DLC and Si doped DLC coatings in 3.5 wt.% seasalt solution.

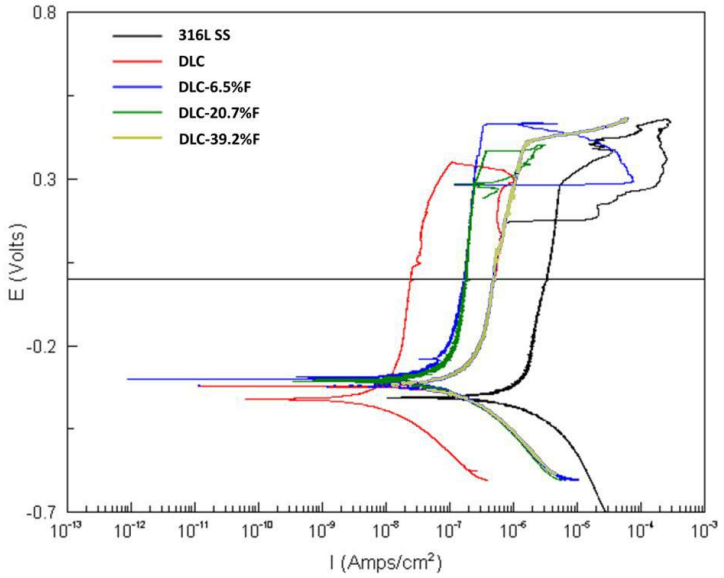

Figure 6.24-(B) Polarization curves of 316L stainless steel, DLC and F doped DLC coatings in 3.5 wt.% seasalt solution.

Sample	β_a (mV/dec)	β_c (mV/dec)	I_{corr} ($\mu A/cm^2$)	E_{corr} (mV)	R_{Corr} (µm/a)
316L SS	146.6	96.5	0.91	-327.9	10.6
DLC	169.8	118.5	0.014	-319.2	0.16
DLC-3.7%Si	288.7	132.9	0.011	-313.7	0.12
DLC-9.7%Si	220.2	156.9	0.008	-285.4	0.09
DLC-19.2%Si	114.4	98.2	0.008	-265.4	0.09
DLC-6.5%F	201.0	132.8	0.08	-260.0	0.9
DLC-20.7%F	209.8	177.3	0.12	-308.4	1.40
DLC-39.2%F	202.7	114.3	0.29	-340.7	3.39

Table 6.3 Electrochemical parameters captured by Tafel method extrapolation on the coatings in PBS.

Sample	β_a (mV/dec)	β_c (mV/dec)	I_{corr} ($\mu A/cm^2$)	E_{corr} (mV)	R_{Corr} (µm/a)
316L SS	322.2	134.6	0.91	-345.0	10.6
DLC	272.1	177.3	0.017	-361.3	0.20
DLC-3.7%Si	196.1	94.7	0.006	-360.0	0.07
DLC-9.7%Si	191.3	87.3	0.006	-350.0	0.06
DLC-19.2%Si	144.3	87.9	0.005	-353.5	0.05
DLC-6.5%F	709.8	131.4	0.08	-297.5	0.97
DLC-20.7%F	476.8	333.0	0.17	-303.4	2.0
DLC-39.2%F	428.1	107.2	0.24	-322	2.84

Table 6.4 Electrochemical parameters captured by Tafel method extrapolation on the coatings in 3.5 wt.% solution.

The corrosion rate (R_{Corr}) can be calculated by Faraday's laws of electrolysis:

$$\Delta m = (\frac{Q}{F})(\frac{M}{n}) \quad (6.2)$$

where Δm is the mass of dissolved metal at anode during corrosion process, Q is the quantity of electricity in corrosion process, F is the Faraday constant = 96485 C/ mol (or A s/mol). M is the molar mass of the substance and n is the valency number of ions of the substance (electrons transferred per ion).

$$\Delta m = \rho R_{corr} S t \quad (6.3)$$

$$\frac{QM}{Fn} = \rho R_{corr} S t \quad (6.4)$$

$$\frac{I_{corr} StM}{Fn} = \rho R_{corr} S t \quad (6.5)$$

$$R_{corr} = \frac{I_{corr} M}{n \rho F} \quad (6.6)$$

R_{corr} is the corrosion rate, which is usually described in mm per year (mm/a) or μm per year (μm/a) in electrochemical corrosion test. And ρ is the density of metals; t is corrosion time and S is the area of the working electrode. For steel metals, like carbon steel and stainless steel:

$$R_{corr} (mm/a) = 11.73 * I_{corr} (mA/cm^2) \quad (6.7)$$

$$MPY = 39.37 * mm/a \quad (6.8)$$

$$R_{corr} (MPY) = 462.2 * I_{corr} (mA/cm^2) \quad (6.9)$$

Table 6.3 and Table 6.4 indicate that the corrosion rates of 316L stainless steel in both PBS and seawater were about 10.6 μm/a; while the corrosion rates of DLC, Si doped DLC coatings and F-doped DLC coatings were only 0.16-0.20μm/a, 0.05-0.12

μm/a and 0.9-3.39μm/a, respectively. The Tables also show that the corrosion rates of the F-doped DLC coatings increased with F content increasing.

The corrosion standard of industrial stainless steel is not higher than 25μm/a (1MPY), the tolerable corrosion rate for metallic implant systems is even more stringent and should be about 0.25μm/a (0.01 MPY). (Mohanty M *et al*., 2003). So based on our test results, the 316L stainless steel fail to meet the demand of the biomaterial in vivo environment, while DLC coating and Si doped DLC coatings are qualified in this indicator. Therefore, it is very necessary to modify the 316L stainless steel with DLC type coating for medical application.

When the corrosion current densities of samples are similar, the corrosion potential is another electrochemical parameter should be taken into consideration. The corrosion potential is representation of the energy barrier in corrosion process, the higher corrosion potential indicates that the occurrence of corrosion has to overcome higher energy barrier and the corrosion resistance is better. The corrosion potentials of different Si/F doped DLC coatings were higher than that of DLC coating, but the differences were not significant. For Si doped DLC coatings, the increasing Si content in DLC coating slightly raised the corrosion potential (-313 to -262 mV in PBS and -361 to -350 mV in seawater), while the higher F content in DLC coating had the opposite effect, namely decrease the corrosion potential (-260 to -340 mV in PBS and -297 to -322mV in seawater). Based on above measurement results, the performances of corrosion resistance of Si/F doped DLC coatings are showed as:

DLC-19.2%Si> DLC-9.7%Si> DLC-3.7%Si

DLC-6.5%F > DLC-20.7%F> DLC-39.2%F

It can be seen clearly that all DLC and doped DLC coatings significantly improved the corrosion resistance of 316L stainless steel, but anti-corrosion performance of the DLC and the doped DLC coatings were different. Since the DLC and doped DLC coatings were prepared by same technology, the coating qualities, including thickness, roughness, and defects and so on, were similar, the different corrosion resistances of the coatings were caused by the doped elements and their contents. The essence of the DLC and doped DLC coatings with the improved corrosion resistance is due to the decrease in the corrosion current density. The chemical inert DLC coatings have very low conductivity, and can hinder the electron transport and the exchange of electrical charges at the samples-electrolyte interface, which are very necessary in the corrosion process (Annett DR *et al.*, 2004). The DLC type coatings in the research were generally metastable amorphous carbon materials (have no dominant crystalline lattice structure) and consist of a mixture of graphite phase (sp^2) and diamond phase (sp^3). It was found that the mechanical properties, like rigidity hardness, fracture toughness, wear resistance and friction resistance, are controlled by sp^3 regions, and the electronic properties of DLC coating, such as band gap and conductivity, are controlled by the sp^2 regions (Robertson J, 2002). The DLC coating with higher sp^3/sp^2 ratio possesses lower conductivity and better corrosion resistance. For Si doped DLC coatings, because silicon cannot form π bonds (Demichelis F *et al.*, 1992), doping Si into DLC coating can increase the sp^3/sp^2 ratio, thereby reach the better corrosion resistance than

original DLC coatings, and the effect raises with Si content increasing. While, doping F element was found can increase the number of sp^2 bonds and the formation of sp^2 clusters in the amorphous network, and the DLC coating becomes more graphitic with the increase of F content (Yu GQ *et al.*, 2003). So, compared with the DLC coatings and Si doped DLC coatings, F doped DLC coatings have weaker corrosion resistances, which decrease with the F content increasing. The corrosion rates of the coatings are consistent with these conclusions.

6.1.4.3 Breakdown potential (E_b) and protection potential (E_p)

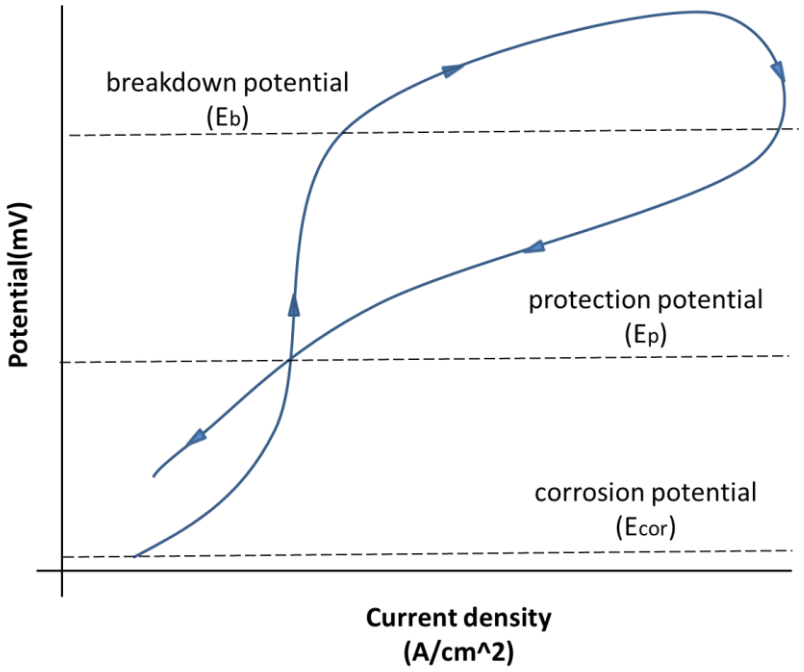

Figure 6.25 Idealized cyclic polarization curve (anodic polarization region) in indicating breakdown potential and protection potential.

Figure 6.25 shows the typical cyclic curve (anodic polarization region) in determining

the breakdown potential and protection potential of test sample. The breakdown potential, which is also referred as pitting potential, is defined as a potential limit where the growth of pits corrosion happen above and a passive film is maintained below (Galvele JR, 2005). So the breakdown potential can indicate the difficulty to break the surface passivation film of metal materials for corrosion attack, and the metal having the higher breakdown potential can maintain a more stable and complete passivation film, which is significant in inhibiting and delaying growth of the pitting corrosion (Frankel GS, 1998). There are also related reports about the fewer pits on stainless steel are due to higher pitting potentials (Leckie HP, 1966). Therefore, the breakdown potential (E_b) is considered as the criterion for evaluating pitting corrosion resistance of materials.

Protection potential (E_p), also called the repassivation potential, is the electrochemical parameter to describe the material's self-recovery capability of surface passivation film after the occurrence of pitting corrosion. Protection potential is the potential at which the reverse scan reaches the anodic polarization curve (passive region). If the hysteresis loop does not close, protection potential (E_p) can be estimated by extrapolating the reverse scan to zero current density. The protection potential (E_p) is influenced by many different factors, including the metal materials, electrolyte environment and also material surface topography (Wilde BE, *et al.*, 1971), so not all the metal materials can steadily show their protection potentials (E_p) in electrochemical corrosion tests. It is generally considered that, after the occurrence pitting corrosion, once the corrosion attack become weak, the metal material having protection potential can repassivate to

repair the surface passivation layer, thereby impede the growth of pitting corrosion and even repair the pitting corrosion holes. So, the protection potential (E_p) is another reference parameter can be used to evaluate the corrosion resistance of metal materials.

Table 6.5 and Table 6.6 are the breakdown potential (E_b) and protection potential (E_p) of the coatings in PBS and seawater. As illustrated, in both PBS and artificial seawater, the breakdown potentials (E_b) of DLC coating and Si/F doped DLC coatings were generally higher than those of 316L stainless steel. Doping more Si in DLC seemed can raise the breakdown potentials (E_b), while the effect of doped F content on breakdown potential (E_b) did not display a clear trend. DLC-19.2%Si and DLC-20.7%F have the highest breakdown potentials in PBS, which were about 500 mV higher than that of uncoated 316L stainless steel.

On the side of protection potential, 316L stainless steel had the protection potential in PBS and seawater, while the DLC coating just showed the protection potential in PBS. And most of the Si doped DLC samples showed no protection potential in both electrolytes, compared with this, the F doped DLC samples showed more stable and better repassivation abilities.

So, DLC type coatings can effectively protect 316L stainless steel from pitting corrosion, furthermore doping more Si and appropriate amount F elements into DLC coating can make further improvement on the pitting corrosion resistance. Compared

with uncoated 316L stainless steel, most of DLC type coatings did not show remarkable advantage on protection potential, but doping F elements seemed can improved the repassivation abilities of DLC coating.

Sample	E_b (mV)	E_p (mV)
316L SS	403	76
DLC	566	518
DLC-3.7%Si	392	246
DLC-9.7%Si	640	-
DLC-19.2%Si	893	-
DLC-6.5%F	892	320
DLC-20.7%F	925	207
DLC-39.2%F	640	631

Table 6.5 Breakdown potential and protection potential of test samples in PBS.

Sample	E_b (mV)	E_p (mV)
316L SS	280	132
DLC	348	-
DLC-3.7%Si	391	-
DLC-9.7%Si	460	-
DLC-19.2%Si	503	-
DLC-6.5%F	464	284
DLC-20.7%F	378	288
DLC-39.2%F	411	-

Table 6.6 The breakdown potential and protection potential of test samples in 3.5 wt.% seasalt solution.

6.1.4.4 Effect of corrosion electrolyte

As PBS and 3.5 wt.% seasalt solution were adopted as the electrolyte in our electrochemical corrosion tests, the effects of electrolyte on corrosion were also studied. By comparing the electrochemical corrosion parameters of test samples, it can be found that the same test sample did not show great difference on corrosion potential and corrosion rate in PBS and seawater. But the breakdown potential of the sample in seawater was much lower than that in PBS, which indicates the passivation layer in seawater is easier to be upset. And fewer samples showed their protection potential in seawater, so there seems to be a lower likelihood for the breakdown of passivation layer to heal in seawater.

This phenomenon should be contributed to the high chlorine ion concentration in seawater, which is considered can interference the stability of passivation layer, although there are still debates about its mechanism, the related explanations are mainly on two theories:

(1) Penetration mechanism. As having tiny ionic radius and aggressive penetration ability, chloride ions can penetrate the passivation layer through the inherent defects and pores on it.(Kimberly E *et al.*, 1997) Therefore, chloride ions can reach the metal-passivation layer interface and form soluble chlorides with metal, thereby

change the structure of passivation layer and lead the passivation become less firm than original.

(2) Adsorption theory. This theory is based on the notion of competitive adsorption of chloride ions and dissolved oxygen.(Uhlig HH, 1950) Compared with dissolved oxygen, the chloride ions are easier to be adsorbed by metal, thereby exclude some dissolved oxygen, which determine the metal passivation, from metal surface. Chloride ions can compete for more adsorption sites on metal surface, and even can replace the passivated ions adsorbed by metal, so accelerate the breakdown of the passivation layer.

6.2 Influence of surface micro/nanostructure on bacterial adhesion

6.2.1 Interaction energy between bacteria and surfaces

6.2.1.1 Interaction energy between rod bacteria and flat surface

As *E. coli* WT (F1693) from the Institute of Infection and Immunity, Nottingham University, UK was used for bacterial adhesion assay in this study, the interaction components (E_{132}^{LW} , E_{132}^{EL}, E_{132}^{AB}) and total interaction energy (E_{132}^{TOT}) between the rod-shaped *E. coli* and the flat PDMS surface 2 in water 3 as a function of separation distance *h* were computed using the equations in section 5.2.2, as shown in Figure 6.26.

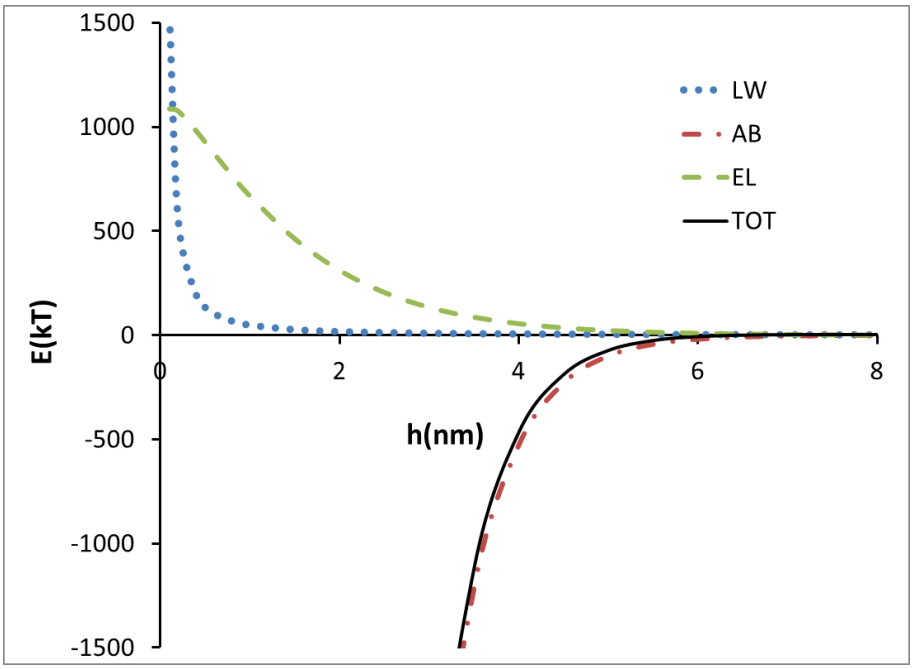

Figure 6.26 Interaction energies between *E.ciol* and flat PDMS surface in water as function of suspension distance h.

The correlation length of the molecules of the water medium λ was taken as 0.6 nm in the calculations. The interaction energies E_{132}^{LW} and E_{132}^{EL} decreased with the separation distance h increasing. The both curves approached the horizontal axis of interaction energy =0 when h > 7 nm; while the interaction energy E_{132}^{AB} increased with h increasing and the curve also approached the horizontal axis when h > 7 nm. Clearly the total interaction energy (E_{132}^{TOT}) curve was very close to the AB interaction energy (E_{132}^{AB}) curve and the two curves almost overlapped. This means that the E_{132}^{AB} component made a major contribution to the total interaction energy E_{132}^{TOT}. Figure 6.26 also indicated that when h was less than 3 nm, the total interaction energy E_{132}^{TOT} dropped sharply with h decreasing. When $h = h_0$, the total interaction energy E_{132}^{TOT} was lowest.

6.2.1.2 Interaction energy between rod bacteria and nanocube array surface

The total interaction energy (E_{132}^{TOT}) between the rod-shaped *E. coli* 1 and the nanocube array surface 2 in water 3 as functions of separation distance *h* and the edge length "*a*" were computed using the equations in Section 5.2.3 (see Figure 5.2 for the nanocube array). If the space distance "a" between the cubes is larger than bacterial radius (R), the computing mode is not so applicable, because the *E. coli* bacteria will be likely to fall into the gaps, and the adhesion situation is similar to that on flat surface. The radius of *E.coli* (R) is about 500-1000nm, Figure 6.27-(A) and Figure 6.27-(B) illustrate the effects of the edge length "a" on the total interaction when bacterial radius (R) was taken 500nm and 1000nm respectively. It can be seen that the total interaction energy E_{132}^{TOT} increased with the suspension distance *h* increasing, when $h = h_0$, the total interaction energy E_{132}^{TOT} was lowest. The modeling results also revealed that the edge length "*a*" had a significant influence on the total interaction energy E_{132}^{TOT}. When the edge length "*a*" was in the range of 0-350 nm, the E_{132}^{TOT} value increased with "*a*" increasing and reached maximum at "*a*" = 350 nm; for the edge length "*a*"> 350nm, when taking different bacterial radius (R), the effects of "*a*" were different, but generally speaking, the E_{132}^{TOT} value is close to or lower than that of "*a*" = 350nm. Furthermore in our observation, the radius of the *E. coli* WT used in our test was about 500nm, so Figure 6.29-(A) was more close to our situation. When *h*>3 nm, the difference was not obvious. After scaling up, the difference became obvious, and Figure 6.28 shows the effect of edge length "*a*" of cubes on the total interaction

energy E_{132}^{TOT} for h = 4 nm when bacterial radius is taken as 500nm. According to the extended DLVO theory, bacterial adhesion decreases with total interaction energy increasing, so the modeling results indicated that the optimum "a" value for inhibiting the adhesion of *E. coli* WT was about 350 nm. Based on the computed optimum "a" with the highest total interaction energy (E_{132}^{TOT}) value, a range of nanocube arrays were designed and produced for further bacterial adhesion tests.

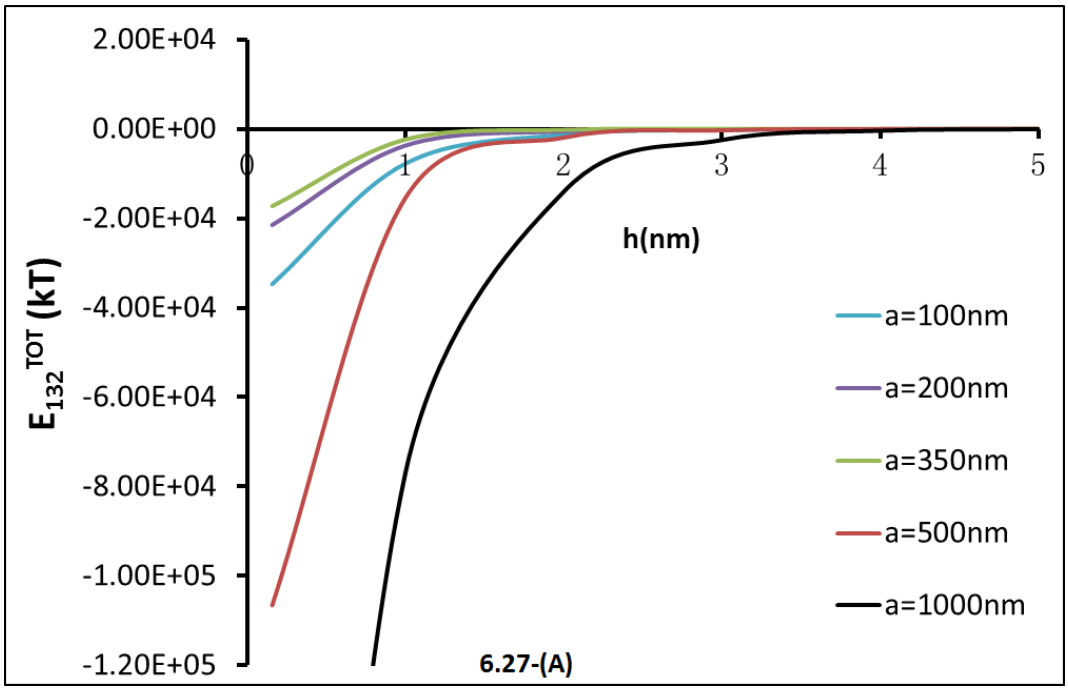

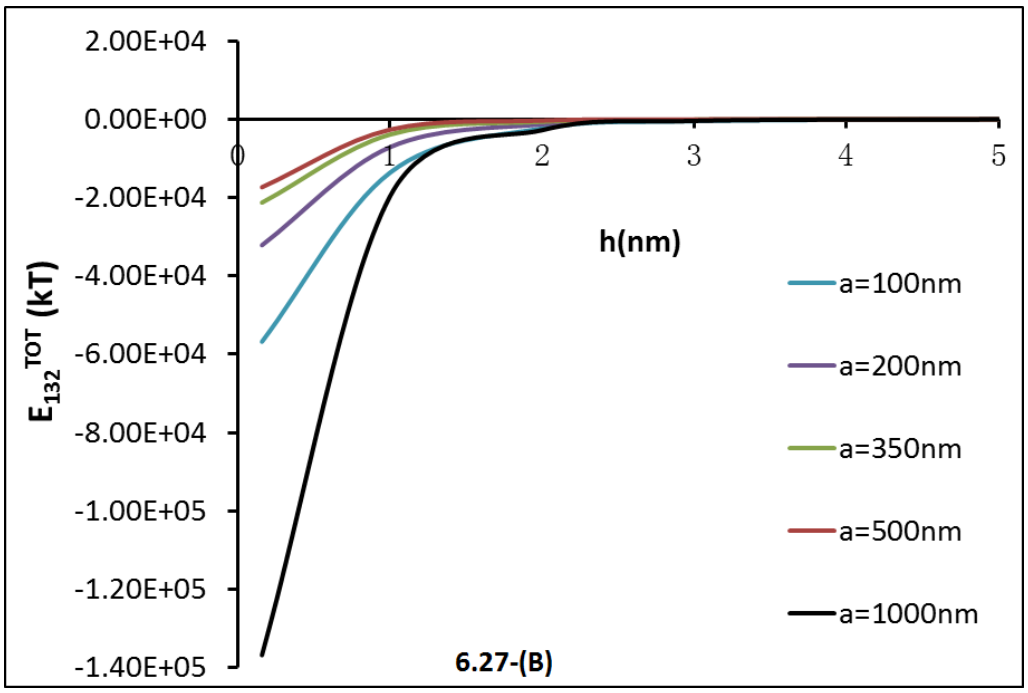

Figure 6.27 Total interaction energy E_{132}^{TOT} between *E.ciol* and nanocube array PDMS surface in water as function of suspension distance *h*. (A): when R=500nm; (B): when R=1000nm

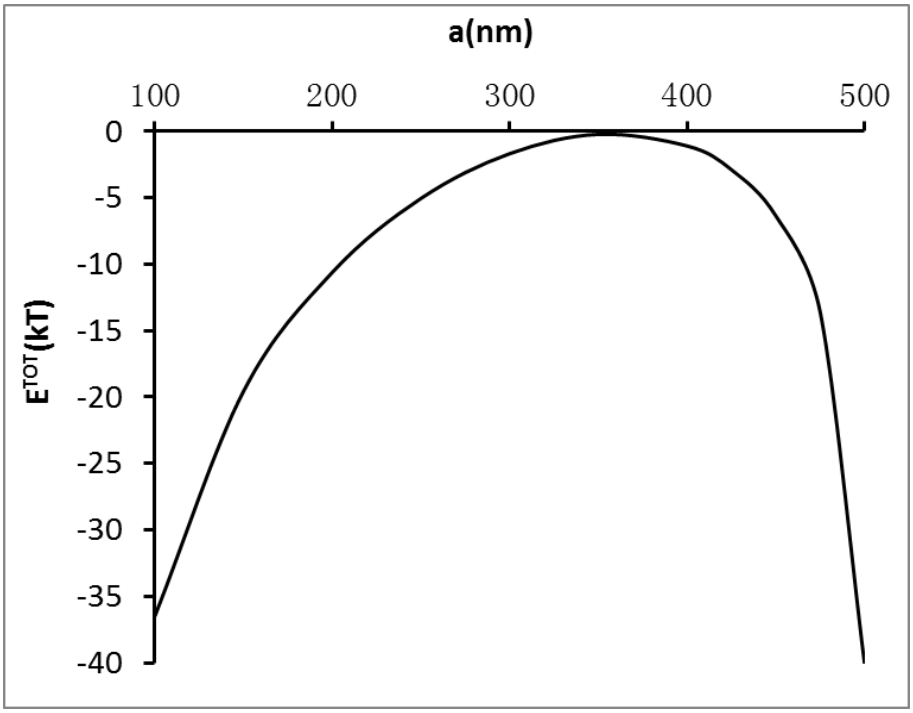

Figure 6.28 Effect of the edge length "*a*" of a cube in nanocube array on the total interaction energy E_{132}^{TOT} for h = 4 nm when bacterial radius is taken as 500nm.

6.2.2 Surface topography by SEM

Figure 6.29 shows the SEM images of the two types of nanocube arrays with the cube edge length of 1000nm and 350 nm respectively. It can be seen that structures with different feature sizes are clear and neat, the measured edge lengths have been listed in Table 2.1, which are close to the design values, so the formation situation of surface pattern is satisfactory and in general met our preliminary design requirements. But it should also be noticed that there are some difference between the sample surface pattern and design. At first, the cubes are trend to be rounded rectangle, this phenomenon was mainly caused by the optimization of making the silicon master by the BFI, which can reduce the technical difficulties and cost, but do not affect original design intention. Furthermore, the PDMS samples with smaller structure pattern showed more deformations and defects. Of cause, there were also some failure samples. As shown by Figure 6.30, unfortunately, the 500nm (B) silicon master was broke for lack of experience of cleaning silicon master and preparing PDMS sample in a high temperature, so the final PDMS sample with 500nm (B) pattern showed some micro-nanostructure structure but the formation situation was bad.

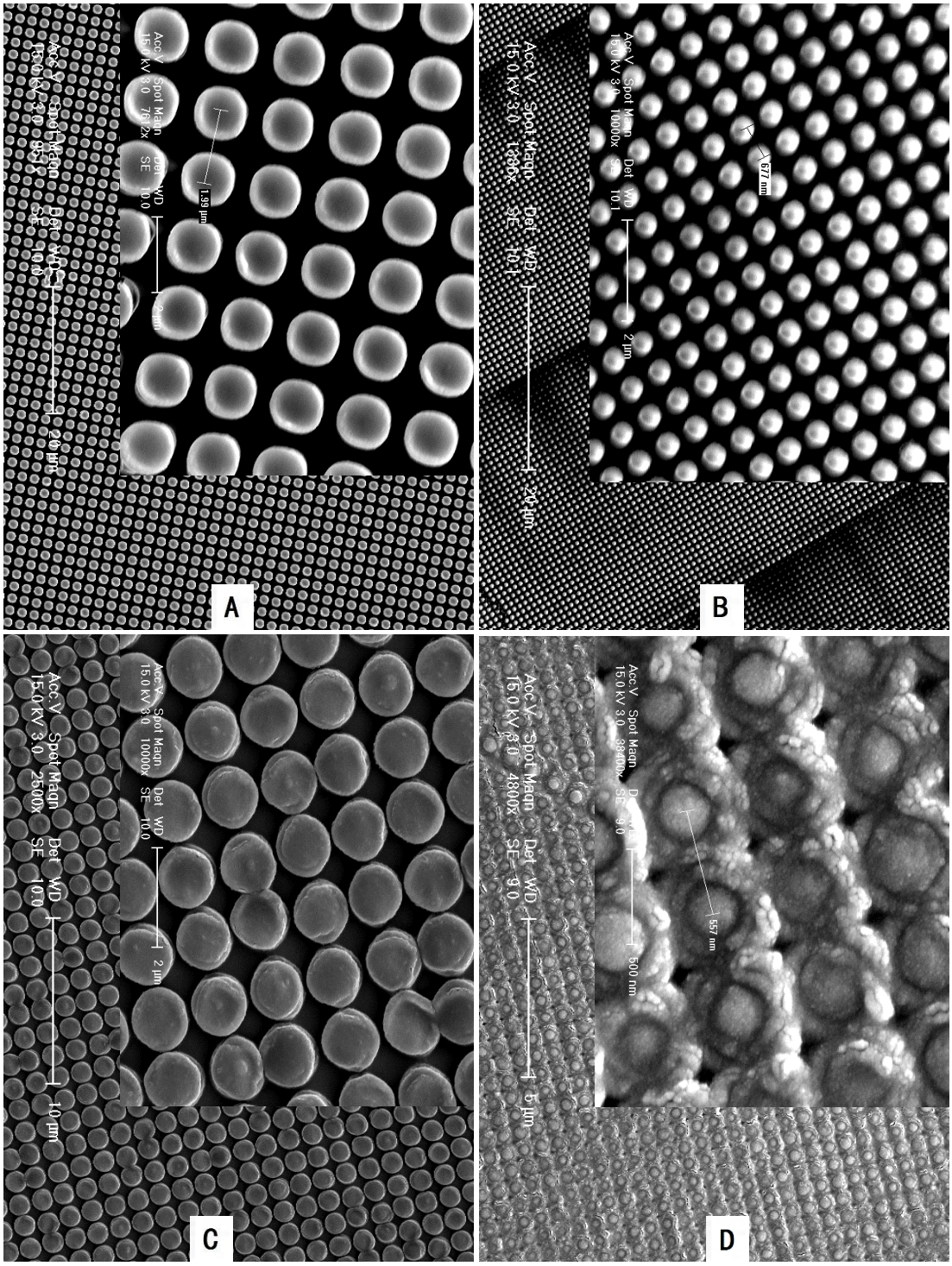

Figure 6.29 SEM of PDMS samples: (A):1000nm A; (B):350nm A; (C):1000nm B; (D): 350nm B

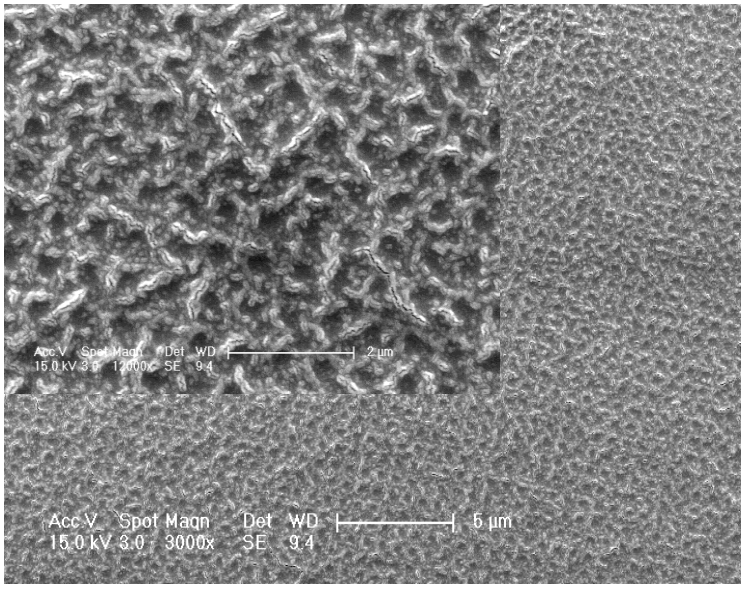

Figure 6.30 SEM of the 500nm B sample with bad formation situation

6.2.3 Contact angle

Cassie raised the Cassie wetting state model (showed in Figure 6.31) to investigate the effect of surface roughness or topography on contact angle, and he presented the following equation

$$\cos\theta^{c} = f(\cos\theta_{o} + 1) - 1 \tag{6.10}$$

Here, θ_o is the standard contact angle of original smooth surface, θ^c is theoretical contact angle of rough surface, f is the radio of effective contact area and macro contact area (Cassie ABD *et al.*, 1944). Taking the pattern shape observed from the SEM results into consideration, f_A and f_B for pattern A and B of the PDMS samples are 0.25-0.39 and 0.5-0.78 respectively.

According to the measured contact angle on original smooth PDMS surface (θ_o) and

the f data, the theoretical contact angle θ_r^c for the PDMS samples were calculated, as shown in Table 6.7.

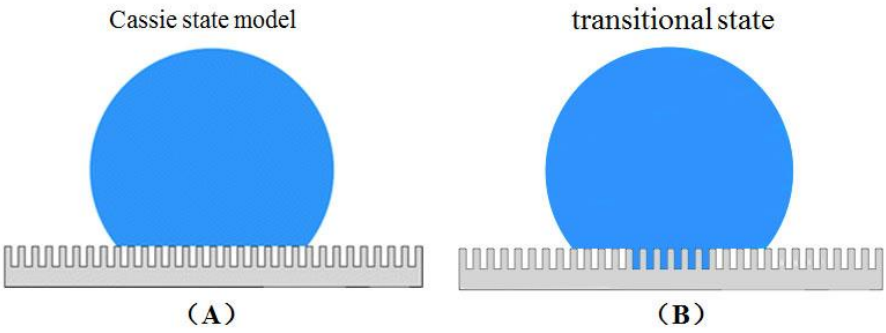

Figure 6.31 Cassie wetting state model

PDMS sample	Theoretical contact angle(°)	Measured contact angle(°)
original	114.70±1.77	
1000nm(a)	144.3±4.1	142.7±0.8
500nm(a)	144.3±4.1	140.2±0.9
400nm(a)	144.3±4.1	138.4±1.0
350nm(a)	144.3±4.1	139.3±0.8
1000nm(b)	128.6±6.1	134.5±0.1
500nm(b)	128.6±6.1	118.4±0.8
400nm(b)	128.6±6.1	130.0±1.4
350nm(b)	128.6±6.1	124.4±2.8

Table 6.7 Theoretical water contact angle and measured contact angles of PDMS samples

The theoretical contact angle of PDMS samples depend on the types of the pattern, but not the feature size. While the measured values of the contact angle are decided by both the pattern type and the feature size. Compared with theoretical values, samples

with smaller feature size have the smaller measured contact angle, which should be contributed to that there are more deformations and defects on their surface.

6.2.4 Effect of micro-nanostructure on bacterial adhesion

In this study, the eight PDMS samples (see Table 6.7) having two types of nanocube arrays in four feature sizes (1000nm, 500nm, 400nm and 350nm) were used in the bacterial adhesion tests and an flat PDMS sample without any special treatment was also assayed for comparison. *E. coli* WT (F1693) with a concentration of 10^6 CFU/ml was used for bacterial adhesion assays. The bacterial adhesion tests were performed for 3 hours and observed by a fluorescence microscopy. Figure 6.32 shows the effect of surface structures on bacterial adhesion. All the patterned PDMS surfaces with nanotube arrays performed better than the plat PDMS surface in inhibiting bacterial adhesion. The density of adhered bacteria decreased with the edge length "*a*" value decreasing, which is consistent to the theoretical modelling results. The nanotube array with "a" = 350 nm performed best, which reduced bacterial adhesion by 60%, compared with the flat PDMS surface. The 500nm B PDMS sample, which has been mentioned before as a fail sample, displayed a relative weak anti-bacterial performance, which may be influenced by the deformations and defects. And pattern A performed better than the pattern B in inhibiting bacterial adhesion.

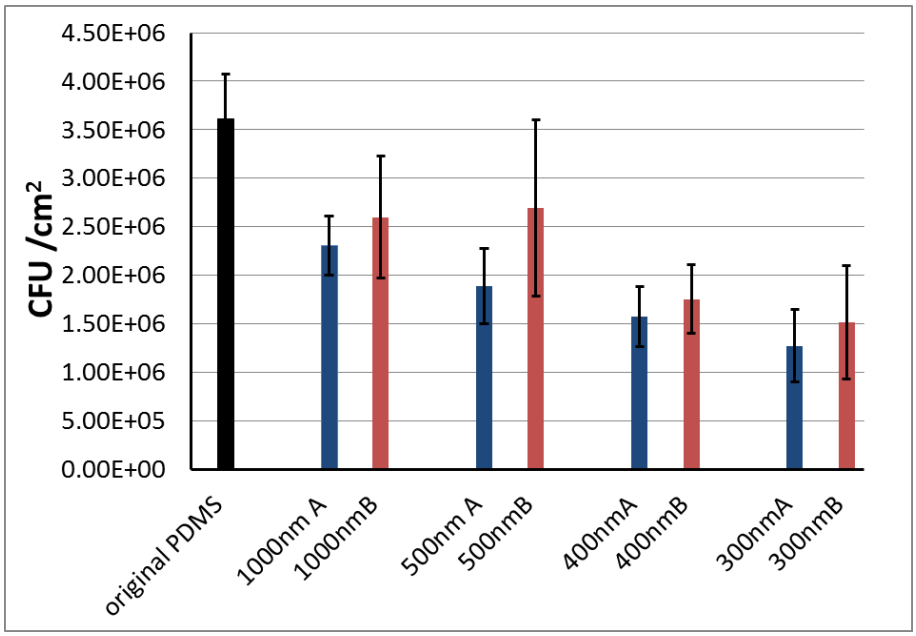

Figure 6.32 Bacterial adhesion on different PDMS samples

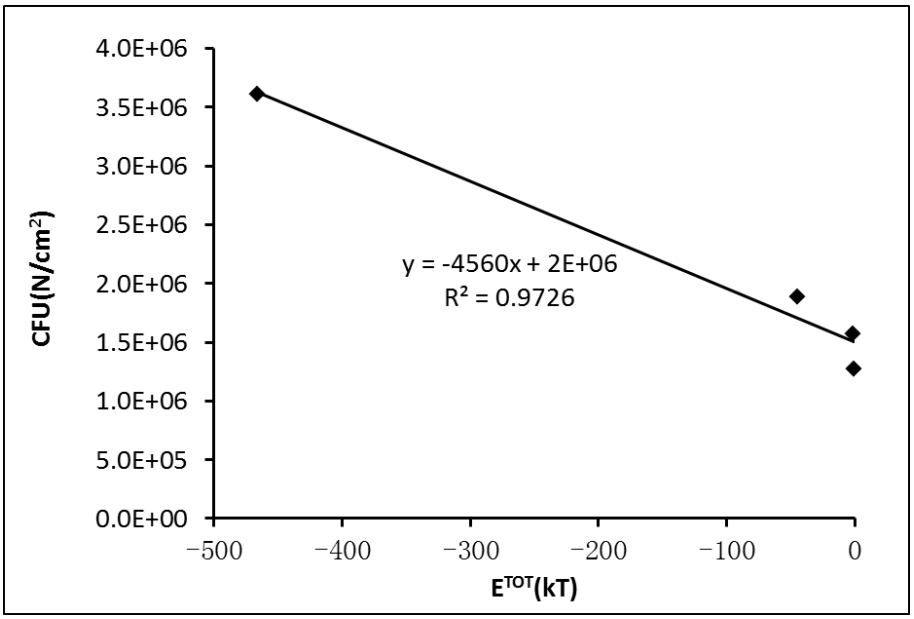

Figure 6.33 Effect of total interaction energy E_{132}^{TOT} on *E. coli* adhesion

Figure 6.33 further shows the effect of total interaction energy E_{132}^{TOT} between the rod-shaped *E. coli* and the PDMS surfaces with the nanotube arrays on bacterial adhesion. The adhered bacteria decreased linearly with the total interaction energy

increasing.

6.2.5 Impact on the attachment mode of bacteria

During the observation by fluorescence microscopy in bacterial adhesion assays, it was found that the surface micro-nanostructure can also affect the adhesion tropism (or direction) of bacteria. Based on the surface pattern, the cube array direction of pattern A was set as the vertical and horizontal directions (0°and 90°, represented as + directions), so the cube array direction of pattern B are 45°and 135° directions (represented as × directions). The clear fluorescence photographs of adhered rod shape *E.coli* on samples (Figure 6.34) were analyzed by Image-Pro Plus software to examine the direction of adhered bacteria. Figure 6.35 is the typical analysis results of bacterial adhesion direction on PDMS samples (flat surface, pattern A and pattern B surface). The percentage of adhered bactera in each direction were counted in three groups, namely + directions (±15°), × directions(±15°) and other directions, as shown in Table 6.8. It can be found from that directions of the adhered bacteria on original PDMS sample were generally random, there showed no special directions that the bacteria prefer to adhere along. But, the bacterial adhesion on PDMS samples with pattern A and pattern B surface structure displayed obvious preference in the adhesion directions. On pattern A PDMS samples, more than half of the bacterial adhered along the + directions, while on pattern B PDMS samples, most of the bacteria preferred to adhere along x directions, so it is obvious that the main adhesion directions of bacteria were

same to the cube array directions of surface pattern. For the samples with 1000nm and 500nm size surface pattern structure, the trends were obvious; while when the structure pattern size decreased to 400nm-350nm, the trends slightly declined. This phenomenon is not a coincidence, the surface pattern and adhered bacteria can be observed simultaneously in the some overexposed fluorescence photographs in the magnification of 1000 (Figure 6.34). It was found that the bacteria preferred to adhere at the space areas (or lower areas) between the adjacent cubes, but not on the top areas of the pattern. Similar phenomenon was also reported in the related research of the surfaces with microscale topography. David Perera-Costa studied the bacterial adhesion situation on different microtopographic surface patterns (6μm protruding and receding square features, 3μm protruding and receding circular features , and 3μm parallel ridges and channels) and found that there are always more bacterial adhered on the lower part of surface structure than the higher part (Perera-Costa D *et al.*, 2014); Katrina e.t. found the bacteria cells' preferentially adhering to polishing scratches (microscale width) on a pyrite surface, and he also observed the polishing direction affected the bacterial adhesion direction (Edwards KJ *et al.*, 2001). So, the material topography not only can influence the bacterial adhesion location, and also affect the bacterial adhesion direction. The latter effect is more obvious on surface with micro-nanoscale patterns, which are close to bacterial size, because the narrow space can limit and guide the possible adhesion direction to certain extent.

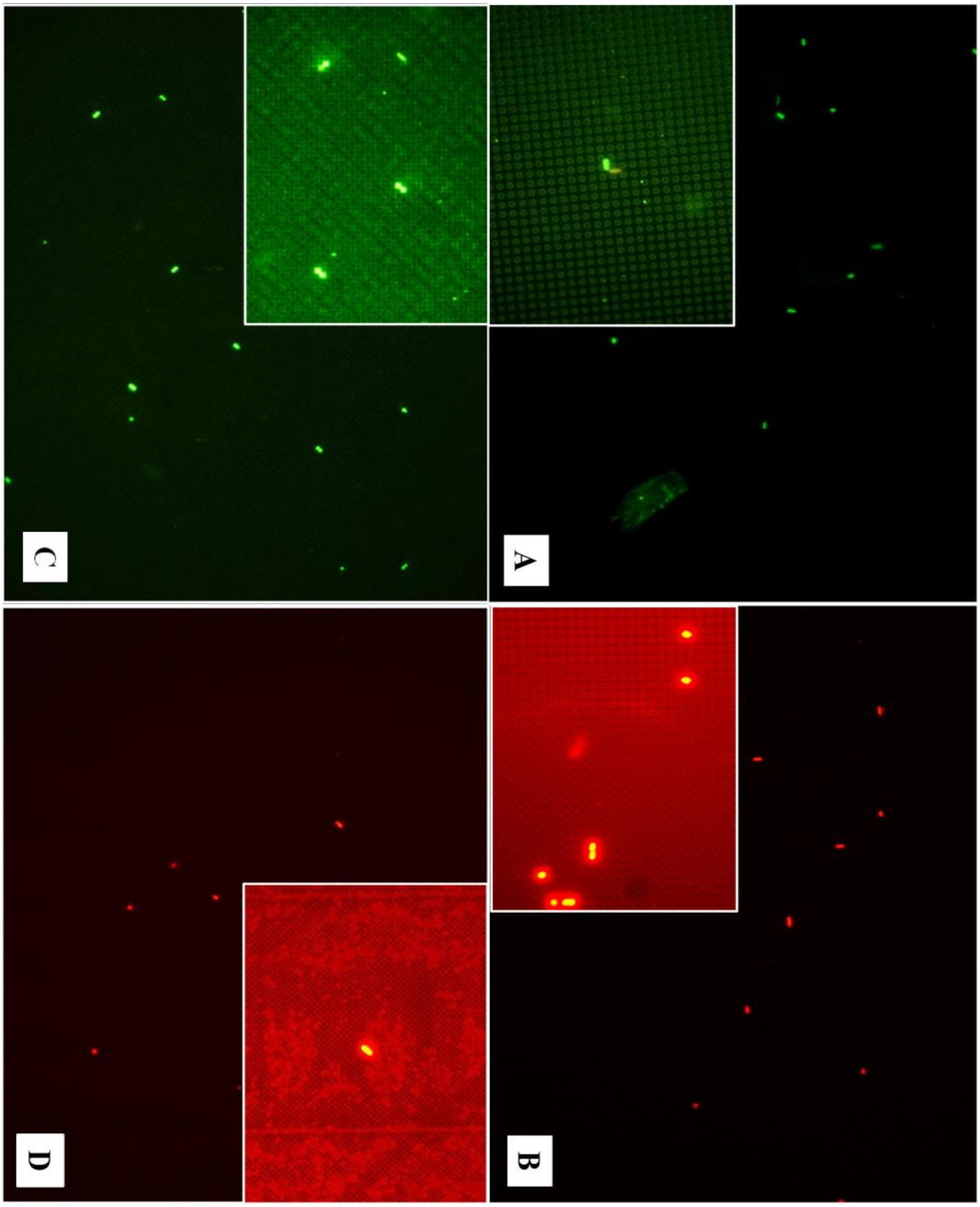

Figure 6.34 Fluorescence photographs of PDMS samples in the magnification 400 and 1000: (A) 1000nmA; (B) 500nmA; (C) 1000nmB; (D) 400nmB.

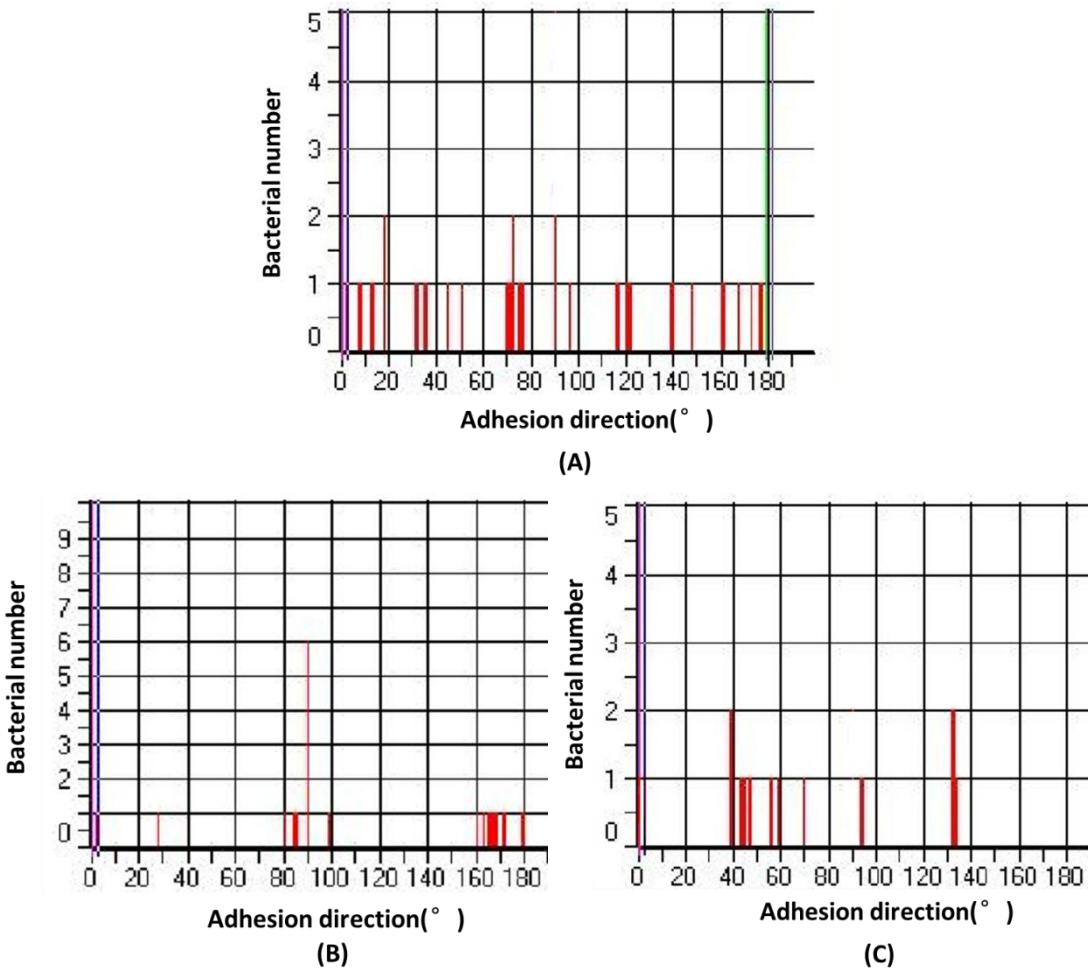

Figure 6.35 Typical analysis results of bacterial adhesion direction on PDMS samples. A: original PDMS sample; B: 500nmA PDMS sample; C: 1000nmB PDMS sample.

	+ directions	x directions	Other directions
Original PDMS	23.4±9.4%	28.7±12.6%	47.8±21.9%
1000nm(A)	69.8±24.5%	2.2±4.5%	28.0±14.5%
500nm(A)	53.15±12.7%	2.0±1.8%	44.8±12.5%
400nm(A)	46.7±4.5%	22.5±5.9%	30.8±13.8%
350nm(A)	42.4±6.5%	17.0±9.9%	40.6±5.0%
1000nm(B)	5.2±2.2%	62.1±9.7%	32.7±12.0%
500nm(B)	17.7±2.1%	60.3±6.9%	21.9±4.8%
400nm(B)	24.2±12.8%	40.4±6.7%	36.4±3.5%
350nm(B)	11.1±15.7%	40.0±13.6%	48.8±28.3%

Table 6.8 Percentage of bacterial adhesion direction on PDMS samples.

6.2.6 Encrustation test in sterile urine

Figure 6.36 shows the photos of the urinary encrustation formation on the 4 PDMS samples after three-week test in sterile artificial urine and Figure 6.37 shows the mass of encrustation deposits on the surfaces of the 4 PDMS samples. Obviously less encrustation deposits formed on the 3 micro-nano-structured surfaces, compaired with the flat PDMS surface. The PDMS samples with 500nm and 350nm surface patterns performed the best against urinary encrustation formation, which reduced urinary encrustation by about 50%, compared with the flat PDMS surface.

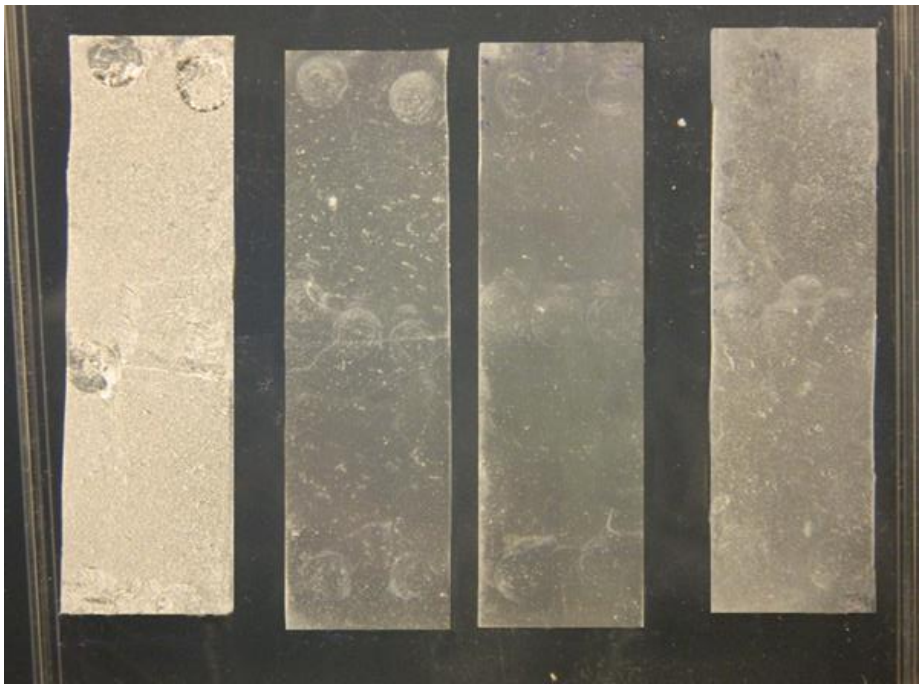

Figure 6.36 Photo of urinary encrustation formation on PDMS surfaces (from left to right: flat PDMS, PDMS with 1000nm surface pattern, PDMS with 500nm surface pattern, PDMS with 350nm surface pattern.

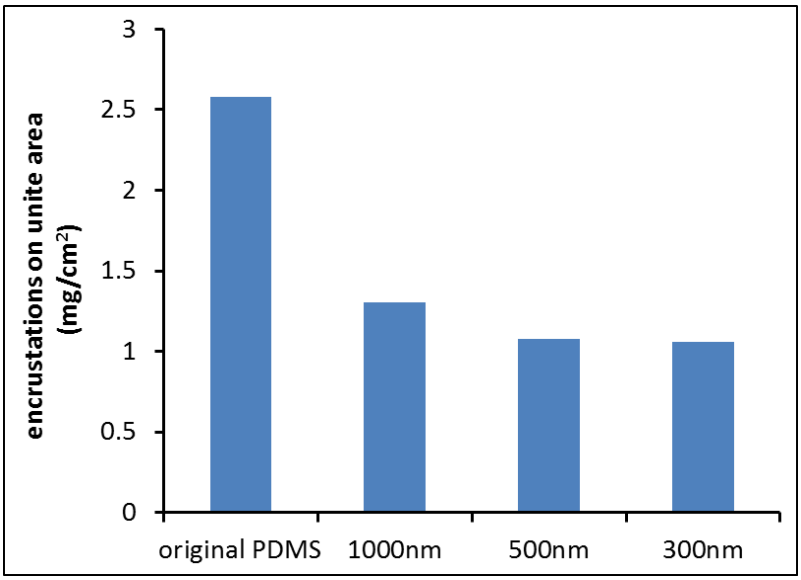

Figure 6.37 Effect of microstructures of PDMS on the mass of urinary encrustation

Figure 6.38 shows the SEM imagines of urinary encrustation on the 4 PDMS samples. The urinary encrustation is mainly composed of two types of crystals, powdery crystals (white arrow on the Figure) and prismatic crystals (red arrow on the Figure). Figure 6.39 is the EDXS analysis of the two types of crystals. Based on EDXS analysis results, combined with crystal morphology showed in SEM images, and with reference to the related literatures (Tunney MM *et al.*, 1996; Maqueda C *et al.*, 1994; Stickler DJ *et al.*, 2002), the powdery crystals are considered as calcium phosphates (tribasic calcium phosphate $Ca_3(PO_4)_2$, dibasic calcium phosphate $CaHPO_4$ and hydroxyapatite $Ca_5(PO_4)_3(OH)$) and prismatic crystals are struvite (NH_4MgPO_4 $6H_2O$).

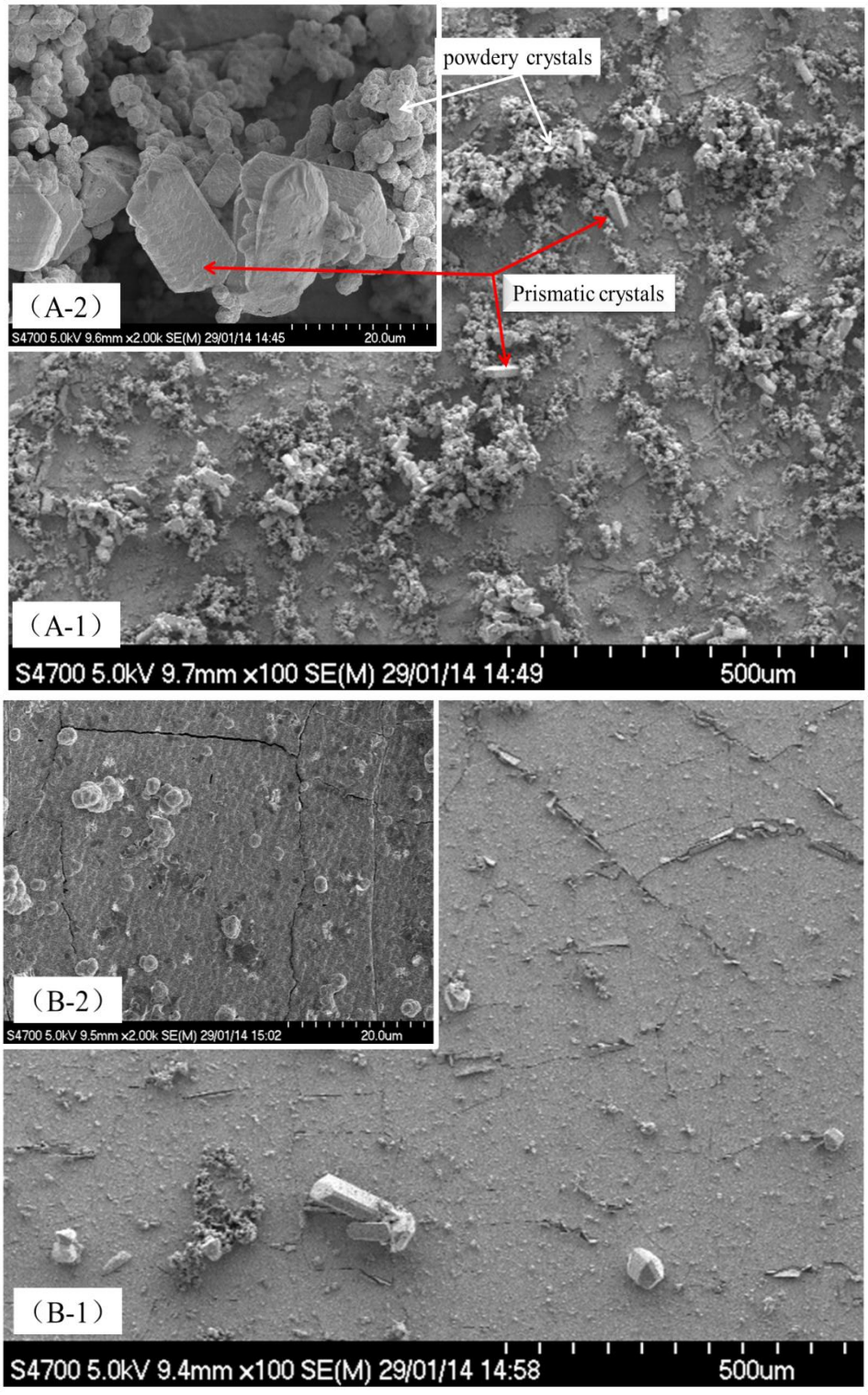
powdery crystals
Prismatic crystals
（A-2）
S4700 5.0kV 9.6mm x2.00k SE(M) 29/01/14 14:45 20.0um
（A-1）
S4700 5.0kV 9.7mm x100 SE(M) 29/01/14 14:49 500um
（B-2）
S4700 5.0kV 9.5mm x2.00k SE(M) 29/01/14 15:02 20.0um
（B-1）
S4700 5.0kV 9.4mm x100 SE(M) 29/01/14 14:58 500um

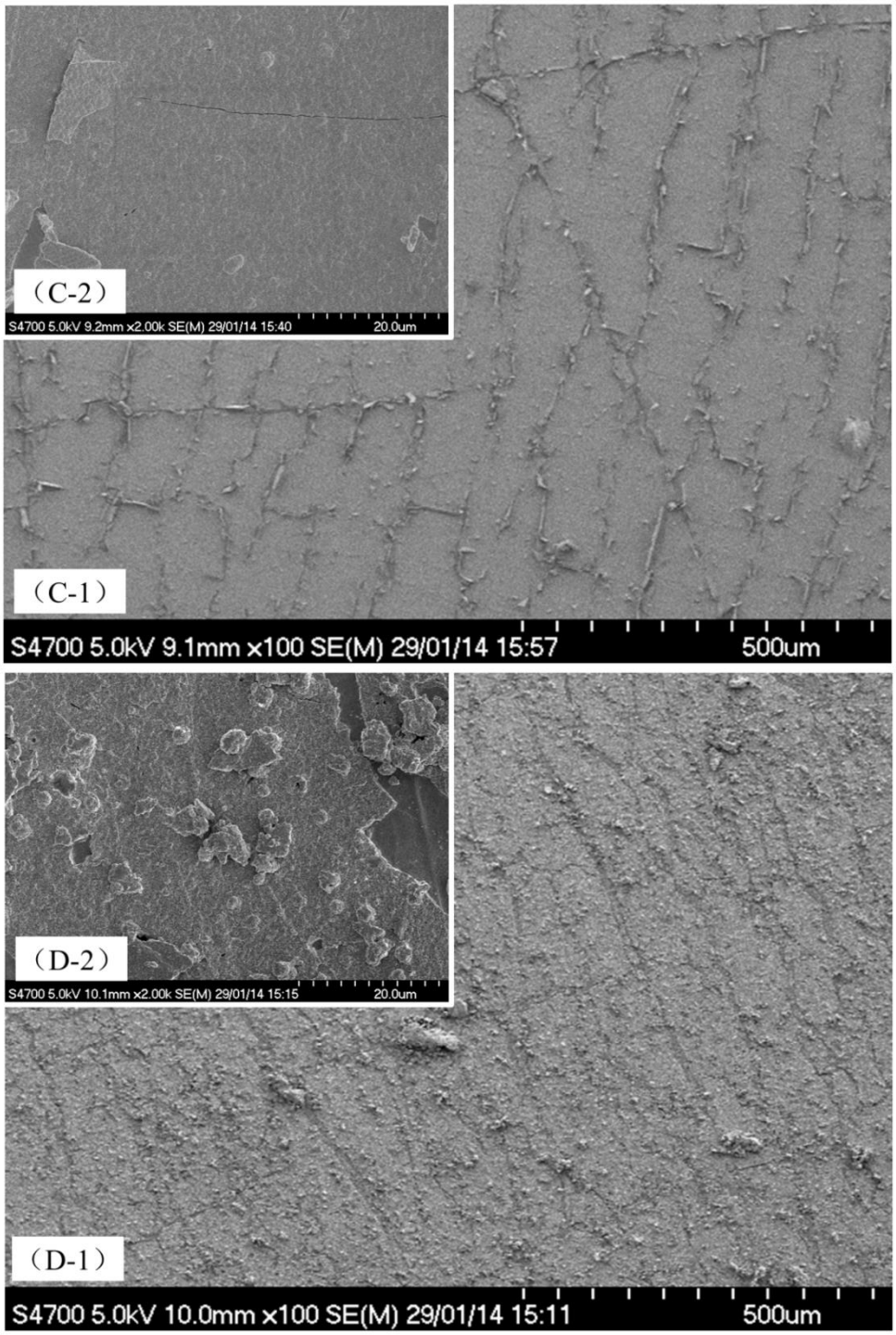

Figure 6.38 The 100 and 2000 magnification SEM images of urinary encrustations on PDMS samples. A: urinary encrustation on flat original PDMS, B: urinary encrustation on 1000nm PDMS, C: urinary encrustation on 500nm PDMS, D: urinary encrustation on 350nm PDMS.

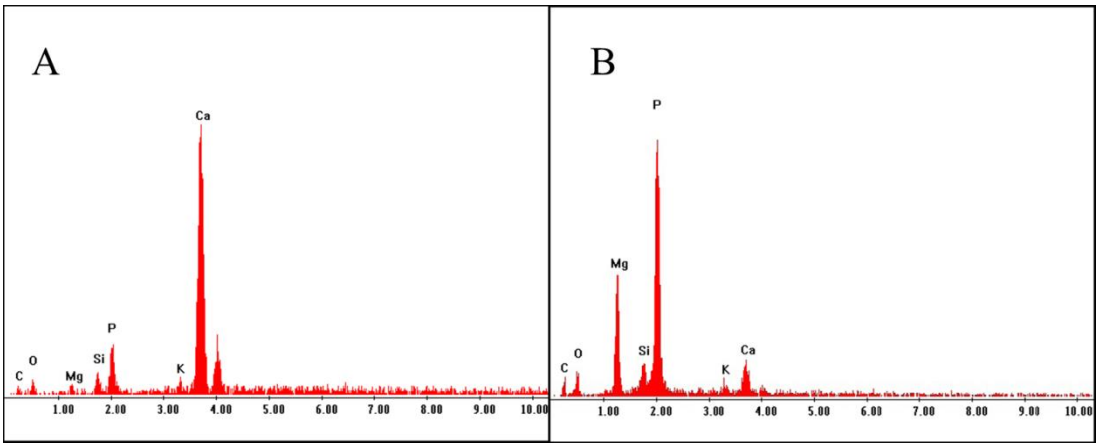

Figure 6.39 EDXS analysis of the element components of the urinary encrustation. A: powdery crystals, B: prismatic crystals.

All the test results indicate that the surface micro-nanostructure has a significant influence on urinary encrustation formation. In general the urinary encrustation mass on the micro-nano-structured PDMS surfaces was only half of that on flat PDMS surface. The PDMS with 500nm and 350nm surface patterns had the lowest urinary encrustation mass at about 1.1 mg/cm^2. The compositions of the encrustation were mainly calcium phosphates and struvite. The SEM imagines in Figure 6.38 show that the encrustation on the flat PDMS surface exhibited much more compact and thicker structures than that on the micro-nano-structured PDMS surfaces. The encrustation on flat PDMS surface had two layers. The bottom layer was made up of relatively flat and dense powdery calcium phosphates deposits, while the top layer was mainly loosely heaped powdery calcium phosphates deposits with prismatic struvite crystals wrapped in them. For the encrustations on surface structured PDMS surfaces, the bottom calcium phosphates layers were more uniform and flat but with more cracking, above it there were much less heaped powdery calcium phosphates deposits and prismatic

struvite crystals. Especially for the 500nm PDMS surface, the encrustation was almost a thin flat layer of calcium phosphates deposits and very few prismatic struvite crystals were observed. These illustrated, during the urinary encrustation process, the calcium phosphate deposits changed from flat, thin and dense to rough, thick and loose. With the help of powdery calcium phosphates deposits, prismatic struvite crystals formed and attached to the surfaces. The less urinary encrustations on structured PDMS surfaces were because the urinary encrustations develop more slowly on these surfaces than on flat surface. When the micro-nano- structured PDMS samples were immersed in artificial urine, air bubbles or even vapor film could form on the solid-liquid interface. These air bubbles could hinder the complete contact between the structured surface and artificial urine and crystallization of encrustation had to overcome the effect from the trapped air bubbles or waited for the escape of these bubbles. Some reports showed that, for hydrophobic materials, like PDMS, the air bubbles generated slowly and preferred to stick on the hydrophobic surface for a longer time even in a relatively high temperature (Zhang T *et al.*, 2011), which had an influence on the formation of urine encrustation on the surface

The adhesion assays of *E. coli* WT and urine encrustation experiments illustrated that the nanotubes arrays structure not only decreased the initial bacterial adhesion, but also reduced urine encrustation formation..

7. Conclusions and future work

7.1 Conclusions

7.1.1 DLC coating and Si/F doped DLC coatings

Standard DLC coating, three Si doped DLC coatings with Si contents of 3.7, 9.7 and 19.2 % and three F-doped DLC coatings with F contents of 6.5%, 20.7% and 39.2% were prepared by radio frequency plasma enhanced chemical vapor deposition (r.f.-PECVD) method. The contact angles of the coatings were measured by both sessile drop method and captive bubble method, and the surface energy components of the coatings were calculated using van Oss approach. The anti-bacterial properties of the coatings were evaluated with the two bacterial strains *Escherichia Coli and Klebsiella pneumonia* under both static and flow conditions.

(1) All the DLC coatings performed better than stainless steel against bacterial adhesion under both static and flow conditions. The doped DLC coatings performed better than the standard DLC. The F-doped DLC coating with high F (39.2 at.%) performed best, which reduced the bacterial adhesion by 60%, compared with the uncoated 316L stainless steel. The Si doped DLC coatings reduced bacterial adhesion by 50% compared with the stainless steel.

(2) In general the numbers of adhered bacteria in flow condition were significant lower than those in static condition. These results indicate that the fluid can generate shearing stress which are help to decrease the bacterial adhesion, or the adhered bacterial can be removed by fluid flow.

(3) The interaction energies between the tested bacteria and the tested surfaces (stainless steel, DLC and Si/F doped DLC coatings) were computed by EDLVO theory. According to the EDLVO theory, bacterial adhesion will decrease with the interaction energy increasing. The F-DLC coating with 39.2% F had the highest interaction energy; while the stainless steel had the lowest interaction energy. All the theoretical modeling results were consistent with the experimental results.

(4) 3 crystal sensors coated with stainless steel, DLC coating and gold were tested by QCM-D system to evaluate *E.coli* adhesion process with time. The adhered bacterial surface density (CFU/cm^2) on the coated sensors as a function of time were obtained. The gold coating showed the lowest bacterial adhesion (about 5×10^5 CFU/cm^2). The bacterial adhesion on the DLC coating was about 7×10^5 CFU/cm^2, which was just half of that on stainless steel surface, so the DLC coating was much better than stainless steel 316L in inhibiting bacterial adhesion. In order to explain the bacterial adhesion behavior obtained by the QCM-D measurements, the interaction energy between the *E. coli* and the coated sensors was computed using the EDLVO theory. The modeling results were consistent with the experiments.

(5) The anti-corrosion performance of the doped DLC coatings was measured using the CS300 Electrochemistry Workstation. The anti-corrosion performance of standard DLC coating and stainless steel was also measured for comparison. The results indicated that the corrosion rates of 316L stainless steel in both PBS and seawater were about 10.6 μm/a; while the corrosion rates of DLC, Si doped DLC coatings and F-doped DLC coatings were only 0.16-0.20 μm/a, 0.05-0.12 μm/a and 0.9-3.39 μm/a, respectively. The corrosion rates of the F-doped DLC coatings increased with F content increasing.

7.1.2 Micro/nano-structured PDMS surfaces

(6) Effect of surface micro-nanostructures on bacterial adhesion.

In this study, the total interaction energy (E_{132}^{TOT}) between the rod-shaped *E. coli* 1 and the nanocube array surface 2 in water 3 as functions of separation distance *h* and the edge length "*a*" were computed using EDLVO theory. The modeling results indicated that when the edge length "*a*" = 350 nm, the total interaction energy reached maximum or bacterial adhesion should be minimum.. To validate the theoretical prediction, 4 types of nanocube arrays with the edge length of 350 nm, 400 nm, 500 nm and 1000 nm were designed and prepared on PDMS substrates by a soft lithography technology. The experimental results on bacterial adhesion indicated that all the patterned PDMS surfaces with nanotube arrays performed better than the plat PDMS surface in inhibiting bacterial adhesion. The numbers of adhered bacteria decreased with the edge

length "*a*" value decreasing, which is consistent to the theoretical modelling results. The nanotube array with "a" =350 nm performed best, which reduced bacterial adhesion by 60%, compared with the flat PDMS surface.

(7) Effect of surface micro-nanostructures on urinary encrustation formation:

The urinary encrustation experiments were performed with 3 types of PDMS nanocube arrays with the edge length of 350 nm, 500 nm and 1000 and a flat PDMS surface in sterile artificial urine for 3 weeks. Less encrustation deposit formed on the 3 micro-nano-structured surfaces, compaired with the flat PDMS surface. The PDMS with 500nm and 350nm surface patterns performed the best against urinary encrustation formation, which reduced urinary encrustation by about 50%, compared with the flat PDMS surface.

7.2 Further work

(1) Try to coat the actual medical equipment and implants with DLC type coatings, and if possible try to perform animal tests to evaluate the anti-infective performances, biocompatibility and reliability of the doped DLC coating in vivo environment.

(2) To apply the anti-adhesion property of the doped DLC coatings to other areas. To

study the feasibility and effectiveness of the doped DLC coating on coronary artery stents to decrease thrombus by reducing platelet adhesion.

(3) To apply the soft lithography and related method to modify the surface structure on other common biomaterials, including polymers, like thermoplastic polyurethane (TPU), UV curing polyurethane (UV-PU), PMMA, and metals, like stainless steels. These can help us verify the general applicability of the photography anti-bacterial strategy and soft lithography technology.

Reference

Aksakal B, Yildirim ÖS and Gul H. Metallurgical failure analysis of various implant materials used in orthopedic applications. Journal of Failure Analysis and Prevention, 2004, Vol 4, 17-23.

Allegranzi B, Report on the burden of endemic health care-associated infection worldwide. WHO Press, 2011.

Alpaslan E, Ercan B, Webster T J. Anodized 20nm diameter nanotubular titanium for improved bladder stent applications. International Journal of Nanomedicine. 2011, 6, 219–225.

AL-Mangour B, Mongrainb R, Irissouc E, Yue S. Improving the strength and corrosion resistance of 316L stainless steel for biomedical applications using cold spray. Surface and Coatings Technology, Vol 216, 2013, 297–307.

Anderson JM, Biological responses to materials. Annual Review of Materials Research, 2001, Vol 3, 81-110.

Andersson AS, Backhed F, von EA, Richter-Dahlfors A, Sutherland D and Kasemo B. Nanoscale features influence epithelial cell morphology and cytokine production. Biomaterials, 2003, Vol 24, 3427-3436.

Andersson AS, Brink J, Lidberg U and Sutherland DS. Influence of systematically varied nanoscale topography on the morphology of epithelial cells. IEEE transactions on nanobioscience, 2003, Vol 2, 49-57.

Annett DR, Schurer C, Irmer G and Muller E. Electrochemical corrosion behavior of uncoated and DLC coated medical grade Co28Cr6Mo. Surface Coating Technology, 2004, Vol 177, 830–837.

Anselme K. Osteoblast adhesion on biomaterials. Biomaterials, 2000, Vol 21, 667-681.

Anselme, K.; Davidson, P.; Popa, A. M.; Giazzon, M.; Liley, M.; Ploux, L. The interaction of cells and bacteria with surfaces structured at the nanometre scale. Acta Biomaterialia, 2010, 6, 3824-3846.

Antoci V, Ono CM, Antoci V Jr, Raney EM. Pin-tract infection during limb lengthening using external fixation. American journal of orthopedics (Belle Mead, N.J.), 2008, 37(9), 150-154.

Bailey RC, Stevenson KJ and Hupp JT. Assembly of micropattened colloidal gold thin films via microtransfer molding and electrophoretic deposition. Advanced materials 2000, Vol 12,1930-1934.

Bai XD. Corrosion and control of materials, Beijing : Qing hua da xue chu ban she, 2005, chapter 7, 220.

Balamurugan A, Kannan S and Rajeswari S. Structural and electrochemical behaviour of sol-gel zirconia films on 316L stainless-steel in simulated body fluid environment. Materials Letters, 2003, Vol 57, 4202–4205.

Barrientos S, Stojadinovic O, Golinko MS, Brem H and Tomic-Canic M. Growth factors and cytokines in wound healing. Wound Repair and Regeneration, 2008, Vol 16, 585-601.

Barth E, Myrvik QM, Wagner W and Gristina AG. In vitro and in vivo comparative

colonization of Staphylococcus aureus and Staphylococcus epidermidis on orthopaedic implant materials. Biomaterials, 1989, Vol 10, 325–328.

Bates DW. Global priorities for patient safety research. British Medical Journal, 2009, Vol 338:b1775.

Baum C, Meyer W, Stelzer R, Fleischer LG and Siebers D. Average nanorough skin surface of the pilot whale Globicephala melas: consideration on the self-cleaning abilities based on nanoroughness. Marine Biology, 2002,Vol 140, 653-657.

Bauer S , Park J , Faltenbacher J, Berger S, von der Mark K, Schmuki P. Size selective behavior of mesenchymal stem cells on ZrO2 and TiO2 nanotube arrays. Integrative Biology. 2009, 1, 525–532.

Beyth N, Houri-Haddad Y, Baraness-Hadar L, Yudovin-Farber I, Domb AJ, Weiss EI. Surface antimicrobial activity and biocompatibility of incorporated polyethylenimine nanoparticles.Biomaterials,2008, Vol 29, 4157–4163.

Berry CW, Moore TJ, Safar JA, Henry CA and Wagner MJ. Antibacterial activity of dental implant metals. Implant Dentistry, 1992, Vol 1, 59-65.

Bridges AW and Garcia AJ. Anti-inflammatory polymeric coatings for implantable biomaterials and devices. Journal of Diabetes Science and Technology, 2008, Vol 2, 984-994.

Bridier A, Briandet R, Thomas V, Dubois-Brissonnet F. Resistance of bacterial biofilms to disinfectants: a review. Biofouling. 2011, 27(9),1017-32.

Bone Q, Moore R H. Biology of Fishes. 3rd Ed. New York, NY: Taylor & Francis, 2009.

Boontheekul T and Mooney DJ. Protein-based signaling systems in tissue engineering. Current Opinion in Biotechnology, 2003, Vol 14, 559-565.

Buchholz HW, Elson RA, Engelbrecht E, Lodenkämper H, Röttger J and Siegel A. Management of deep infection of total hip replacement. The Journal of Bone & Joint Surgery, 1981, Vol 63-B, 342-353.

Burke JP. Infection control - a problem for patient safety. New England Journal of Medicine, 2003, Vol 348, 651–656.

Busscher HJ, Rinastiti M, Siswomihardjo W and van der Mei HC. Biofilm formation on dental restorative and implant materials. Journal of Dental Research. **2010**, Vol 89, 657–665.

Buffet-Bataillon S, Tattevin P, Bonnaure-Mallet M, Jolivet-Gougeon A. Emergence of resistance to antibacterial agents: the role of quaternary ammonium compounds – a critical review. International Journal of Antimicrobial Agents, 2012, 39, 381–389.

Campoccia D, Montanaro L and Arciola CR. A review of the biomaterials technologies for infection-resistant surfaces. Biomaterials, 2013 Vol 34, 8533-8554.

Carmen ML, Estes TG, Feinberg AW, Schumacher JF, Wilkerson W, Wilson LH, Callow M E, Callow JA and Brennan AB. Engineered antifouling microtopographies–correlating wettability with cell attachment. Biofouling, 2006, Vol 22, 11-21.

Cassie ABD and Baxter S, Wettability of porous surfaces. Transactions of the Faraday Society, 1944, Vol 40, 546-551.

Chapekar MS, Regulatory concerns in the development of biologic-biomaterial combinations. Journal of Biomedical Materials Research. 1996, Vol 33, 199-203.

Chambers LD, Stokes KR, Walsh FC and Wood RJK. Modern approaches to marine antifouling coatings. Surface and Coatings Technology, 2006, Vol 201, 3642-3652.

Charnley M, Textor M, Acikgoz C. Designed polymer structures with antifouling–antimicrobial properties. Reactive and Functional Polymers, 2011, Vol 71, 329–334.

Chen S, Jones JA, Xu Y, Low HY, Anderson JM and Leong KW. Characterization of topographical effects on macrophage behavior in a foreign body response model. Biomaterials, 2010, Vol 31, 3479-3491.

Choong S, Wood S, Fry C and Whitfield H. Catheter associated urinary tract infection and encrustation. International Journal of Antimicrobial Agents, 2001, Vol 17, 305-10.

Cook G, Costerton JW and Darouiche RO, Direct confocal microscopy studies of the bacterial colonization in vitro of a silver-coated heart valve sewing cuff. International Journal Antimicrob Agents 2000, Vol 13, 169-173.

Crawford RJ, Webb HK, Truong VK, Hasan J and Ivanova EP. Surface topographical factors influencing bacterial attachment. Advances in Colloid and Interface Science, 2012, Vol 179–182, 142-149.

Dalby MJ, Riehle MO, Johnstone H, Affrossman S and Curtis AS. In vitro reaction of endothelial cells to polymer demixed nanotopography. Biomaterials, 2002, Vol 23, 2945-2954.

Dalby MJ, Pasqui D, Affrossman S. Cell response to nano-islands produced by

polymer demixing: a brief review. IEE Proceedings–Nanobiotechnology, 2004 , Vol 151, 53-61.

Darouiche RO, Preventing Infection in Surgical Implants, US Surgery, 2007, 40-44.

Dastjerdi R, Montazer M. A review on the application of inorganic nano-structured materials in the modification of textiles: focus on anti-microbial properties. Colloids and Surfaces B: Biointerfaces, 2010, 79(1), 5-18.

De Bastiani G, Aldegheri R and Renzi Brivio L. The treatment offractures with a dynamic axial fixator. The Journal of bone and joint surgery, 1984, Vol 66, 538-545.

Demichelis F, Pirri CF and Tagliaferro A. Influence of silicon on the physical properties of diamond-like films. Materials Science and Engineering: B. 1992, Vol 11, 313–316.

Edin-Liljegren A, Hedelin H.H, Grenabo L and Pettersson S. Impact of Escherichia coli on urine citrate and urease-induced crystallization. Scanning Microscope.1995, Vol 9, 901-905.

Edwards KJ and Rutenbergb AD. Microbial response to surface microtopography: the role of metabolism in localized mineral dissolution. Chemical Geology, 2001, Volume 180, Pages 19–32.

Elliott TS, Moss HA, Tebbs SE, Wilson IC, Bonser RS, Graham TR, Burke LP and Faroqui MH. Novel approach to investigate a source of microbial contamination of central venous catheters. European Journal of Clinical Microbiology & Infectious Diseases, 1997, Vol 16, 210-213.

Elshahawy W, Biocompatibility. Advances in Ceramics - Electric and Magnetic

Ceramics, Sikalidis C, ed. 2011, 359-378.

Erbil HY. Surface Chemistry of Solid and Liquid Interfaces, 2006, charpter 9, 309.

Espositoa S, Purrellob SM, Bonnetc E, Novellid A, Tripodia F, Pascalea R, Unale S, Milkovichf G. Central venous catheter-related biofilm infections: An up-to-date focus on meticillin-resistant Staphylococcus aureus. Journal of Global Antimicrobial Resistance, 2013, Vol 1, 71-78.

Evelyn L, Lindsay EN, Susan EC and Carolyn G. Strategies to Prevent Catheter-Associated Urinary Tract Infections in Acute Care Hospitals: 2014 Update. Infection Control and Hospital Epidemiology, 2014, Vol. 35, No. 5.

Fathi MH, Salehi M, Saatchi A, Mortazavi V and Moosavi SB. In vitro corrosion behavior of bioceramic, metallic, and bioceramic-metallic coated stainless steel dental implants. Dental Materials, 2003, 19, 188-198.

Fink J, Fuhrmann R, Scharnweber T and Franke RP. Stimulation of monocytes and macrophages: possible influence of surface roughness. Clinical Hemorheology and Microcirculation, 2008, Vol 39, 205-212.

Fitzgerald RH Jr, Infections of hip prostheses and artificial joints. Infectious Disease Clinics of North America, 1989, Vol 3, 329-338.

Fitzgerald RH Jr. Infected total hip arthroplasty: Diagnosis and treatment. Journal of the American Academy of Orthopaedic Surgeons, 1995, Vol 3, 249–262.

Frankel GS. Pitting Corrosion of Metals A Review of the Critical Factors. Journal of

the Electrochemical Society, 1998, Vol 145, 2186-2198.

Francis R and Powell G. The Corrosion Performance of Metals for the Marine Environment: A Basic Guide. European Federation of Corrosion Series, 2012, Vol 63.

Fujita S, Ohshima M and Iwata H. Time-lapse observation of cell alignment on nanogrooved patterns. Journal of the Royal Society Interface, 2009, Vol 6, 269–277.

Galvele JR, Tafels law in pitting corrosion and crevice corrosion susceptibility. Corrosion Science, 2005, Vol 47, 3053-3067.

Gao G, Lange D, Hilpert K, Kindrachuk J, Zou Y, Cheng JT, Kazemzadeh-Narbat M, Yu K, Wang R, Straus SK, Brooks DE, Chew BH, Hancock RE, Kizhakkedathu JN. The biocompatibility and biofilm resistance of implant coatings based on hydrophilic polymer brushes conjugated with antimicrobial peptides. Biomaterials, 2011, Vol 32(16), 3899-3909.

George MW and Darren JL. Soft nanotechnology: ‘‘structure’’ vs. ‘‘function’. Faraday Discussions, 2009, Vol 143, 373-84.

Glagov S, Zarins C, Giddens DP and Ku DN. Hemodynamics and atherosclerosis. Insights and perspectives gained from studies of human arteries. Archives of Pathology & Laboratory Medicine, 1988, Vol 112, 1018-1031.

Grill A, Review of the tribology of diamond-like carbon. Wear, 1993, Vol 168, 143-153.

Gristina AG and Costerton JW. Bacterial adherence to biomaterials and tissue: The significance of its role in clinical sepsis. The Journal of Bone & Joint Surgery, 1985, Vol 67, 264–273.

Guangji Li, Jiarui Shen and Yinlan Zhu, A study of pyridinium-type functional polymers. I. Preparation and characterization of soluble pyridinium-type functional polymers. Journal of Applied Polymer Science, Vol 62, 2247-2255.

Guntupalli R, Sorokulova I, Olsen E, Globa L, Pustovyy O and Vodyanoy V. Biosensor for Detection of Antibiotic Resistant Staphylococcus Bacteria. Journal of Visualized Experiments, 2013, Vol 75, e50474.

Gutman J, Walker Sl, Freger V and Herzberg M. Bacterial Attachment and Viscoelasticity: Physicochemical and Motility Effects Analyzed Using Quartz Crystal Microbalance with Dissipation (QCM-D). Environmental Science & Technology, 2013, Vol 47, 398−404.

Harris LG, Tosatti S, Wieland M, Textor M and Richards RG. Staphylococcus aureus adhesion to titanium oxide surfaces coated with non-functionalized and peptide-functionalized poly(L-lysine)-grafted-poly(ethylene glycol) copolymers. Biomaterials, 2004, Vol 25, 4135–4148.

Hedelin H, Edin-Liljegren A, Grenabo L, Hugosson J, Larsson P, Pettersson S. E. coli and urease-induced crystallisation in urine. Scandinavian Journal of Urology. 1990,24(1): 57-61.

Hedelin H, Bratt CG, Eckerdal G and Lincoln K. The relation between urease-producing bacteria, urine pH and encrustations on indwelling urinary catheters. British Journal of Urology, 1991, Vol 67, 527.

Hench LL and Wilson J, An Introduction to Bioceramics. World Scientific. 1993.

Hilbert LR, Bagge-Ravnb D, Koldc J and Gram L. Influence of surface roughness of stainless steel on microbial adhesion and corrosion resistance. International Biodeterioration & Biodegradation, 2003 ,Volume 52, 175–185.

Hoek EMV and Agarwal GK. Extended DLVO interactions between spherical particles and rough surfaces. Journal of Colloid and Interface Science, 2006, Vol 298, 50–58.

Hoipkemeier-Wilson L, Schumacher JF, Carman ML, Gibson AL, Feinberg AW, Callow ME, Finlay JA, Callow JA, Brennan AB. Antifouling Potential of Lubricious, Micro-engineered, PDMS Elastomers against Zoospores of the Green Fouling Alga Ulva (Enteromorpha). Biofouling, 2004, Vol 20, 53-63.

Höök F, Kasemo B, Nylander T, Fant C, Sott K and Elwing H. Variations in coupled water, viscoelastic properties, and film thickness of a Mefp-1 protein film during adsorption and cross-linking: a quartz crystal microbalance with dissipation monitoring, ellipsometry, and surface plasmon resonance study. Analytical Chemistry, 2001, Vol 73, 5796-804.

Hotta A, Hasebe T. Diamond-Like Carbon Coated on Polymers for Biomedical Applications. Biological and Medical Physics, Biomedical Engineering, 2013, 171-228.

Hosoya N, Honda K, Iino F and Arai T. Changes in enamel surface roughness and adhesion of Streptococcus mutans to enamel after vital bleaching. Journal of Dentistry, 2003, Vol 31, 543-548.

Hulbert S, The use of alumina and zirconia in surgical implants. An Introduction to Bioceramics, Hench LL and Wilson J, ed. World Scientific.1993, 25-40.

Illingworth B, Bianco RW, Weisberg S. In Vivo Efficacy of Silver-Coated Fabric Against Staphylococcus Epidermidis, The Journal of Heart Valve Disease, 2000, Vol 9, 135-141.

Ivanova EP, Hasan J, Truong VK, Wang JY, Raveggi M, Fluke C and Crawford RJ. The influence of nanoscopically thin silver films on bacterial viability and attachment. Applied Microbiology and Biotechnology, 2011,91, 1149–1157.

Jansen B, Peters G, Schareina S, Steinhauser H, Schumacher-Perdreau F, Pulverer G. Development of Polymers with anti-infections properties.Applied Bioactive Polymeric Materials. Plenum Press, 1988, 97.

Jeyachandran YL, Narayandass SaK, Mangalaraj D, Bao CY, Li W and Liao YM. A study on bacterial attachment on titanium and hydroxyapatite based films. Surface and Coatings Technology, 2006, Vol 201, 3462–3474.

Jeyachandran YL, Venkatachalam S, Karunagaran B, Narayandass SaK, Mangalaraj D and Bao CY. Bacterial adhesion studies on titanium, titanium nitride and modified hydroxyapatite thin films. Materials Science and Engineering: C, 2007, Vol 27, 35–41.

Jones DS, Djokic J, McCoy CP and Gorman SP, Poly(ε-caprolactone) and poly(ε-caprolactone)-polyvinylpyrrolidone-iodine blends as ureteral biomaterials: characterisation of mechanical and surface properties, degradation and resistance to encrustation in vitro. Biomaterials, 2002, Vol 23, 4449–4458.

Kamachimudali U, Sridhar TM and Raj B. Corrosion of bio implants. Sadhana, 2003, Vol 28, 601-637.

Kane RS, Takayama S and Ostuni E. Patterning proteins and cells using soft lithography. Biomaterials, 1999, Vol 20, 2363-2376.

Kawabata N and Nishiguchi M, Antibacterial activity of soluble pyridinium-type polymers. Applied and Environmental Microbiology, 1988, Vol 54, 2532-2535.

Keating JF, Gardner E, Leach WJ, Macpherson S and Abrami G. Management of tibial fractures with the Orthofix dynamic external fixator. Journal of the Royal College of Surgeons of Edinburgh, 1991, Vol 36, 272–277.

Kenawy ER, Worley SD, Broughton R. The chemistry and applications of antimicrobial polymers: a state-of-the-art review. Biomacromolecules, 2007, 8(5), 1359-84.

Katsikogianni M and Missirlis YF. Concise review of mechanisms of bacterial adhesion to biomaterials and of techniques used in estimating bacteria material interactions, European cells & materials, 2004, Vol 8, 37-57.

Kelly PJ, Li H, Whitehead KA, Verran J, Arnell RD. A study of the antimicrobial and tribological properties of TiN/Ag nanocomposite coatings. Surf. Coat. Technol. 2009, 204, 1137–1140.

Kesel A and Liedert R. Learning from Nature: Non-toxic Biofouling Control by Shark Skin Effect. Comparative Biochemistry &. Physiology. A, 2007, Vol 146, 130.

Kohler-Ockmore J and Feneley RC, Long-term catheterization of the bladder: prevalence and morbidity. British Journal of Urology, 1996, Vol 77, 347-51.

Kristinsson KG. Adherence of staphylococci to intravascular catheters. Journal of Medical Microbiology, 1989, Vol 28, 249-257.

Kruger J. Fundamental aspects of corrosion of metallic implants. In Corrosion and degradation of implant materials, Syrett BC and Acharya A ed, 1979, 107-113.

Kurtis KE and Mehta K. A Critical Review of Deterioration of Concrete Due to Corrosion of Reinforcing Steel. International Concrete Abstracts Portal, 1997, Vol 170, 535-554.

Kunin CM and McCormack RC. Prevention of catheter-induced urinary-tract infections by sterile closed drainage. The New England Journal of Medicine, 1966, Vol 274,1155-1161.

Kubitschek HE, Cell Volume Increase in Escherichia coli after Shifts to Richer Media. Journal of Bacteriology, 1990, Vol 172, 94-101.

Langone JJ, Immunotoxicity testing guidance. Draft Document, Center for Devices and Radiological Health, Food and DrugAdministration . 1999.

Labow RS, Meek E and Santerre JP. Neutrophil-mediated biodegradation of medical implant materials. Journal of Cellular Physiology, 2001, Vol 186, 95-103.

Lai L-C, Tyson DR, Clayman RV and Earthman JC, Encrustation of nanostructured Ti in a simulated urinary tract environment. Materials Science and Engineering C,2008, Vol 28, 460–464.

LaQue F L. Marine Corrosion: Causes and Prevention. John Wiley & Sons Inc, 1975.
Lakes RS, Polymeric implant materials. Biomaterials: an introduction, 2007, 173-205.

Leckie HP and Uhlig HH. Environmental factors affecting the critical potential for pitting in 18–8 stainless steel. Journal of The Electrochemical Society, 1966,Vol 113,1262-1267.

Lee JH, Burner KD, Fealey ME, Edwards WD, Tazelaar HD, Orszulak TA, Wright AJ

and Baddour LM. Prosthetic valve endocarditis: clinicopathological correlates in 122 surgical specimens from 116 patients (1985-2004). Cardiovascular Pathology, 2011, Vol 20, 26-35.

Liu Y and Zhao Q. Influence of surface energy of modified surfaces on bacterial adhesion. Biophysical Chemistry, 2005, Vol 117, 39-45.

Liu X, Chu P, Ding C. Surface modification of titanium, titanium alloys, and related materials for biomedical applications. Materials Science and Engineering: R: Reports, 2004, 47, 49–121.

Long CJ, Schumacher JF, Robinson PA 2nd, Finlay JA, Callow ME, Callow JA and Brennan AB. A model that predicts the attachment behavior of Ulva linza zoospores on surface topography. Biofouling. 2010, Vol 26, 411-419.

Love CA, Cook RB, Harvey TJ, Dearnley PA, Wood RJK. Diamond like carbon coatings for potential application in biological implants—a review.Tribology International, 2013, Vol 63, 141–150.

Magin CM, Cooper SP and Brennan AB. Non-toxic antifouling strategies. Materials Today，2010, Volume 13, 36–44.

Magill SS, Edwards JR, Bamberg W, Beldaus ZG, Dumyati G, Kainer MA, Lynfield R, Maloney M, McAllister-Hollod L, Nadle J, Ray SM, Thompson D, Wilson LE, Fridkin SK, Multistate point-prevalence survey of health care-associated infections. The New England Journal of Medicine, 2014, 370, 1198-1208.

Mahan J, Selgison D, Henry SL, Hynes P and Dobbins J. Factors in pin tract infections. Orthopedics, 1991, Vol 14, 305–308.

Maki DG and Tambyah PA. Engineering out the risk for infection with urinary catheters. Emerging Infectious Diseases journal, 2001, Vol 7, 342-347.

Malic S, Waters M, Basil L, Stickler DJ and Williams DW. Development of an "early warning" sensor for encrustation of urinary catheters following Proteus infection. Journal of Biomedical Materials Research Part B: Applied Biomaterials. 2012, Vol 100B, 122-137.

Malte H. The DLVO theory in microbial adhesion. Colloids and Surfaces B: Biointerfaces, 1999, Vol 14, 105–119.

Manivasagam G, Dhinasekaran D and Rajamanickam A. Biomedical Implants: Corrosion and its Prevention - A Review. Recent Patents on Corrosion Science, 2010, Vol 2, 40-54.

Maqueda C, Pérez Rodríguez JL and Lebrato J. Study of struvite precipitation in anaerobic digesters. Water Research, 1994, Vol 28, 411–416.

Ma Y, Chen M, Jones JE, Ritts AC, Yu Q and Sun H. Inhibition of staphylococcus epidermidis biofilm by Trimethylsilane Plasma Coating. Antimicrobial Agents and Chemotherapy, 2012, Vol 56, 5923–5937.

McMillan PW. Glass-Ceramics. Academic Press.1979.

Meinert K and Wolf GK. Corrosion Studies of Stainless-Steel 316L, Modified by Ion-Beam Techniques, Under Simulated Physiological Conditions. SURFACE & COATINGS TECHNOLOGY;SURFACE & COATINGS TECHNOLOGY, 1996, 1148-1156.

Mohanty M, Baby S and Menon KV. Spinal fixation device: a 6-year postimplantation

study. Journal of Biomaterials Applications, 2003, Vol 18,109-121.

Murdoch DR, Corey GR, Hoen B, Miró JM, Fowler VG Jr *et al.* Clinical presentation, etiology, and outcome of infective endocarditis in the 21st century: the International Collaboration on Endocarditis-Prospective Cohort Study. Archives of Internal Medicine, 2009, Vol 169, 463-473.

Murata H, Koepsel RR, Matyjaszewski K, Russell AJ. Permanent, non-leaching antibacterial surfaces – 2: how high density cationic surfaces kill bacterial cells. Biomaterials, 2007, 28, 4870–4879.

Nicolle LE. Catheter associated urinary tract infections. Antimicrobial Resistance and Infection Control, 2014, 3, 23.

Odom TW, Love JC and Wofle DB. Improved pattern transfer in soft lithography using composite stamps. Langmuir, 2002, Vol 18, 5314-5320.

O'Grady NP, Alexander M, Burns LA, Dellinger EP, Garland J, Heard SO, Lipsett PA, Masur H, Mermel LA, Pearson ML, Raad II, Randolph AG, Rupp ME, Saint S. Guidelines for the prevention of intravascular catheter-related infections. Clinical Infectious Diseases, 2011, Vol 52, e162-193.

Oldani C and Dominguez Alejandro. Titanium as a Biomaterial for Implants, Recent Advances in Arthroplasty, Dr. Samo Fokter (Ed.), InTech, 2012.

Olsson AL, van der Mei HC, Busscher HJ and Sharma PK. Influence of cell surface appendages on the bacterium-substratum interface measured real-time using QCM-D. Langmuir, 2009, Vol 25, 1627-1632.

Parameswaran AD, Roberts CS, Seligson D. Pin Tract Infection With Contemporary

External Fixation: How Much of a Problem? Journal of Orthopaedic Trauma, 2003,Vol 17 ,7, 503-507.

Patton JP, Nash DB and Abrutyn E. Urinary tract infection: economic considerations. Medical Clinics of North America, 1991, Vol 75, 495-513.

Pavithra D and Doble M. Biofilm formation, bacterial adhesion and host response on polymeric implants--issues and prevention. Biomed Material.2008, Vol 3, 1-13.

Papaioannou TG and Stefanadis C. Vascular wall shear stress: basic principles and methods. The Hellenic Journal of Cardiology, 2005, Vol 46, 9-15.

Pazzaglia UE, Beluffi G, Colombo A, Marchi A, Coci A and Ceciliani L. Myositis ossificans in the newborn. A case report. The Journal of Bone & Joint Surgery, 1986, 68, 456-458.

Perera-Costa D, Bruque JM, González-Martín ML, Gómez-García AC and Vadillo-Rodríguez V. Studying the Influence of Surface Topography on Bacterial Adhesion using Spatially Organized Microtopographic Surface Patterns. Langmuir, 2014, Vol 30, 4633-4641.

Privett BJ, Youn J, Hong SA, Lee J, Han J, Shin JH and Schoenfisch MH. Antibacterial fluorinated silica colloid superhydrophobic surfaces. Langmuir, 2011, Vol 27, 9597–9601.

Qin D, Xia Y and Whitesides GM. Solithography for micro- and nanoscale patterning. Nature Protocols, 2010, Vol 5, 491-502.

Raad II, Sabbagh MF, Rand KH and Sherertz RJ. Quantitative tip culture methods and the diagnosis of central venous catheterrelated infections. Diagnostic Microbiology and Infectious Disease, 1992, Vol 15,13-20.

Rai-Choudhury P. Handbook of Microlithography, Micromachining, and Microfabrication. Bellingham. 1997, SPIE Press. Vol 1.

Ratner BD, Hoffman AS, Schoen FJ, Lemons JE, Editors. Biomaterials Science: An introduction to materials in medicine. London: Elsevier Academic Press; 2012.

Ren DW, Zhao Q, Bendavi A. Anti-bacterial property of Si and F doped diamond-like carbon coatings. Surface and Coatings Technology, 2013, Vol 226, 1–6.

Pereni, CI, Zhao Q, Liu Y and Abel E. Surface free energy effect on bacterial retention. Colloids and Surfaces B: Biointerfaces, 2006,Vol 48, 143-147.

Respet P, Kleinman P and Meinhard B. Pin tract infection: a caninemodel. Journal of Orthopaedic Research, 1987, Vol 5, 600–603.

Pinto F .Adaptive optics actuation by means of van der waals forces:a novel nanotechnology strategy to steer light by light. Optomechatronic Technologies, 2008， Vol 7266, 1~16.

Riedl CR, Witkowski M, Plas E and Pflueger H. Heparin coating reduces encrustation of ureteral stents: a preliminary report. International Journal of Antimicrobial Agents, 2002, Vol 19, 507-510.

Robertson J. Diamond-like amorphous carbon. Materials Science and Engineering R, 2002, Vol 37,129-281.

Rodahl M and Kasemo M. On the measurement of thin liquid overlayers with the quartz-crystal microbalance. Sensors and Actuators A: Physical, 1996,Volume 54, 448–456.

Roosjen A, van der Mei HC, Busscher HJ and Norde W. Microbial adhesion to poly(ethyle oxide) brushes: Influence of polymer chain length and temperature. Langmuir, **2004**, Vol 20, 10949-10955.

Roosjen A, Norde W, van der Mei HC and Busscher HJ. The use of positively charged or low surface free energy coatings versus polymer brushes in controlling biofilm formation. Progress in Colloid and Polymer Science, 2006, Vol 132, 138–144.

Rosenthal VD. Device-associated nosocomial infections in limited-resources countries: findings of the international nosocomial infection control consortium (INICC). American Journal of Infection Control, 2008, Vol 36, S171.e7-12.

Rosato DV. Polymers, processes and properties of medical plastics: including markets and applications, Biocompatible Polymers, Metals, and Composites, M. Szycher, ed. PubL. Lancaster.1983, 1019-1067.

Rutter PR and Vincent B. Microbial adhesion to surface. Berkely RCW ed,Ellis orwood Ltd,1980.

Saeki D, Tanimoto T and Matsuyama H. Prevention of bacterial adhesion on polyamide reverse osmosis membranes via electrostatic interactions using a cationic phosphorylcholine polymer coating. Colloids and Surfaces A: Physicochemical and Engineering Aspects. 2014, Vol 443, 171–176.

Sandhyarani M, Rameshbabu N, Venkateswarlu K. Surface morphology, corrosion resistance and in vitro bioactivity of P containing ZrO2 films formed on Zr by plasma electrolytic oxidation. Journal of Alloys and Compounds, 2013, Vol 553, 324–332.

Sahly H and Podschun R. Clinical, bacteriological, and serological aspects of *Klebsiella* infections and their spondylarthopathic sequelae. Clinical and Vaccine Immunology, 1997, Vol 4, 393–399.

Sa ́nchez-Lo ́pez JC, Donnet C, Fontaine J, Belin M, Grill A, Patel V and Jahnes C. Diamond-like carbon prepared by high density plasma. Diamond and Related Materials, 2000, Vol 9, 638–642.

Scardino AJ, Hudleston D, Peng Z, Paul NA and de Nys R. Biomimetic characterisation of key surface parameters for the development of fouling resistant materials. Biofouling, 2009, Vol 25, 83-93.

Schalamon J, Petnehazy T, Ainoedhofer H, Zwick EB, Singer G and Hoellwarth ME, Pin tract infection with external fixation of pediatric fractures, Journal of Pediatric Surgery, 2007, Vol 42, 1584-1587.

Schierholz JM, Yücel N, Rump AF, Beuth J and Pulverer G. Antiinfective and encrustation-inhibiting materials--myth and facts. International Journal of Antimicrobial Agents, 2002, Vol 19, 511-516.

Schulte VA, Diez M, Moller M and Lensen MC. Surface topography induces fibroblast adhesion on intrinsically nosnadhesive poly(ethylene glycol) substrates. Biomacromolecules, 2009, Vol 10, 2795-2801.

Schumacher JF, Aldred N, Callow ME, Finlay JA, Callow JA, Clare AS and Brennan AB. Species-specific engineered antifouling topographies: correlations between the settlement of algal zoospores and barnacle cyprids. Biofouling, 2007, Vol 23, 307-317.

Schumacher JF, Carman ML, Estes TG, Feinberg AW, Wilson LH, Callow ME, Callow JA, Finlay JA and Brennan AB. Engineered antifouling microtopographies -

effect of feature size, geometry, and roughness on settlement of zoospores of the green alga Ulva. Biofouling, 2007, Vol 23, 55-62.

Shabtai L, Dolkart O, Chechik O, Amar E, Steinberg E, Mozes G, Maman E. Incidence and Severity of Infections After Closed Reduction and External Fixation of Proximal Humeral Fractures. Journal of Orthopaedic Trauma, 2013, Volume 27, Issue 4, e81–e86.

Shah H, Bosch W, Thompson KM and Hellinger WC. Intravascular Catheter-Related Bloodstream Infection. Neurohospitalist, 2013, 3(3), 144-151.

Shaw GL, Choong SK and Fry C. Encrustation of biomaterials in the urinary tract, Urological Research, 2005, Vol 33,17-22.

Shirai T, Tsuchiya H, Shimizu T, Ohtani K, Zen Y and Tomita K, Prevention of pin tract infection with titanium-copper alloys. Journal of Biomedical Materials Research Part B: Applied Biomaterials, 2009, Vol 91, 373-380.

Sitges-Serra A and Girvent M, Catheter-related bloodstream infection. World Journal of Surgery, 1999, Vol 23, 589-595.

Sivakumar M, Mudali KU and Rajeswari S. Investigation of failures in stainless steel orthopaedic implant devices: fatigue failure due to improper fixation of a compression bone plate. Journal of Materials Science, 1994, Vol 13,142-145.

Sivakumar M, Kumar S, Dhanadurai K, Rajeswari S, ThulasiramanV. Failures in stainless steel orthopaedic implant devices: A survey. Journal of Materials Science Letters, 1995, Vol 14, 351-354.

Skogberg K, Lyytikäinen O, Ruutu P, Ollgren J and Nuorti JP. Increase in bloodstream

infections in Finland, 1995-2002. Epidemiology & Infection, 2008, Vol 136, 108-114.

Smith B S. Titania nanotube arrays: Interfaces for implantable devices. Colorado State University. 2012.

Sopyana I, Melb M, Rameshc S and Khalidd KA, Porous hydroxyapatite for artificial bone applications. Science and Technology of Advanced Materials. 2007, Vol 8, 116-123.

Stark RP and Maki DG. Bacteriuria in the catheterized patient. What quantitative level of bacteriuria is relevant? The New England Journal of Medicine, 1984, Vol 311, 560-564.

Stickler DJ, Evans A, Morris N and Hughes G. Strategies for the control of catheter encrustation. International Journal of Antimicrobial Agents, 2002, Vol 19,499-506.

Stickler DJ and Feneley RC. The encrustation and blockage of long-term indwelling bladder catheters: a way forward in prevention and control. Spinal Cord, 2010, Vol 48(11), 784-90.

Stickler DJ. Clinical complications of urinary catheters caused by crystalline biofilms: something needs to be done. Journal of Internal Medicine, 2014, Vol 276(2), 120-129.

Subbaraman LN, Borazjani R, Zhu H, Zhao Z, Jones L, Willcox MD. Influence of protein deposition on bacterial adhesion to contact lenses. Optometry and Vision Science, 2011, 88(8), 959-66.

Tadmor R. Line energy and the relation between advancing, receding, and young contact angles, Langmuir, 2004, Vol 20, 7659-7664.

Tathe A, Ghodke M and Nikalje AP. A Brief review: biomaterials and application. International Journal of Pharmacy and Pharmaceutical Sciences. 2010, Vol 2, 19-23.

Tiller JC, Liao CJ, Lewis K and Klibanov AM. Designing surfaces that kill bacteria on contact. Proceedings of the National Academy of Sciences of America, 2001, 98, 5981–5985.

Tiwari SK, Sahu RK, Pramanick AK, Singh R. Development of conversion coating on mild steel prior to sol gel nanostructured Al_2O_3 coating for enhancement of corrosion resistance. Surface and Coatings Technology, Vol 205, 4960–4967.

Truong TT, Lin RS and Jeon S. Soft Lithography Using Acryloxy Perfluoropolyether Composite Stamps. Langmuir, 2007, Vol 23, 2898-2905.

Truong VK, Lapovok R, Estrin YS, Rundell S, Wang JY, Fluke CJ, Crawford RJ and Ivanova EP. The influence of nano-scale surface roughness on bacterial adhesion to ultrafine-grained titanium. Biomaterials, 2010, Vol 31, 3674-3683.

Tunney MM, Keane PF, Jones DS and Gorman Sp. Development of model for assessment of biomaterial encrustation in upper urinary tract. Biomaterials, 1996, Vol 12,1025-1029.

Uhlig HH. Adsorbed and Reaction ‐ Product Films on Metals. Journal of The Electrochemical Society, 1950, Vol 97, 215-220.

Unger MA, Chou HP and Thorsen T. Monolithic microfabricated values and pumps by multilayer soft lithography. Science, 2000, Vol 288, 113-116.

Urban RM, Jacobs JJ, Gilbert JL and Galante JO. Migration of corrosion products from modular hip prostheses. The Journal of Bone & Joint Surgery, 1994, Vol 76, 1945-59.

van Dyke ME, Clarson SJ, Arshady R. Silicone biomaterials, PBM Series. Introduction to polymeric biomaterials, 2003, Vol 1,109-135.

Van Oss CJ, Chaudhury MK and Good RJ. Interfacial Lifshitz-van der Waals and polar interactions in macroscopic systems. Chemical Reviews, 1988, Vol 88, 927–941.

Van Oss CJ, Interfacial Forces in Aqueous Media, New York, 1994.

Voinova M V, Rodahl M, Joson M and Kasemo B. Viscoelastic acoustic response of Layered Polymer Films at fluid-solid interfaces: Continuum Mechanics approach. Physica Scripta.1999, Vol 59, 391-396.

Wang R, Neoh KG. Antifouling coating with controllable and sustained silver release for long‐term inhibition of infection and encrustation in urinary catheters. Journal of Biomedical Materials Research Part B: Applied Biomaterials, 2014, DOI: 10.1002/jbm.b.33230.

Warren JW. The catheter and urinary tract infection. The Medical Clinics of North America，1991, Vol 75, 481-493.

Warren LJ. Shear-flocculation of ultrafine scheelite in sodium oleate solutions. Journal of Colloid and Interface Science.1975, Vol 50, 307-318.

Warnes SL and Keevil CW. Mechanism of copper surface toxicity in vancomycin-resistant Enterococci following wet or dry surface contact. Appl. Environ Microbiol. 2011, 77, 6049–6059.

Washburn NR, Yamada KM, Simon CG Jr, Kennedy SB and Amis EJ. High-throughput investigation of osteoblast response to polymer crystallinity: influence of nanometer-scale roughness on proliferation. Biomaterials, 2004, Vol

25,1215-1224.

Whitehead KA, Colligon J, Verran J. Retention of microbial cells in substratum surface features of micrometer and sub-micrometer dimensions. Colloids and Surfaces B: Biointerfaces, 2005, 41(2-3), 129-38.

Wika SF. Pitting and crevice corrosion of stainless steel under offshore conditions. Chemical Engineering and Biotechnology, 2012.

Wilde BE, Williams E, The use of current/voltage curves for the study of localized corrosion and passivity breakdown on stainless steels in chloride media. Electrochimica Acta, 1971, Vol 11, 1971-1985.

Williams DF, Biomaterials and tissue engineering in reconstructive surgery. Sadhana, 2003, Vol 28, 563-574.

Wilson J, Pigott1 GH, Schoen FJ and Hench LL. Toxicology and biocompatibility of bioglasses. Journal of Biomedical Materials Research. 1981, Vol 15, 805-817.

Wu J, Zhang GL, LIU J. Synthesis, characteristics, and antibacterial activity of a rare-earth samarium/silver/titanium dioxide inorganic nanomaterials. Journal of Rare Earths, 2014, Vol 32, 727-732.

Xu Z and Yoon RH. A study of hydrophobic coagulation. Journal of Colloid and Interface Science.1990, Vol 134, 427-434.

Yates A. The causes and management of catheter encrustation. Continence Essentials, Vol 1, 2008.

Yim EK and Leong KW. Significance of synthetic nanostructures in dictating cellular

response. Nanomedicine, 2005, Vol 1, 10-21.

Yinnon AM, Butnaru A, Raveh D, Jerassy Z and Rudensky B. Klebsiella bacteraemia: community versus nosocomial infection. QJ, 1996, Vol 89, 933-941.

Yu GQ, Tay BK, Sun Z and Pan LK. Properties of fluorinated amorphous diamond like carbon films by PECVD. Applied Surface Science, 2003, Vol 219, 228-237.

Yuhta T, Kikuta Y, Mitamura Y, Nakagane K, Murabayashi S and Nishimura I. Blood compatibility of sputter-deposited alumina films. Journal of Biomedical Materials Research, 1994, Vol 28, 217-224.

Zarb P, Coignard B, Griskevicienne J, Muller A, Vankerckho ven Weist K, Goossens MM, Vaerenberg S, Hopkins S, Catry B, Monnet DL, Goosens H, Suetens C. The European Centre for Disease Prevention and Control (ECDC) pilot point prevalence survey of healthcare-associated infections and antimicrobial use. Euro Surveill, 2012, 17, 46.

Zhang T, Wang JM, Chen L, Zhai Z, Song YL and Jiang L. High-Temperature Wetting Transition on Micro- and Nanostructured Surfaces. Angewandte Chemie, 2011, Vol 50, 5311–5314.

Zhang ZY, Luo J. Diamond-Like Carbon Coatings. Encyclopedia of Tribology, 2013, 742-751.

Zhao Q, Liu Y, Müller-Steinhagenb H and Liuc G, Graded Ni–P–PTFE coatings and their potential applications. Surface and Coatings Technology, 2002, Volume 155, 279–284.

Zhao Q, Liu C, Sua X, Zhanga Z, Song W, Wang S, Ning G, Ye J, Lin Y and Gong W.

Antibacterial characteristics of electroless plating Ni–P–TiO2 coatings, Applied Surface Science, 2013, Vol 274, 101-104.

Zhao L, Chu PK, Zhang Y and Wu Z. Antibacterial coatings on titanium implants. Journal of Biomedical Materials Research Part B: Applied Biomaterials. 2009, 91, 470–480

Zhen HD, Izumi M and Nobuyoshi H. Effects of Environmental Parameters on Marine Corrosion of Aluminium Alloy. Advanced Materials Research, 2012, Vol 569, 95.